AD-A174 493 FUNDAMENTAL STUDIES IN FATIGUE AND FRACTURE MECHANICS PHASE 1(U) CARNEGIE-MELLON UNIV PITTSBURGH PA DEPT OF MECHANICAL ENGINEE.. G B SINCLAIR 07 OCT 86 SM-86-13 1/1

UNCLASSIFIED AFOSR-TR-86-1077 AFOSR-85-0030 F/G 20/11 NL

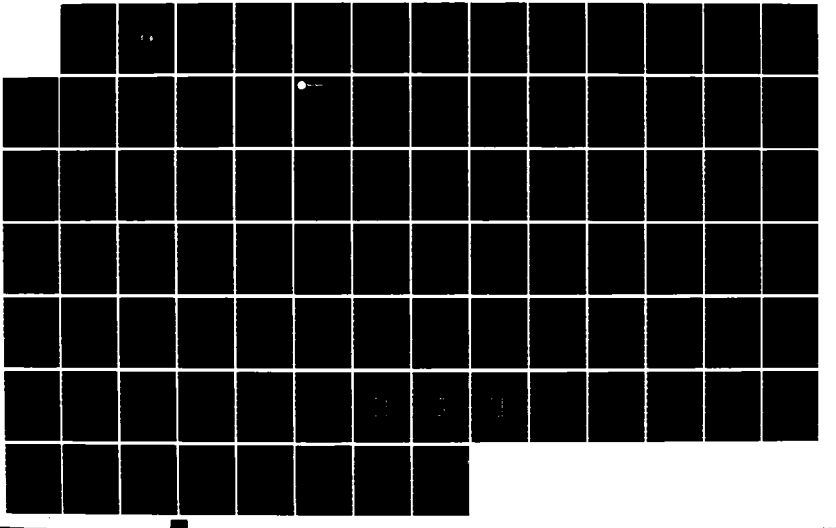

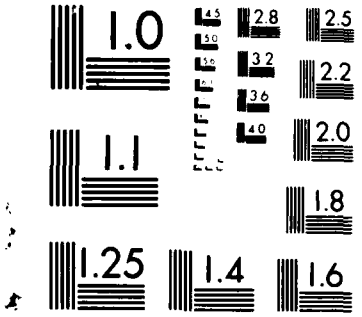

FUNDAMENTAL STUDIES IN FATIGUE AND FRACTURE MECHANICS (Phase I)

Final Report on Air Force Office of Scientific Research

Contract No. AFOSR-85-0030

G. B. Sinclair

SM 86-13

September, 1986

Department of Mechanical Engineering
Carnegie Institute of Technology
Carnegie-Mellon University
Pittsburgh, Pennsylvania 15213

DISCLAIMER NOTICE

THIS DOCUMENT IS BEST QUALITY PRACTICABLE. THE COPY FURNISHED TO DTIC CONTAINED A SIGNIFICANT NUMBER OF PAGES WHICH DO NOT REPRODUCE LEGIBLY.

Unclassified

SECURITY CLASSIFICATION OF THIS PAGE

REPORT DOCUMENTATION PAGE

1a. REPORT SECURITY CLASSIFICATION: Unclassified	1b. RESTRICTIVE MARKINGS: None
2a. SECURITY CLASSIFICATION AUTHORITY: None	3. DISTRIBUTION/AVAILABILITY OF REPORT: Unlimited
2b. DECLASSIFICATION/DOWNGRADING SCHEDULE: N/A	
4. PERFORMING ORGANIZATION REPORT NUMBER(S): SM 86-13	5. MONITORING ORGANIZATION REPORT NUMBER(S): AFOSR-TR- 86-1077
6a. NAME OF PERFORMING ORGANIZATION: G.B. Sinclair, Carnegie-Mellon University; 6b. OFFICE SYMBOL (If applicable): N/A	7a. NAME OF MONITORING ORGANIZATION: Air Force Office of Scientific Research
6c. ADDRESS (City, State and ZIP Code): Department of Mechanical Engineering, Carnegie-Mellon University, Pittsburgh, PA 15213	7b. ADDRESS (City, State and ZIP Code): Bolling Air Force Base, Washington, D.C. 20332
8a. NAME OF FUNDING/SPONSORING ORGANIZATION: Air Force Office of Scientific Research; 8b. OFFICE SYMBOL (If applicable): N A	9. PROCUREMENT INSTRUMENT IDENTIFICATION NUMBER: AFOSR-85-0030
8c. ADDRESS (City, State and ZIP Code): AFOSR / NA, Building 410, Bolling AFB, D.C. 20332	10. SOURCE OF FUNDING NOS.

PROGRAM ELEMENT NO.	PROJECT NO.	TASK NO.	WORK UNIT NO
61102F	2302	B2	

11. TITLE (Include Security Classification): Fundamental Studies in Fatigue and Fracture Mechanics (Phase I)

12. PERSONAL AUTHOR(S): G. B. Sinclair

13a. TYPE OF REPORT	13b. TIME COVERED	14. DATE OF REPORT (Yr., Mo., Day)	15. PAGE COUNT
Final Report	FROM 1/15/85 TO 4/14/86	1986, October 7	83

16. SUPPLEMENTARY NOTATION

17. COSATI CODES			18. SUBJECT TERMS (Continue on reverse if necessary and identify by block number)
FIELD	GROUP	SUB GR	

19. ABSTRACT (Continue on reverse if necessary and identify by block number)

The need to examine the very foundations of fracture mechanics became evident at the close of an earlier AFOSR program [1]. In essence, the basic tenet of fracture mechanics is that the stress intensity factor, K, controls fracture and fatigue: here the former claim is critically examined. The underlying supporting arguments - the original energy argument of Griffith and the more modern K-controlled region view - are considered. These considerations demonstrate that there are questionable assumptions in both, so that the viability of K as a damage parameter for fracture has to be established by the physical evidence. The first question then is whether or not the critical value of K, K_{Ic}, is a material parameter: checking data shows it need not be. The second question is can the technology be usefully predictive, even in the most simple of situations: checking the data shows it to be unreliable in this role. At this time then, it remains to ask similar questions (cont'd)

20. DISTRIBUTION/AVAILABILITY OF ABSTRACT	21. ABSTRACT SECURITY CLASSIFICATION	
UNCLASSIFIED/UNLIMITED ☒ SAME AS RPT ☐ DTIC USERS ☐	Unclassified	
22a. NAME OF RESPONSIBLE INDIVIDUAL: George K. Haritos, Major, USAF NA	22b. TELEPHONE NUMBER (Include Area Code): (202) 767-4937	22c. OFFICE SYMBOL: NA

DD FORM 1473, 83 APR EDITION OF 1 JAN 73 IS OBSOLETE.

Unclassified

SECURITY CLASSIFICATION OF THIS PAGE

19. ABSTRACT (cont'd.)

concerning the role of K in fatigue crack growth and, certainly for the monotonic loading case, develop alternatives: these are the objectives of the second phase of the program.

FUNDAMENTAL STUDIES IN FATIGUE AND FRACTURE MECHANICS (PHASE I)

TABLE OF CONTENTS

SUMMARY

The need to examine the very foundations of fracture mechanics became evident at the close of an earlier AFOSR program [1]. In essence, the basic tenet of fracture mechanics is that the stress intensity factor, K, controls fracture and fatigue: here the former claim is critically examined. The underlying supporting arguments – the original energy argument of Griffith and the more modern K-controlled region view – are considered. These considerations demonstrate that there are questionable assumptions in both, so that the viability of K as a damage parameter for fracture has to be established by the physical evidence. The first question then is whether or not the critical value of K, K_{Ic}, is a material parameter: checking data shows it need not be. The second question is can the technology be usefully predictive, even in the most simple of situations: checking the data shows it to be unreliable in this role. At this time then, it remains to ask similar questions concerning the role of K in fatigue crack growth and, certainly for the monotonic loading case, develop alternatives: these are the objectives of the second phase of the program.

INTRODUCTION

In general, the primary objective of fracture mechanics is to predict when a component will fail when the analysis of the associated configuration leads to singular stresses. This is not an easy task, since the theory is saying that physically unsustainable infinite stresses result from even infinitesimal loadings. At this time, the accepted approach for dealing with such anomalous findings is Linear Elastic Fracture Mechanics (LEFM), at least in the instance of cracked geometries. Essentially, LEFM selects the coefficient of the stress singularity, the stress intensity factor, as the parameter which governs fracture provided response is sufficiently brittle. As a result of an earlier AFOSR research program [1], it became quite clear that this choice and the surrounding technology needed a full examination. This report describes work undertaken in a one year study to this end.

In somewhat greater detail, the principal current activities within a fracture mechanics treatment of a monotonic loading situation may be classified as follows:

- Singularity recognition
- Evaluation of singularity participation
- Interpretation of the resulting quantified singular behaviour

We discuss findings with respect to each of these in turn in what follows.

OVERVIEW OF RESULTS OBTAINED IN RESEARCH PROGRAM

Singularity recognition

Typically the presence and character of singularities is well understood – seldom does the fracture mechanics community stumble on this all-important first step. This is especially so for the elastic analysis of geometries containing cracks. It is also usually the case for the elastic treatment of other configurations, and for the handling of cracks within nonlinear theories. Asymptotic analyses continue to be contributed in these latter instances, e.g., respectively, [2]* and some excellent articles in the recent conference [3]. These last, incidentally, demonstrate that the nonphysical nature of singular stresses is retained when one entertains yielding, i.e., the problem of interpreting singularities is not circumvented by admitting plastic flow. Basically this is because, physically, elastic response must precede plastic and elastic analyses to date continue to be plagued by singularities.**

Singularity participation

In two dimensions, analytical solutions provide explicit and exact values of singularity participation or stress intensity, K, in some situations. In practice, though, even two-dimensional geometries are often too complex to be tractable to a purely analytical approach. Here, however, numerical analysis can be employed to good effect. Principally, the finite element method, when used in conjunction with a path independent integral, furnishes a reliable and accurate means of determining K. This is primarily because the finite element method readily adapts to the various and diverse geometries encountered in engineering, while path independent integrals are orthogonal to any other regular fields present in the analysis of a particular configuration. Moreover, the approach is sufficiently efficient so as to meet engineering accuracy requirements in return for modest computational effort. Such efficiency levels can be demonstrated on test problems with

---

*Copy appended for convenience.

**There do exist elastic analyses of cracks which are apparently free from singularities – these, however, either fail to load the crack tip or involve an integration/finite length scale in effect and therefore do not really overcome the difficulty.

known exact solutions. For example, the path independent integrals devised in [4]*, [5]* can be used to determine K to within 1% using fewer than 200 constant-strain-triangle elements. In all then, the development of the ability to establish singularity participation is well in hand, at least in two-dimensional instances. And the extension of such methods to three dimensions is not seen as a further development of any great significance in the overall question of the performance of fracture mechanics, [6]**.

There are in use at present, nonetheless, some other methods of determining singularity participation which can be shown to be quite unreliable, [7]*, [8]*. In substance, these methods employ some kind of fit of local field data to infer K: the basic reasons for the potential unreliability of such local procedures are as follows. First, all local procedures must consider quantities near but not at the crack tip. Second, at such stations fields other than the key singular ones can contribute. Third, the extent of such participation cannot be either completely controlled or fully accounted for. As a consequence, for any given local procedure there exist problems on which it produces unacceptably erroneous results.

A corollary of the unreliability of local fitting procedures is that fracture criteria based on some local field value cannot be reliably connected to the stress intensity involved. This means that criteria entailing crack opening displacement, crack opening angle, or some so-called critical stress or strain at a nearby station, all fail in the second aspect of fracture mechanics, namely establishing singularity participation. The successful completion of this aspect is a prerequisite to successful interpretation. Accordingly it is unreasonable to expect that any of today's local fracture criteria should prove of genuine and significant value in practice.

---

*Copy appended for convenience.

**Copy sent earlier to AFOSR (final report on Contract No. AFOSR-79-0078).

Singularity Interpretation

The first argument suggested in support of the singularity coefficient, or stress intensity factor, as the controlling parameter in brittle fracture was, in effect, Griffith's energy balance. In Griffith's approach, the energy source is the strain (potential) energy released on fracture, while the sink is a surface energy term. Thus the controlling function at the onset of fracture is the energy release rate, G. Irwin showed that G has a simple relationship to K independent of geometry, so that Griffith's energy balance is equivalent to the choice of the stress intensity factor as a damage parameter.

Griffith's work represented a major step forward at that time. Since, however, a number of questions have been raised concerning the extent of its validity (e.g., Goodier [9]). Moreover, if one simply applies the ideas to the fracture of a truly brittle material in a unaxial tension test, one obtains [10]*

$$\sigma_u \propto \frac{1}{\sqrt{\ell}}. \tag{1}$$

Here σ_u is the ultimate stress, ℓ is the length of the specimen. Equation (1) stems from the fact that the energy source has dimensions of F.L, where as the energy sink has dimensions of F alone, F being force, L being length. For the application to the tensile test, L transpires to be ℓ, the specimen length. While (1) is trendwise correct in that fracture stress decreases with increasing size, it is oversimplified. This is because σ_u can also depend on other dimensions and σ_u's dependence on length need not be to the $-\frac{1}{2}$ exponent, or even particularly close to this precise relation. Indeed, for sufficiently large specimens, σ_u is generally regarded as a material properly, independent of geometry. Thus this simple application of Griffith's ideas raises a question as to whether or not the assumption of a surface energy term as the dominant energy source is really valid, or even sufficiently accurate in certain circumstances. The answer, as far as cracked geometries are concerned, has to lie with the physical evidence.

---

*Copy included in [1].

The more modern argument suggested in support of the stress intensity as the controlling factor in brittle fracture is as follows. For the K-field alone at the crack-tip, the associated field quantities are clearly in violation of the underlying yet unpoliced assumptions of linear elasticity, viz, infinitesimal displacement gradients, stresses in the elastic range, etc. However, some distance away from the crack tip these K-fields do comply with underlying assumptions and may be regarded as being valid. To fix ideas, call the radius from the crack tip outside which the K-fields are valid r_v. Conversely, as one approaches the crack tip for any configuration, there comes a point after which the K-fields dominate any regular fields present. Call this radius r_d. As a result, if $r_v < r_d$, an annulus is formed which may reasonably be viewed as K controlled, i.e. a region in which K sets the boundary conditions in effect for the process zone at the crack tip. Thus under these circumstances, given similar fracture processes in the same material, K determines when fracture occurs.

The drawback to this argument clearly is that r_v may not be less than r_d. Some indication that this can occur is contained in [11]*, [12]*, wherein three very similar pac-man geometries under the same loading are treated. By changing the roof of the pac-man's mouth slightly, K switches from on to off to on again. Here in some sense r_d is going from some finite value, to zero, to some finite value. Hence at some point in this sequence, no K-controlled annulus exists. And further examples can also be constructed. Thus the question arises as to whether or not this approach is sufficiently reliable to be useful in practice: again the answer rests with the physical evidence.

Turning to the physical evidence, perhaps the most basic question is to what extent is the critical value of K, the fracture toughness, a material constant. In particular, to what degree is the plane strain fracture toughness, K_{Ic}, a material constant, since this is probably the most carefully governed by standards in measurement of all parameters in fracture mechanics today. A review for two materials which possibly have had the most extensive

---

*Copy appended for convenience

testing in this regard of all steel and aluminum alloys, respectively, is given in [13]*. A summary of the results is contained in Table 1 (bars indicate mean values, Δ indicates 95% confidence limit, σ_Y is yield stress, K_c plane stress fracture toughness). In sum, K_{Ic} is about five times more variable than the yield stress and accordingly quite dubious as a material property.

Table 1. Critical value of K as a material property

Material	Property ranges		
	$\Delta\sigma_Y$	ΔK_{Ic}	ΔK_c
7075 T6 Al	$\pm 11\%\ \bar{\sigma}_Y$	$\pm 81\%\ \bar{K}_{Ic}$	$\pm 55\%\ \bar{K}_c$
4340 Steel	$\pm 9\%\ \bar{\sigma}_Y$	$\pm 50\%\ \bar{K}_{Ic}$	-

A second basic question in terms of physical evidence is how well can K be used to predict fracture in the simplest of situations. Focusing on geometrically similar configurations subject to a change of scale alone – arguably the most fundamental of tests of predictive capability – an extensive, if not comprehensive, survey of all the pertinent data is furnished in [14]**, [15]**. The answer found is summarized in Fig 1. This figure shows the percentage of times LEFM is within 10% of predicting fracture – useful agreement – and the percentage of times it is within 5% – good agreement. These percentages are shown as a function of scaling with the number of independent tests involved for each class of scale factors given in parentheses. When scaling is small (2-3) there is really little to predict even so K fails to furnish useful predictions over 70% of

*Copy appended for convenience.

**Copy included in [1].

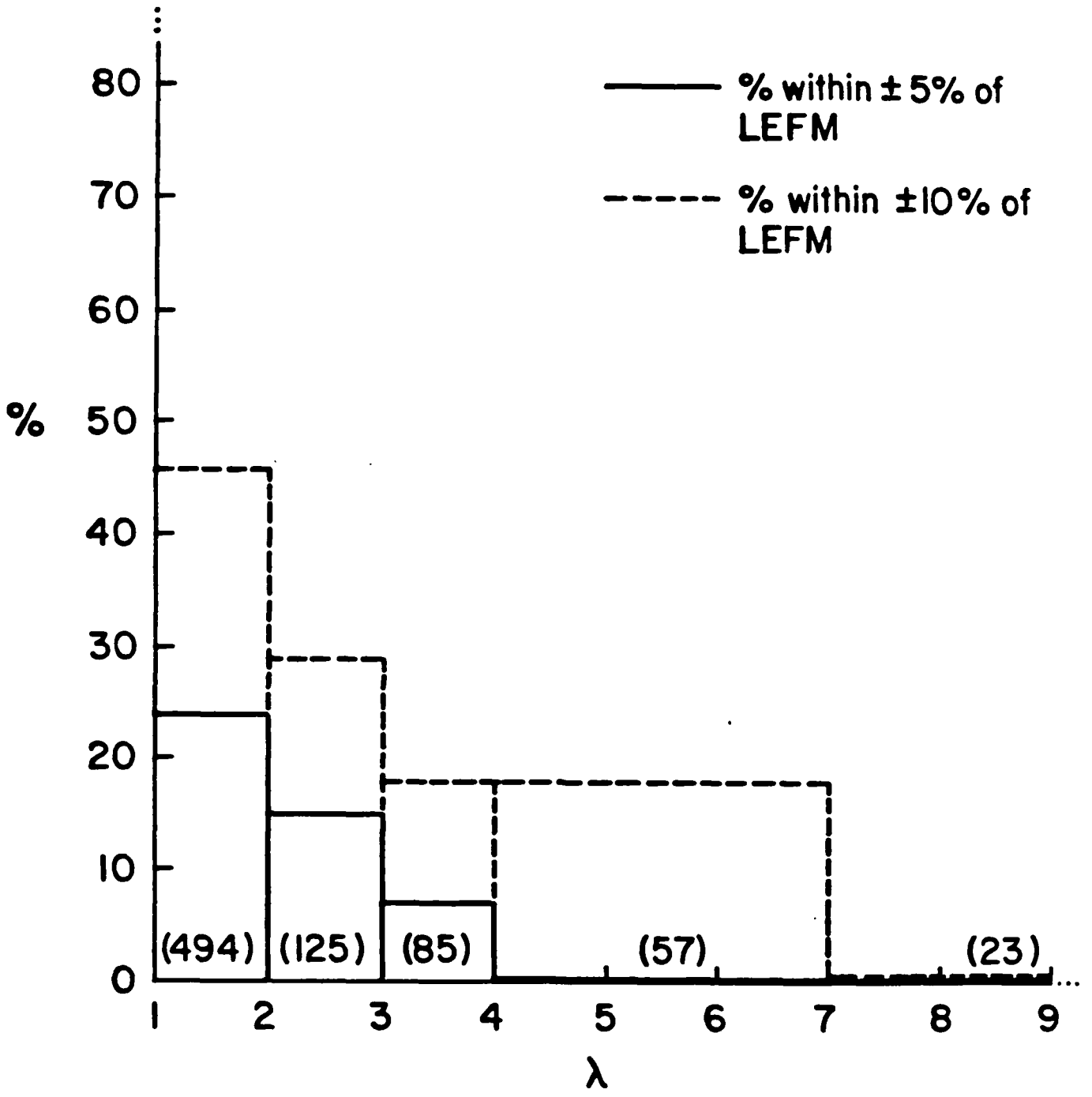

Fig. 1. Predictive capability of K for changes of scale alone.

the time. When scaling is moderate (3-4), K fails to furnish useful results over 80% of the time, while when it is significant (>4) it fares somewhat worse until eventually there are no instances of satisfactory performance. And good predictive capability is even more rare. This performance in such carefully controlled laboratory situations could perhaps have been expected given the outcome of the earlier question concerning K_{Ic} as a material constant, but is nonetheless most unsatisfactory.

CONCLUDING REMARKS

Fracture mechanics today typically is successful in identifying and quantifying singularities, prerequisites to a useful technology. The present interpretation of the resulting quantified singularity, however, is not good enough. More precisely, the choice of the stress intensity factor as the parameter governing brittle fracture under monotonic loading, while appealing in its simplicity, is not up to handling the complex phenomena involved. There is a serious and immediate need to improve our technology here.

Further investigations are warranted regarding the performance of fracture mechanics in the fatigue or cyclic life arena. Given the unsatisfactory performance of fracture mechanics in the simpler monotonic loading instance, there would seem to be little reason for optimism here. Probably significantly different alternatives will need to be developed for both monotonic and cyclic loading before engineering can be provided with an adequate technology.

Acknowledgements - We are pleased to acknowledge the continued valuable benefit of discussions during the course of this work with J.W. Griffin of the Department of Mechanical Engineering at Carnegie-Mellon University. The financial support of the Air Force Office of Scientific Research is also appreciated.

REFERENCES

1. G.B. Sinclair, On the role of dimensionless elastic fracture mechanics. Report SM 85-14, Dept. of Mechanical Engineering, Carnegie-Mellon University (1985).

2. W.S. Burton and G.B. Sinclair, On the singularities in Reissner's theory for the bending of elastic plates. *Journal of Applied Mechanics*, Vol. 53, pp. 220-222 (1986).

3. Tenth U.S. National Congress of Applied Mechanics, Abstracts of Papers. University of Texas at Austin (1986).

4. G.B. Sinclair, M. Okajima and J.H. Griffin, Path independent integrals for computing stress intensity factor at sharp notches in elastic plates. *International Journal for Numerical Methods in Engineering*, Vol. 20, pp. 999-1008 (1984).

5. G.B. Sinclair, A remark on the determination of Mode I and Mode II stress intensity factors for sharp re-entrant corners. *International Journal of Fracture*, Vol. 27, pp. R81-R85 & Vol. 25, p. R17 (1985).

6. W.S. Burton, G.B. Sinclair, J.S. Solecki and J.L. Swedlow, On the implications for LEFM of the three-dimensional aspects in some crack/surface intersection problems. *International Journal of Fracture*, Vol. 25, pp. 3-32 (1984).

7. G.B. Sinclair, Some inherently unreliable practices in present day fracture mechanics. *International Journal of Fracture*, Vol. 28, pp. 3-16 (1985).

8. G.B. Sinclair, Further examples of the unreliability of stress intensity estimates found via local fitting. Report SM 84-13, Department of Mechanical Engineering, Carnegie-Mellon University (1984).

9. J.N. Goodier, Mathematical theory of equilibrium cracks. In *Fracture* (editor H. Liebowitz), Vol. 2, Academic Press, New York (1968).

10. G.B. Sinclair, Some comments on the Griffith-Irwin approach to fracture mechanics. *Proceedings of the Nineteenth Midwestern Mechanics Conference*, Columbus, Ohio, pp. 139-140 (1985).

11. G.B. Sinclair and A.E. Chambers, On the capricious nature of elastic singularities. In [3], (1986).

12. A.E. Chambers and G.B. Sinclair, The elastic analysis of three re-entrant corners. Report SM 86-10, Department of Mechanical Engineering, Carnegie-Mellon University (1986).

13. A.E. Chambers and G.B. Sinclair, On obtaining fracture toughness values from the literature. *International Journal of Fracture*, Vol. 30, pp. R11-R15 (1986).

14. G.B. Sinclair and A.E. Chambers, Strength size effects and fracture mechanics: What does the physical evidence say? *Engineering Fracture Mechanics*, in press.

15. G.B. Sinclair and A.E. Chambers, A bibliography of strength size effects for cracked specimens. Report SM 85-10, Department of Mechanical Engineering, Carnegie-Mellon University 1984).

APPENDIX 1: ON THE SINGULARITIES IN REISSNER'S THEORY FOR THE BENDING OF ELASTIC PLATES

Journal of Applied Mechanics

Brief Notes

A Brief Note is a short paper that presents a specific solution of technical interest in mechanics but which does not necessarily contain new general methods or results. A Brief Note should not exceed *1500 words or equivalent* (a typical one-column figure or table is equivalent to 250 words; a one line equation to 30 words). Brief Notes will be subject to the usual review procedures prior to publication. After approval such Notes will be published as soon as possible. The Notes should be submitted to the Technical Editor of the JOURNAL OF APPLIED MECHANICS. Discussions on the Brief Notes should be addressed to the Editorial Department, ASME, United Engineering Center, 345 East 47th Street, New York, N. Y. 10017, or to the Technical Editor of the JOURNAL OF APPLIED MECHANICS. *Discussions on Brief Notes appearing in this issue will be accepted until two months after publication.* Readers who need more time to prepare a Discussion should request an extension of the deadline from the Editorial Department.

On the Singularities in Reissner's Theory for the Bending of Elastic Plates

W. S. Burton[1] and G. B. Sinclair[1]

Wedge-shaped elastic plates under bending, with the edges forming the wedge vertex being either stress-free, clamped or simply supported, are characterized as to possible singular behavior within the context of Reissner's plate theory.

Introduction

Probably the first singularity analysis of an angular elastic plate under bending is William's treatment using the *classical theory* [1]. In the classical theory it is possible to satisfy stress-free conditions at an edge solely in an approximate way, since only two boundary conditions can be enforced and there are three stress resultants. As the boundary conditions play an important role in governing singular behavior at the vertex of any corner in a plate it is to be expected that *Reissner's theory* [2], which admits three, physically-natural, boundary conditions on an edge, may offer an improved, albeit singular, representation in these instances. This is the expectation that possibly motivated other analysts (e.g., Wang [3]) to perform analyses of complete, individual, crack problems using Reissner's theory rather than the classical, and indeed more physically sensible results are derived in these analyses. Specifically, for the crack-tip on the tensile face of the plate the same hydrostatic singular field ahead of the crack as occurs in the extensional case of a cracked plate under tension is found; this is in contrast to the classical bending theory in which the principal stresses ahead of the crack differ in sign and magnitude. As a result it would seem reasonable to attempt the analogue of Williams' study for the classical theory [1] and explore the singularities in Reissner's plate theory for a wider range of geometries than that investigated elsewhere and for a full range of boundary conditions; this is the intent of the present note.

We begin by formulating a class of problems for a wedge-shaped elastic plate under bending within the context of Reissner's theory. Next we establish suitable solution forms for the dominant asymptotic response near the wedge vertex and set down conditions for the existence of these fields. The conditions basically involve the analysis of an eigenequation for each pair of edge conditions considered. The note concludes by displaying these eigenequations and discussing the eigenvalues satisfying them which give rise to singularities.

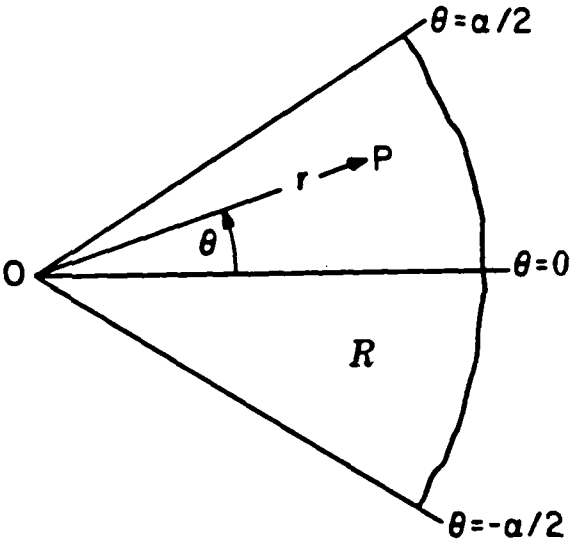

Fig. 1 Geometry and coordinates for the plate

Formulation

The plate has thickness h and occupies the open wedge region, R,

$$R = \{(r,\theta)\,|\,0<r<\infty, -\alpha/2<\theta<\alpha/2\}(0<\alpha\leq 2\pi), \qquad (1)$$

where (r,θ) are the polar coordinates of a point P in the wedge with respect to the origin, 0, at the wedge vertex, and α is the vertex angle (Fig. 1).

The plate is comprised of a homogeneous, isotropic, and

[1]Department of Mechanical Engineering, Carnegie-Mellon University, Pittsburgh, PA 15213.

Manuscript received by ASME Applied Mechanics Division, December 19, 1983; final revision July 15, 1985.

Table 1 Eigenequations for Reissner's plate theory generating singular moment resultants

Edge Conditions	Eigenequation	Constants
Stress-free/stress-free	$\sin\lambda\alpha = C_1\lambda$	$C_1 = (-)^k\sin\alpha$
Clamped/clamped	$\sin\lambda\alpha = C_2\lambda$	$C_2 = (-1/\kappa)^{k+1}\sin\alpha$
Clamped/stress-free	$\sin^2\lambda\alpha = C_3 - C_4\lambda^2$	$C_3 = 4/\kappa(1+\nu)^2$
		$C_4 = (1/\kappa)\sin^2\alpha$
Stress-free/simply supported	$\sin2\lambda\alpha = C_5\lambda$	$C_5 = \sin2\alpha$
Clamped/simply supported	$\sin2\lambda\alpha = C_6\lambda$	$C_6 = (-1/\kappa)\sin2\alpha$
Simply supported/simply supported	$\cos\lambda\alpha = C_7$	$C_7 = (-)^k\cos\alpha$

Note: $k = 1,2$ for symmetric or anti-symmetric loading, respectively, and $\kappa = (3-\nu)/(1+\nu)$.

linear elastic material having Young's modulus, E, and Poisson's ratio, ν. For this plate the stress resultants and rotations of Reissner's plate theory, in the absence of surface loading, can be expressed in terms of the out of plane deflection, $w(r,\theta)$, and a single stress potential, $\chi(r,\theta)$. That is,

$$V_r = \frac{1}{r}\frac{\partial\chi}{\partial\theta},\quad V_\theta = -\frac{\partial\chi}{\partial r},$$

$$M_\theta = 2\gamma\left(\frac{1}{r^2}\frac{\partial\chi}{\partial\theta} - \frac{1}{r}\frac{\partial^2\chi}{\partial r\partial\theta}\right)$$

$$-D\left(\nu\frac{\partial^2 w}{\partial r^2} + \frac{1}{r}\frac{\partial w}{\partial r} + \frac{1}{r^2}\frac{\partial^2 w}{\partial\theta^2}\right),$$

$$M_r = 2\gamma\frac{\partial}{\partial r}\left(\frac{1}{r}\frac{\partial\chi}{\partial\theta}\right) - D\left(\frac{\partial^2 w}{\partial r^2} + \frac{\nu}{r}\frac{\partial w}{\partial r} + \frac{\nu}{r^2}\frac{\partial^2 w}{\partial\theta^2}\right),$$

$$M_{r\theta} = \gamma\left(\frac{1}{r^2}\frac{\partial^2\chi}{\partial\theta^2} - r\frac{\partial}{\partial r}\left(\frac{1}{r}\frac{\partial\chi}{\partial r}\right)\right) \tag{2}$$

$$-(1-\nu)D\frac{\partial}{\partial r}\left(\frac{1}{r}\frac{\partial w}{\partial\theta}\right),$$

$$\beta_\theta = -\frac{2\gamma}{D(1-\nu)}\frac{\partial\chi}{\partial r} - \frac{1}{r}\frac{\partial w}{\partial\theta},$$

$$\beta_r = \frac{2\gamma}{D(1-\nu)}\frac{1}{r}\frac{\partial\chi}{\partial\theta} - \frac{\partial w}{\partial r},$$

on R, where V_r, V_θ, the shear resultants, M_θ, M_r, $M_{r\theta}$, the moment resultants and β_θ, β_r, the rotations, are functions of r, θ, defined in the usual manner, with $\gamma = h^2/10$, $D = Eh^3/12(1-\nu^2)$, the last being the flexural rigidity. Then the *field equations* of Reissner's theory are reduced to the Cauchy-Riemann equations for the functions $\chi - \gamma\nabla^2\chi$ and $D\nabla^2 w$, i.e.,

$$\frac{\partial}{\partial r}(\chi - \gamma\nabla^2\chi) = \frac{1}{r}\frac{\partial}{\partial\theta}(D\nabla^2 w),$$

$$\frac{1}{r}\frac{\partial}{\partial\theta}(\chi - \gamma\nabla^2\chi) = \frac{-\partial}{\partial r}(D\nabla^2 w), \tag{3}$$

on R. Here ∇^2 is the Laplacian operator in cylindrical polar coordinates.

On each wedge face three homogeneous boundary conditions are to be satisfied. These three boundary conditions are combined in sets of *edge conditions* to model various edges as follows:

Stress-free	$M_\theta = M_{r\theta} = 0$,	$V_\theta = 0$,
Clamped	$\beta_\theta = \beta_r = 0$,	$w = 0$, (4)
Simply supported	$M_\theta = 0$,	$\beta_r = 0$, $w = 0$,

on $\theta = \pm\alpha/2$ $(0 \le r < \infty)$. These three cases combine to give six *distinct problems for the wedge*. When the same conditions apply on each face, it is possible to distinguish between symmetric and anti-symmetric contributions. Thus, in effect, nine problems are considered. Ensuring bounded displacements concludes our formulation and limits the singular behavior admitted-while this formulation is then still not complete, it suffices given our objective of characterizing *possible* singular *fields at the wedge vertex*. We next consider the construction of suitable sets of asymptotic solutions.

Singularity Analysis

From the form of the relations in (2), observe that if $w = O(r^{\lambda+1})$, $\chi = O(r^{\lambda+1})$, as $r \to 0$ on R, λ a constant, then the shear resultants and rotations are $O(r^\lambda)$, while the moment resultants are $O(r^{\lambda-1})$. Accordingly we seek to construct separable solutions for w, χ satisfying the governing equations (3) which furnish six independent constants multiplying these dominant contributions as $r \to 0$, thereby providing a means of satisfying the six boundary conditions contained in any pair of the edge conditions (4). To this end, and noting that $\chi - \lambda\nabla^2\chi$ and $D\nabla^2 w$ are harmonic functions and the interrelations in (3), we therefore take as our asymptotic solution forms for χ and w, the biharmonic functions[2]

$$\chi = r^{\lambda+1}F(\lambda,\theta) + O(r^{\lambda+3}),$$
$$w = r^{\lambda+1}G(\lambda,\theta) + O(r^{\lambda+3}), \tag{5}$$

as $r \to 0$ on R, where

$$F(\lambda,\theta) = (b_1\cos(\lambda+1)\theta + b_2\sin(\lambda+1)\theta + b_3\cos(\lambda-1)\theta + b_4\sin(\lambda-1)\theta),$$

$$G(\lambda,\theta) = (b_5\sin(\lambda+1)\theta + b_6\cos(\lambda+1)\theta - \gamma b_3\sin(\lambda-1)\theta + \gamma b_4\cos(\lambda-1)\theta)/D.$$

The stress and moment resultants and the rotations in (2) may then be written as

$$V_r = r^\lambda F' + O(r^{\lambda+2}),\quad V_\theta = -(\lambda+1)r^\lambda F + O(r^{\lambda+2}),$$
$$M_\theta = r^{\lambda-1}[-2\gamma\lambda F' - D((\lambda+1)(1+\nu\lambda)G + G^*)] + O(r^{\lambda+1}),$$
$$M_r = r^{\lambda-1}[2\gamma\lambda F' - D((\lambda+1)(\lambda+\nu)G + \nu G^*)] + O(r^{\lambda+1}),$$
$$M_{r\theta} = r^{\lambda-1}[\gamma(F^* - (\lambda+1)(\lambda-1)F) - D(1-\nu)\lambda G'] + O(r^{\lambda+1}),$$
$$\beta_\theta = r^\lambda\left[\frac{-2\gamma}{D(1-\nu)}(\lambda+1)F - G'\right] + O(r^{\lambda+2}), \tag{6}$$
$$\beta_r = r^\lambda\left[\frac{2\gamma}{D(1-\nu)}F' - (\lambda+1)G\right] + O(r^{\lambda+2}),$$

as $r \to 0$ on R, where the primes denote differentiation with respect to θ.

With this set of separable functions for w and χ the singularity analysis proceeds in a manner similar to that developed by Williams [4] for power singularities and by Dempsey and Sinclair [5] for logarithmic singularities. Imposing the displacement regularity requirements on (6) and con-

[2] Note that one cannot use Reissner's solution [2] and have a sufficient number of independent constants available for the asymptotic analysis.

fining attention to singular solutions, the resulting conditions may be summarized by

$\mathbf{M} = 0(r^{\lambda-1})$ for real λ satisfying $D = 0, 0 < \lambda < 1$,

$$\mathbf{M} = 0\left(r^{\lambda-1}\begin{Bmatrix}\sin(\eta \ln r)\\ \cos(\eta \ln r)\end{Bmatrix}\right) \text{ for complex } \lambda = \xi + i\eta$$

$$\text{satisfying } D = 0, 0 < \Delta Re\lambda < 1, \tag{7}$$

$\mathbf{M} = 0(r^{\lambda-1}\ln r)$ *for real* λ *satisfying*

$$\frac{d^{n-m}D}{d\lambda^{n-m}} = 0,\ m < n,\ 0 < \lambda \le 1,$$

$$\mathbf{M} = 0\left(r^{\lambda-1}\ln r\begin{Bmatrix}\sin(\eta \ln r)\\ \cos(\eta \ln r)\end{Bmatrix}\right) \text{ for complex } \lambda = \xi + i\eta$$

$$\text{satisfying } \frac{d^{n-m}D}{d\lambda^{n-m}} = 0,\ m < n,\ 0 < Re\lambda \le 1,$$

as $r \to 0$ on R, where $\mathbf{M} = (M_\theta, M_r, M_{r\theta})$ *is the vector of moment resultants.* In (7), D is the determinant of the coefficient matrix stemming from the substitution of (6) into a set of edge conditions drawn from (4) and n is the order of this matrix, m its rank. For any particular combination of the edge conditions (4) for a wedge angle α, the values of λ in the ranges given in (7) may be regarded as the singular *eigenvalues* of the *eigenequation*, $D = 0$. We now investigate the eigenequations resulting from such expansions.

Eigenequations

For the particular problem of the symmetric bending of a stress-free/stress-free wedge, substituting (6) with $b_1 = b_3 = b_5 = 0$ therein into the first of (4) and expanding the determinant of the resulting 3×3 coefficient matrix leads to

$$\sin(\lambda + 1)\alpha/2(\lambda \sin\alpha + \sin\lambda\alpha) = 0 (0 < \alpha \le 2\pi). \tag{8}$$

Equation (8) factors into two equations; however, the first of these, while not generating a completely trivial solution, does not give rise to any moment resultants and therefore contributes no singular fields. Consequently, it may be discarded leaving as our eigenequation for this case only the second factor. The eigenequations for the remaining combinations of the edge conditions each possess similar, non-singular, multiplicative factors. *In Table 1, we suppress these and list* only those parts of each eigenequation that have attendant singular fields.

Comparison of the first three cases in Table 1 with the corresponding extensional cases given in Williams [4] shows the eigenequations to be identical. Examining the fourth and fifth cases in Table 1 and noting that the conditions for the simply supported edge in (4) are the same as anti-symmetry requirements, we see these eigenequations are equivalent to the anti-symmetric parts of the first and second eigenequations, respectively, for a wedge of angle 2α. It follows that these two cases are also effectively contained in Williams' extensional analysis [4]. Finally, taking as the physical analogue of the simply supported/simply supported edge condition, the extensional anti-symmetry conditions, $u_r = 0$, $\sigma_\theta = 0$ where u_r is the radial displacement and σ_θ is the tangential normal stress, we find that the last case too has a corresponding extensional eigenequation. The significance of this correspondence is that discussions in the literature on the extensional eigenequations are directly applicable to elastic wedges generated by Reissner's bending theory.

Solutions for the dominant singular real part of λ are given for the first three cases in Table 1 by Williams [4] and are decomposed in effect into symmetric and anti-symmetric parts by Kalandiia [6], thus accounting for the first five cases. The roots for the last case, simply supported/simply supported, can be determined by inspection. Some of the eigenvalues given in [4, 6] are actually the real parts of complex solutions; however, no truly comprehensive search for complex roots appears to be available in the literature. Such a parameter study is outside the scope of the present work. Nonetheless, for any given application the determination of complex eigenvalues proceeds routinely on separating the pertinent eigenequation for the specific α-value into real and imaginary parts and solving the resulting, simple, simultaneous pair of transcendental equations. Likewise, logarithmic singularities have not been exhaustively searched for, but are straight forward to check for in any specific instance.

In conclusion we remark that the correspondence between the singular fields in Reissner's theory and those in extensional plate theory is not restricted merely to the singular eigenvalues, but carries over to the actual eigenfunctions which share the same *r and* θ dependences, as can be deduced from the solution (6) and its counterpart in Williams [4].

References

1 Williams, M. L., "Surface Stress Singularities Resulting From Various Boundary Conditions in Angular Corners of Plates Under Bending," *Proceedings of the First U.S. National Congress of Applied Mechanics*, 1951, pp. 325-329.

2 Reissner, E., "The Effect of Transverse Shear Deformation on the Bending of Elastic Plates," ASME JOURNAL OF APPLIED MECHANICS, Vol. 12, 1945, pp. A-69-A-77.

3 Wang, N-M., "Effects of Plate Thickness on the Bending of an Elastic Plate Containing a Crack," *Journal of Mathematics and Physics*, Vol. 47, 1968, pp. 371-390.

4 Williams, M. L., "Stress Singularities Resulting from Various Boundary Conditions in Angular Corners of Plates in Extension," ASME JOURNAL OF APPLIED MECHANICS, Vol. 19, 1952, pp. 526-528.

5 Dempsey, J. P., and Sinclair, G. B., "On the Stress Singularities in the Plane Elasticity of the Composite Wedge," *Journal of Elasticity*, Vol. 9, 1979, pp. 373-391.

6 Kalandiia, A. L., "Remarks on the Singularity of Elastic Solutions Near Corners," *Prikladnaia Matematika i Mekhanika*, Vol. 33, 1969, pp. 132-135.

Dynamic Behavior of Beam Structures Carrying Moving Masses

S. Saigal[1]

Introduction

The dynamic response of structures carrying moving masses is a problem of widespread practical significance. A detailed survey of research efforts in this field was given by Stanišić et al. [2]. The original problem is nonlinear in both local and convective derivatives [3] and is complicated by the presence of a Dirac-Delta function as a coefficient in the differential equation of motion. Previous methods [2] applied for the solution of this problem are approximate in nature and tedious in their hierarchy of mathematical operation. Recently, Stanišić [3] expressed the solution in terms of eigenfunctions satisfying the boundary, initial and transient conditions, for a heavy mass moving over a simply supported beam. However, in engineering practice there are problems that involve more complex boundary conditions and, therefore, it is of phenomenological interest to look into the physics of the dynamical behavior of a clamped and a cantilever beam under the action of heavy moving masses. The present study extends Stanišić's theory [3] to study the dynamic behavior of a

[1]School of Aeronautics and Astronautics, Purdue University, West Lafayette, Indiana 47907. Student Member, ASME.

APPENDIX 2: PATH INDEPENDENT INTEGRALS FOR COMPUTING STRESS INTENSITY FACTORS AT SHARP NOTCHES IN ELASTIC PLATES / A REMARK ON THE DETERMINATION OF MODE I AND MODE II STRESS INTENSITY FACTORS FOR SHARP RE-ENTRANT CORNERS

INTERNATIONAL JOURNAL FOR NUMERICAL METHODS IN ENGINEERING, VOL. 20, 999–1008 (1984)

PATH INDEPENDENT INTEGRALS FOR COMPUTING STRESS INTENSITY FACTORS AT SHARP NOTCHES IN ELASTIC PLATES

G. B. SINCLAIR, M. OKAJIMA AND J. H. GRIFFIN

Department of Mechanical Engineering and the Center for the Joining of Materials, Carnegie-Mellon University, Pittsburgh, Pennsylvania, U.S.A.

SUMMARY

A set of path independent integrals is constructed for the calculation of the generalized stress intensity factors occurring in elastic plates having sharp re-entrant corners or notches with stress-free faces and subjected to Mode I, II or III type loading. The Mode I integral is then demonstrated to enjoy a reasonable degree of numerical path independence in a finite element analysis of a test problem having an exact solution. Finally, this integral is used on the same problem in conjunction with a regularizing, finite element, procedure or superposition method. The results indicate that sufficiently accurate estimates of these stress intensity factors for engineering purposes can be achieved with little computational effort.

INTRODUCTION

In a number of engineering structures, sharp re-entrant corners or notches are introduced, usually to facilitate fabrication. At the vertices of these notches, stress concentrations arise making them likely sites for fatigue crack initiation and therefore the potential sources of ultimate failure. Elastic analyses of such configurations result in stress singularities (see, e.g., References 1 and 2). While these singularities are physically unrealistic in themselves, it is possible that, with a sufficiently accurate determination of their nature and participation, an extension of the now accepted notion of a *stress intensity factor* K might prove of value. Although such a generalization lacks the thermodynamic argument in terms of energy release rates that underlies the physical significance of K for cracks, it could lead to an improvement over present practice in initiation calculations for notches. One current approach to such calculations is to *assume* that a crack has actually formed at the notch tip, then compute the usual stress intensity factor variation under cyclic loading, ΔK, and compare it with material threshold values to see if crack growth commences: with a generalized K for the notch itself, the ΔK could be computed directly and compared with an accompanying set of experimental threshold values *for the notch*. In this way, increased life could be detected in circumstances in which load levels are too low for the formation of a crack at the notch tip. The intent of this investigation is to contribute to the analytical component of such a technology by developing an efficient computational procedure for accurately assessing generalized stress intensity factors at stress-free notches in elastic plates, one which is readily applicable to the wide range of complex configurations encountered in practice.

The basis of our approach to meet the foregoing objective lies in the development of a set of *path independent integrals* which pick off the K at notches. Such path independent integrals for singular elasticity problems probably owe their origin to Eshelby's work[3] in the early 1950s, and a number of different forms for these integrals have evolved over the intervening years

0029–5981/84/060999–10$01.00

Received May 1982
Revised 20 March 1983

(e.g. Sanders' integral;[4] see also Freund[5] and the references contained therein). All of the foregoing integrals apply to a crack. Recently Stern and Soni[6] developed an integral for a right-angle corner under fixed-free conditions; here we follow the ideas in Reference 6 and construct a set of like integrals, termed H integrals, for a stress-free notch in an elastic plate.

The computational advantage of path independent integrals in the analysis of singular elasticity problems stems from the fact that the only numerical errors accrued in their calculation derive from the numerical approximations being used—there is no additional source of errors such as that due to the truncation of an eigenfunction expansion as in local fitting methods. It is to be expected therefore that, when used in conjunction with a finite element method which recognizes and handles the singularity present or some equivalent numerical approach, a procedure results which is easily adapted to varying configurations yet which yields the necessary resolution for practical purposes in return for a modest computational effort. Such is indeed demonstrated to be the case in the second section of the paper, wherein the numerical path independence of an H integral drawn from the previous section is examined, following which the same integral is used in conjunction with the regularizing procedure of Sinclair and Mullan.[7] The paper then closes with some remarks on other applications and extensions.

CONSTRUCTION OF THE PATH INDEPENDENT INTEGRALS

Here we first focus on the in-plane symmetric loading of a notch in an elastic plate and develop a path independent integral for the stress intensity factors in this class of problems. We then discuss other integrals for anti-symmetric and out-of-plane configurations.

To formulate our initial class of symmetric, in-plane, notch problems we consider a plane finite wedge subtending an angle 2α at its vertex ($\pi/2 < \alpha < \pi$), let (x_1, x_2) be rectangular cartesian co-ordinates having origin at the wedge vertex, the x_1-axis bisecting the angle there, and take R to be the open region defined by that part of the wedge in the upper half-plane, with ∂R being its boundary (Figure 1). To facilitate further the formulation and subsequent

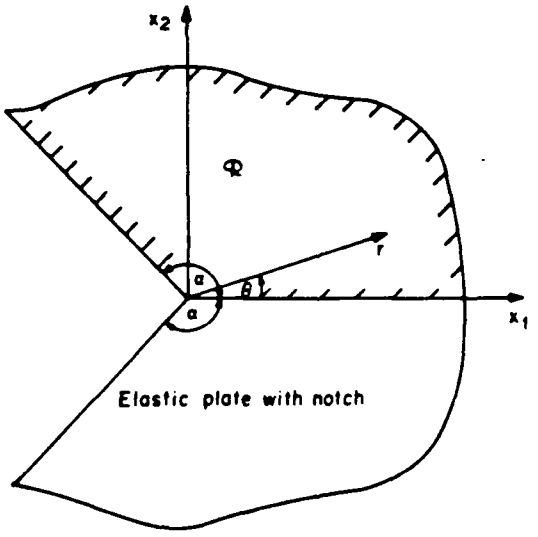

Figure 1. Geometry and co-ordinates for the region R

analysis, we introduce companion cylindrical polar co-ordinates (r, θ) related to (x_1, x_2) by the transformations,

$$x_1 = r\cos\theta \qquad x_2 = r\sin\theta \quad (0 \leq r < \infty, -\pi < \theta \leq \pi) \tag{1}$$

Then, in general, we seek the stresses σ_{ij} and displacements $u_i (i, j = 1, 2)$ throughout R as functions of x_1, x_2 satisfying the following. The two-dimensional stress equations of equilibrium in the absence of body forces,†

$$\sigma_{ij,j} = 0 \quad \text{on } R \tag{2}$$

The stress–displacement relations for a homogeneous and isotropic, linear elastic plate,

$$\sigma_{ij} = \mu[((3-\kappa)/(\kappa-1))\delta_{ij}u_{k,k} + u_{i,j} + u_{j,i}] \quad \text{on } R \tag{3}$$

wherein μ is the shear modulus, κ equals $3-4\nu$ for plane strain and $(3-\nu)/(1+\nu)$ for plane stress ν being Poisson's ratio, and δ_{ij} is the Kronecker delta. The stress-free conditions on the notch face,

$$\sigma_{ij}n_j = 0 \quad \text{on } \partial R \text{ when } x_1/x_2 = \cot\alpha \tag{4}$$

where n_j are the components of the unit outward normal to ∂R. The symmetry requirements ahead of the notch tip,

$$\sigma_{12} = 0 \qquad u_2 = 0 \quad \text{on } \partial R \text{ when } x_2 = 0 \tag{5}$$

The boundary conditions prescribing the tractions or displacements on the remainder of ∂R,

$$\sigma_{ij}n_j = s_i^0 \quad \text{on } \partial_1 R \qquad u_i = u_i^0 \quad \text{on } \partial_2 R \tag{6}$$

wherein s_i^0, u_i^0 are the applied tractions and displacements and $\partial_1 R$, $\partial_2 R$ are complementary subsets of ∂R excluding the intervals in (4), (5). And finally the regularity requirements at the notch-tip which insist that the displacements are bounded there,

$$u_i = O(1) \quad \text{on } R \text{ as } r \to 0 \tag{7}$$

Specifically we seek to extract from the stress and displacement fields meeting these requirements the *generalized stress intensity factor* present defined by

$$K_1 = \lim_{x_1 \to 0^-} \sqrt{(2\pi)}x_1^{1-\lambda}\sigma_{22} \quad \text{on } x_2 = 0 \tag{8}$$

Here the subscript I denotes the opening symmetric mode, Mode I, and λ is the singular eigenvalue characterizing the only singular stress field possible at the re-entrant corner as identified after Williams.[2]‡ That is, λ is the root of the transcendental eigenequation,

$$\sin 2\lambda\alpha = -\lambda \sin 2\alpha \qquad (0 < \lambda < 1) \tag{9}$$

with an associated eigenfunction having stresses and displacements in the neighbourhood of the notch tip behaving in accordance with

$$\sigma_{ij} = O(r^{\lambda-1}) \qquad u_i = O(r^{\lambda}) \quad \text{on } R \text{ as } r \to 0 \tag{10}$$

† Although the lower case subscripts only range over the integers (1, 2), the usual index notation conventions apply: repeated subscripts imply summation and a subscript preceded by a comma indicates partial differentiation with respect to the corresponding cartesian co-ordinate.

‡ See Gregory[8] for a completeness argument for Williams' eigenfunctions.

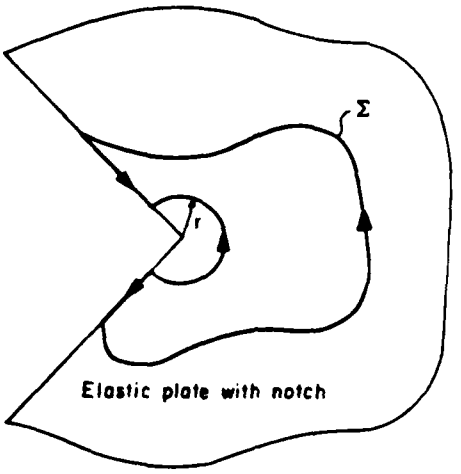

Figure 2. H_1 integral paths

To construct a *path independent integral* for computing K_1 we proceed as follows. In general, path independent integrals can be devised by invoking the divergence theorem of Gauss on ensuring the divergence of the integrand is zero: in elasticity, this can be done in effect with Betti's reciprocal theorem (refer, e.g., to Reference 9, p. 355) which, in a plane, can be stated as

$$\int_\Gamma (\sigma_{ij} u_i^* - \sigma_{ij}^* u_i) n_j \, ds = 0 \tag{11}$$

In (11), the integration is performed in a counter-clockwise sense around Γ which is any closed contour in R, σ_{ij}^*, u_i^* are complementary fields satisfying the same field equations as σ_{ij}, u_i, namely (2), (3), n_j are now the components of the unit outward normal to Γ, and ds is an infinitesimal line segment of Γ. Next we choose Γ as the contour comprised of any path Σ which emanates on the lower notch flank and terminates on the upper, a circular path of radius r from the upper flank to the lower, and two closing straight paths along the flanks (Figure 2). On letting the radius of the inner circular arc shrink to zero it is clear that only those parts of the integrand which behave like $O(1/r)$ as $r \to 0$ can contribute to this portion of the integral in (11). In order that such contributions stem from the singular K_1 fields alone we therefore require that

$$\sigma_{ij}^* = O(r^{-\lambda-1}), \qquad u_i^* = O(r^{-\lambda}) \quad \text{on } R \text{ as } r \to 0 \tag{12}$$

Then (10), (12) imply that the product of the K_1 terms with the complementary field in (11) has the desired $1/r$ behaviour while all other fields in σ_{ij}, u_i contribute terms $o(1/r)$ as $r \to 0$ by virtue of the fact that the K_1 singularity is the dominant one present. Unfortunately, under this limiting procedure the possibility of divergent integrals along the flanks arises because of the potential of $1/r$ terms there. Fortunately, if λ is an eigenvalue satisfying (9) so is $-\lambda$, so that the complementary fields can be further required to be eigenfunctions themselves, thereby rendering both $\sigma_{ij} n_j$ and $\sigma_{ij}^* n_j$ zero on the flanks and making the integrals there identically zero. Under these conditions the integral around Σ equals the counter-clockwise integral around the circular arc in the limit as $r \to 0$ which, with the selection of appropriate participation factor

in the complementary eigenfunction, can be adjusted to recover K_I. That is, we define H_I by

$$H_I = \int_\Sigma (\sigma_{ij} u_i^* - \sigma_{ij}^* u_i) n_j \, ds \tag{13}$$

and scale the complementary eigenfunction satisfying (2)–(5), (12) so that

$$H_I = K_I \tag{14}$$

The actual forms for the complementary eigenfunction are most readily established in polar co-ordinates and can be derived along the lines of Williams' analysis[2] yielding

$$\begin{aligned}
\sigma_{rr}^* &= -K_I^* r^{-\lambda-1}[(\lambda+3)\cos(\lambda+1)\theta - \beta\cos(\lambda-1)\theta] \\
\sigma_{\theta\theta}^* &= K_I^* r^{-\lambda-1}[(\lambda-1)\cos(\lambda+1)\theta - \beta\cos(\lambda-1)\theta] \\
\sigma_{r\theta}^* &= -K_I^* r^{-\lambda-1}[(\lambda+1)\sin(\lambda+1)\theta - \beta\sin(\lambda-1)\theta] \\
u_r^* &= \frac{K_I^* r^{-\lambda}}{2\mu\lambda}[(\lambda+\kappa)\cos(\lambda+1)\theta - \beta\cos(\lambda-1)\theta] \\
u_\theta^* &= \frac{K_I^* r^{-\lambda}}{2\mu\lambda}[(\lambda-\kappa)\sin(\lambda+1)\theta - \beta\sin(\lambda-1)\theta]
\end{aligned} \tag{15}$$

with

$$K_I^* = \frac{\sqrt{(8\pi)}\mu\lambda(\lambda\sin^2\alpha + \sin^2\lambda\alpha)}{(1+\kappa)(\sin 2\alpha + 2\alpha\cos 2\lambda\alpha)} \qquad \beta = \frac{\lambda^2-1}{\lambda\cos 2\alpha + \cos 2\lambda\alpha}$$

Before moving on to the application of the H_I integral of (13), several remarks concerning its use and some simple extensions are in order. First, because of the symmetry involved, it is clear that H_I can be computed as twice the integral around that part of Σ within R alone. Second, (14) holds in the limit $\alpha \to \pi$ and the notch becomes a *crack*. Third, the pure traction conditions on $\partial_1 R$ and the pure displacement conditions on $\partial_2 R$ are solely for convenience in the formulation and can be relaxed to accommodate admissible mixtures of traction and displacement components. Fourth, extension to the *antisymmetric* or Mode II case is straightforward and leads to

$$H_{II} = K_{II} = \int_\Sigma (\sigma_{ij} u_i^* - \sigma_{ij}^* u_i) n_j \, ds \tag{16}$$

where K_{II} is the Mode II, stress intensity factor defined as the natural generalization to a notch of the Mode II factor for a crack, the σ_{ij}, u_i components now fulfil antisymmetry requirements instead of symmetry, i.e.

$$\sigma_{22} = 0 \qquad u_1 = 0 \quad \text{on } \partial R \text{ when } x_2 = 0 \tag{17}$$

and, in polar co-ordinates, the antisymmetric complementary fields are given by:

$$\begin{aligned}
\sigma_{rr}^* &= -K_{II}^* r^{-\lambda-1}[\beta'\sin(\lambda-1)\theta - (\lambda+3)\sin(\lambda+1)\theta] \\
\sigma_{\theta\theta}^* &= K_{II}^* r^{-\lambda-1}[\beta'\sin(\lambda-1)\theta - (\lambda-1)\sin(\lambda+1)\theta] \\
\sigma_{r\theta}^* &= K_{II}^* r^{-\lambda-1}[\beta'\cos(\lambda-1)\theta - (\lambda+1)\cos(\lambda+1)\theta] \\
u_r^* &= \frac{K_{II}^* r^{-\lambda}}{2\mu\lambda}[\beta'\sin(\lambda-1)\theta - (\lambda+\kappa)\sin(\lambda+1)\theta] \\
u_\theta^* &= -\frac{K_{II}^* r^{-\lambda}}{2\mu\lambda}[\beta'\cos(\lambda-1)\theta - (\lambda-\kappa)\cos(\lambda+1)\theta]
\end{aligned} \tag{18}$$

with

$$K_{II}^{*}=\frac{\sqrt{(8\pi)}\mu\lambda(\lambda\sin^2\alpha-\sin^2\lambda\alpha)}{(1+\kappa)(\sin 2\alpha-2\alpha\cos 2\lambda\alpha)} \qquad \beta'=\frac{\lambda^2-1}{\lambda\cos 2\alpha-\cos 2\lambda\alpha}$$

where λ is now the root of the antisymmetric eigenvalue equation, namely (9) with the minus sign changed to plus. Fifth, for problems entailing a mixture of Modes I and II, the fields need to be separated into their respective symmetric and antisymmetric parts in accordance with

$$u_i^{*}=[u_i(x_1,x_2)\mp(-)^i u_i(x_1,-x_2)]/2 \tag{19}$$

where u_i^{+} and the stresses derived from substituting u_i^{+} into (3) constitute the symmetric part, u_i^{-}, etc., the antisymmetric, then treated individually using (13) and (16), respectively. Sixth and last, extension to include the outstanding *out-of-plane* mode, Mode III, also proceeds routinely and results in

$$H_{III}=K_{III}=\int_{\Sigma}(\sigma_{3j}u_3^{*}-\sigma_{3j}^{*}u_3)\,ds_j \tag{20}$$

where K_{III} is the generalized, Mode III, stress intensity factor for a notch, the σ_{3j}, u_3 components are now the out-of-plane responses ($j=1,2$), and, in polar co-ordinates ($x_3=z$), the out-of-plane complementary fields are:

$$\sigma_{zr}^{*}=-\frac{\mu\pi}{2\alpha r}u_z^{*}=\frac{K_{III}^{*}}{\sqrt{(2\pi)}r^{1+\pi/2\alpha}}\sin\frac{\pi\theta}{2\alpha}$$
$$\sigma_{\theta z}^{*}=\frac{K_{III}^{*}}{\sqrt{(2\pi)}r^{1+\pi/2\alpha}}\cos\frac{\pi\theta}{2\alpha} \qquad K_{III}^{*}=\frac{\mu\pi^2}{2\alpha^2} \tag{21}$$

TEST PROBLEM

In this section a plane elastic notch problem having an exact solution is set up and analysed using a finite element approach and the H_1 integral. The results found enable the numerical path independence of the integral to be examined and its efficiency as a computational device assessed.

For simplicity we fix attention on a problem drawn from the restricted class formulated in the previous section. One means of setting up a problem within this class having an exact solution is to superimpose symmetric eigenfunctions for a notch on some region R, and we adopt this simple device here. In order to thoroughly evaluate the performance of the integral when used with the simplest of finite elements, the constant-stress triangle, we select for combination the first three eigenfunctions for the notch since these contain: the necessary singular stress field; a stress field which, while continuous, is not continuously differentiable and may therefore be regarded as just barely being a regular field for constant-stress elements; and, lastly, a stress field which is relatively smooth and is continuously differentiable.† More precisely, we consider a plate with a 90° re-entrant corner ($\alpha=3\pi/4$) and take R to be the trapezium within the upper half-plate (Figure 3) defined by

$$R=\{(x_1,x_2)|-x_2<x_1<a, 0<x_2<a\} \tag{22}$$

† By a 'regular' field with respect to a given element we mean one which does not impair the normal maximum convergence the element can enjoy; thus fields are regular for analysis using a constant-stress element if the stresses are continuous (see Reference 10, Section 2.2, for a full discussion of the regularity requirements for various finite elements).

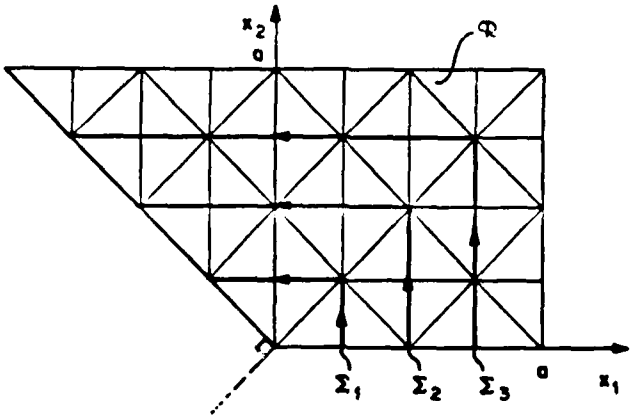

Figure 3. Geometry for the test problem, coarse grid and integration paths

On this region we are to place the first three symmetric eigenfunctions for the 90° notch, admissible in the sense of (7), and associated with the first three eigenvalues of (9) with $\alpha = 3\pi/4$ there and having Re $\lambda > 0$. The forms for superposition are therefore those of (15) with K_1^* therein being replaced by the constants K_1, C_2, C_3 and λ being exchanged for $-\lambda$ then set equal to the three corresponding eigenvalues, λ_1, λ_2, λ_3, provided the real parts of the expressions in (15) are taken in the event of a complex eigenvalue. In the interests of brevity we suppress details of these fields here and merely list the required eigenvalues determined numerically from (9):

$$\lambda_1 = 0{\cdot}544 \qquad \lambda_2 = 1{\cdot}629 + i\,0{\cdot}231 \qquad \lambda_3 = 2{\cdot}972 + i\,0{\cdot}374 \tag{23}$$

The corresponding eigenfunctions satisfy the two-dimensional field equations of elasticity (2), (3), the stress-free boundary conditions on the upper notch face (4), and the symmetry conditions ahead of the crack (5). In combining them we first adjust the participation of the λ_1-fields so that

$$K_1/\sigma^0\sqrt{(2\pi)}a^{1-\lambda_1} = 1 \tag{24}$$

Here K_1 is the generalized stress intensity factor defined in (8) and σ^0 equals σ_{11} for λ_1 at $x_1 = a$, $x_2 = 0$. Then, to complete our test problem, we add together all three eigenfunctions with the λ_2-, λ_3-fields having participation factors C_2, C_3 such that they share the same σ_{11} magnitude at $x_1 = a$, $x_2 = 0$ as the λ_1-field (namely σ^0) and take, as the boundary conditions on the remainder of ∂R ($x_1 = a, 0 < x_2 < a$; $-a < x_1 < a, x_2 = a$), the tractions that result there from their superposition. In this manner all three fields contribute to a comparable degree to the test problem.

The application of a constant-stress triangle, finite element code and the calculation of the H_1 integral for this test problem proceeds routinely. Since the issue of interest is the computational performance of the integral, we discretize R *uniformly* with a set of 45° isosceles triangles. To examine convergence we employ a sequence of three grids—a coarse, a medium and a fine—with the medium and fine grids being formed from the coarse by successively halving the element sides. The coarse grid has 48 elements and 35 nodes (Figure 3), the medium 192 elements and 117 nodes, and the fine 768 elements and 425 nodes. To examine path independence we use three contours $\Sigma_n (n = 1, 2, 3)$ which have nodes common to all three grids

(Figure 3) and along these contours use the mid-point rule to evaluate the integral in (13)—a quadrature rule of like accuracy to that of the finite element discretization. The results so found are presented in the first half of Table I.

Table I. Numerical values of the dimensionless stress intensity factor for the test problem (exact value 1)

Grid	Direct calculation using (13) on three integration paths			Calculation using regularizing procedure (25) on three paths		
	Σ_1	Σ_2	Σ_3	Σ_1	Σ_2	Σ_3
Coarse	1·044	0·843	0·883	0·979	0·975	0·978
Medium	0·913	0·939	0·940	0·992	0·994	0·994
Fine	0·972	0·973	0·972	0·998	0·998	0·999

Of course the problem at hand is *singular* and accordingly results from the foregoing direct treatment can be expected to be poor; needed is an approach which recognizes the singularity present and takes it into account if better results are to be realized. One procedure with this attribute is described by Sinclair and Mullan[7] and belongs to a class of *superposition methods* which, in essence, treat the singular part of any problem analytically with scant regard for boundary conditions remote from the singularity source, then use a simple numerical method to complete the satisfaction of the boundary conditions in what is now a regular problem. What basically distinguishes the procedure in Reference 7 from other superposition methods is the use of path independent integrals to balance the analytical and numerical contributions and it thus seems natural to apply it here. The end result so far as the stress intensity factor is concerned is (see Reference 7 for details of the surrounding argument)

$$K_1 \doteq \bar{H}_1/\bar{H}_1' \tag{25}$$

wherein $\bar{H}_1$ is the numerical estimate of H_1 for the problem of interest, $\bar{H}_1'$ the numerical estimate of H_1' for an associated singular problem formed by taking corresponding boundary conditions on ∂R as prescribed in effect by the singular eigenfunction alone with a participation factor of unity. What (25) says, in effect, is not that either $\bar{H}_1$ or $\bar{H}_1'$ represent accurate estimates of H_1 or H_1', respectively, but rather that they constitute roughly equally crude estimates with the errors cancelling in large part. Central to this cancellation is the use of an underlying method for calculating K_1 which has predictable errors due solely to the discretization—hence the need for the path independent integrals in (25).†

Application of (25) to the test problem is straightforward: the $\bar{H}_1$ values that have already been computed are simply divided by the numerical values of H_1 found on the *same* grid and path for the singular problem in which the boundary conditions on ∂R are established by the placing of the λ_1-fields alone on R with a dimensionless participation factor of unity, i.e. as in (24). The results so found are presented in the second half of Table I

The numbers in Table I illustrate the degree to which the H_1 integral is *numerically path independent*. The variation between the different paths is of the order of 20 per cent for the direct coarse analysis and converges to approximately 0·1 per cent for the fine grid; the variation between paths is yet smaller for the regularizing procedure (25) with the differences being actually less than 0·5 per cent for the coarse grid, 0·04 per cent for the fine. Moreover these

† See Reference 7 for a fuller discussion of the advantages of path independent integrals relative to methods such as local collocation in this regard.

results are the worst experienced in a number of numerical experiments since the *signs* of the participation factors here are such that errors accrue rather than compensate. Accordingly it would appear that the choice of integration path is not a major concern in applying the H_1 integral, especially when doing so in conjunction with the regularizing procedure. The numbers in Table I also indicate the sort of convergence to be expected with H_1 integral. To illustrate this more clearly we model the errors for each analysis with

$$e = e_0 h^c \tag{26}$$

where e is the absolute percentage error in the dimensionless stress intensity factor for a dimensionless grid size of h: e_0 is thus the error for unit grid size and reflects the initial *accuracy* of an analysis, while the constant c gauges its rate of *convergence*. We fit (26) to the medium and fine grid results in Table I since we expect that c is more likely to have converged to a constant itself for these grids. To check (26) as an error model we then use it to predict the errors for the coarse grid; with the exception of the direct calculation of H_1 on Σ_1 these predictions agree well with the actual errors supporting the use of (26). The results of applying it can be summarized by the average values determined. For the direct calculations,

$$e_0 = 13\,(\%) \qquad c = 1{\cdot}1 \tag{27}$$

For the regularizing procedure results,

$$e_0 = 3\,(\%) \qquad c = 2{\cdot}1 \tag{28}$$

Equations (27), (28) show that for this test problem the regularizing procedure not only leads to markedly better convergence as expected, but in addition is about a factor of four more accurate. Further, the regularizing procedure was observed to enjoy a similar superiority over direct computation in other test problems and the sort of relative improved performance demonstrated in (27), (28) is characteristic of that obtained in earlier applications of the procedure to crack problems (refer to Reference 7 wherein average values of e_0 and c are 42 per cent and 0·15 for a direct calculation using the J integral, in contrast to 8 per cent and 1·4 for the procedure). It would thus seem that the use of the path independent integrals developed here, together with a regularizing procedure as in (25), offers an attractive and efficient computational approach for singular elastic notch problems.

CONCLUDING REMARKS

The path independent integrals described furnish engineers with a useful tool for determining generalized stress intensity factors in elastic notch problems. This is especially so when used with a regularizing procedure such as that of Reference 7; then accurate results can readily be obtained using any standard, constant-stress, finite element code. Improved usage over that demonstrated here can be brought about by introducing mesh refinement with the grid gradation being tuned to the complete problem in the instance of a direct calculation, and to the residual regular problem when employing the procedure in Reference 7.

Extension of these integrals to treat problems involving loaded notch flanks is elementary via superposition when such loads are constant but otherwise awkward. Extension to composite configurations is possible at the expense of some algebra and is being undertaken at this time; extension to anisotropic notch problems is possible in principle but does require significant algebra. Extension to three-dimensional geometries in which the notch tip traces out a sufficiently smooth curve is also possible in the light of Aksentian's analysis[11] which shows the singular character in such instances to be that of the two-dimensional problem. However, for

geometries that are more significantly three-dimensional, such as the intersection of a notch with a free surface, the integrals given here would not be appropriate and the development of suitable new integrals would appear to represent a considerable analytical task.

ACKNOWLEDGEMENTS

We are most grateful to one of the reviewers of this paper for some very constructive criticism and, in particular, for drawing our attention to the work of Stern and Soni,[6] thereby leading to more elegant and computationally efficient forms for the H_I and H_{II} integrals. We also appreciate being given access to the code PLANDJ, originally written by J. L. Swedlow of the Department of Mechanical Engineering, Carnegie-Mellon University, and the financial support of the Center for the Joining of Materials at CMU under a grant from the National Science Foundation.

REFERENCES

1. J. H. A. Brahtz, 'Stress distribution in a reentrant corner', *Trans. A.S.M.E. (J. Appl. Mech.)*, **55**, 31–37 (1933).
2. M. L. Williams, 'Stress singularities resulting from various boundary conditions in angular corners of plates in extension', *J. Appl. Mech.* **19**, 526–528 (1952).
3. J. D. Eshelby, 'The force on an elastic singularity', *Phil Trans Royal Soc. (Lond.)*, **A244**, 87–112 (1951).
4. J. L. Sanders, 'On the Griffith–Irwin fracture theory', *J. Appl. Mech.* **27**, 352–353 (1960).
5. L. B. Freund, 'Stress intensity factor calculations based on a conservation integral', *Int. J. Solids Struct.* **14**, 241–250 (1978).
6. M. Stern and M. L. Soni, 'On the computation of stress intensities at fixed-free corners', *Int. J. Solids Struct.* **12**, 331–337 (1976).
7. G. B. Sinclair and D. Mullan, 'A simple yet accurate finite element procedure for computing stress intensity factors', *Int. j. numer. methods eng.* **18**, 1587–1600 (1982).
8. R. D. Gregory, 'Green's functions, bi-linear forms, and completeness of the eigenfunctions for the elastostatic strip and wedge', *J. Elasticity*, **9**, 283–309 (1979).
9. I. S. Sokolnikoff, *Mathematical Theory of Elasticity*, 2nd edn, McGraw-Hill, New York, 1956.
10. G. Strang and G. F. Fix, *An Analysis of the Finite Element Method*, Prentice-Hall, New Jersey, 1973.
11. O. K. Aksentian, 'Singularities of the stress–strain state of a plate in the neighborhood of an edge', *J. Appl. Math. Mech. (P.M.M.)*, **31**, 193–202 (1967).

International Journal of Fracture 27 (1985) R81–R85.

A REMARK ON THE DETERMINATION OF MODE I AND MODE II STRESS INTENSITY FACTORS FOR SHARP RE-ENTRANT CORNERS

G.B. Sinclair
Department of Mechanical Engineering, Carnegie-Mellon University
Pittsburgh, Pennsylvania 15213 USA
tel: (412) 578-2504

The independent development in Carpenter [1] and Sinclair, Okajima, and Griffin [2] of path independent integrals for the stress intensity factors at sharp re-entrant corners provides fracture mechanics with a useful analytical tool. Prompted by Carpenter's recent sequel [3] to [1], in which he extends his earlier work so as to be able to individually determine mode I and II factors, the purpose of this note is to point out that such a capability is already available in the integrals of [2]. This attribute may well be obscured in [2] by the overstatement there that mixed mode problems "need" to be split into their symmetric and antisymmetric parts prior to applying the corresponding path independent integral. While this is certainly one approach for distinguishing between mode I and mode II, it is by no means necessary. Simply applying the integral for mode I in [2] to a mixed problem yields the mode I intensity and vice versa. This is basically because the complementary fields in the mode I integral are symmetric so that when they are multiplied by any antisymmetric fields, including the singular mode II field, then integrated, no contribution results. The converse holds true for the mode II integral. In detail the argument is as follows.

Consider an elastic plate with a re-entrant corner, or sharp notch, which has stress-free flanks (Fig. 1). Let x_1, x_2 be rectangular cartesian coordinates aligned such that the negative x_1-axis bisects the opening angle at the corner into two angles of magnitude $\pi - \alpha$. For this geometry we can define the respective stress intensity factors for mode I, mode II by

$$K_I = \lim_{x_1 \to 0^+} \sqrt{(2\pi)}\, x_1^{1-\lambda^+}\, \sigma_{22}, \quad K_{II} = \lim_{x_1 \to 0^+} \sqrt{(2\pi)}\, x_1^{1-\lambda^-}\, \sigma_{22} \tag{1}$$

on $x_2 = 0$. In (1), σ_{22} is the normal component in the x_2-direction of the stress field σ_{ij} $(i, j = 1, 2)$, while λ^+, λ^- are the singular eigenvalues stemming from their corresponding eigenequations,

$$\sin 2\lambda^+\alpha = -\lambda^+ \sin 2\alpha, \quad \sin 2\lambda^-\alpha = \lambda^- \sin 2\alpha \tag{2}$$

with $0 < \lambda^+, \lambda^- < 1$. The elastic fields associated with λ^+ and λ^- are, respectively, symmetric and antisymmetric about the x_1-axis. That is, if $\overset{+}{\sigma}_{ij}$, $\overset{+}{u}_i$ are the stress and displacement components for λ^+ with σ_{ij}, u_i being those for λ^-,

$$\sigma_{ij}^{+}(x_1, -x_2) = (-)^{i+j}\sigma_{ij}^{+}(x_1, x_2),\ u_i^{+}(x_1,-x_2) = -(-)^{i}\, u_i^{+}(x_1, x_2) \quad (3)$$

and

$$\sigma_{ij}^{-}(x_1, -x_2) = -(-)^{i+j}\, \sigma_{ij}^{-}(x_1, x_2),\ u_i^{-}(x_1, -x_2) = (-)^{i}\, u_i^{-}(x_1, x_2) \quad (4)$$

Now from [2] we have, as our path independent integrals for determining the stress intensity factors for these singular fields,

$$H_I = \int_\Sigma (\sigma_{ij}\, u_i^{*} - \sigma_{ij}^{*}\, u_j)n_j ds \quad (5)$$

and

$$H_{II} = \int_\Sigma (\sigma_{ij}\, u_i^{**} - \sigma_{ij}^{**}\, u_j)n_j ds \quad (6)$$

Here, Σ is any contour within the plate commencing on the lower notch flank and terminating on the upper; n_j are components of the unit outward normal to Σ and ds is an infinitesimal element of its length; the integration is to be performed in a counterclockwise sense; and σ_{ij}^{*}, u_i^{*} are the stresses and displacements of the symmetric complementary singular eigenfunction, σ_{ij}^{**}, u_i^{**} those of the antisymmetric (see Appendix for details). The participation factors of these last are adjusted in [2] so that they pick off the corresponding stress intensity factor, i.e.,

$$H_I = K_I,\ H_{II} = K_{II} \quad (7)$$

Turning to their application in mixed mode problems which have both symmetric and antisymmetric singular fields present, we first focus on the use of H_I established for any problem's elastic fields in [2], the general contour Σ can be exchanged for the here more convenient path Γ (Fig. 1). Applying H_I of (5) on Γ, then changing variables so that segments in the lower half-plane ($x_2 < 0$) are expressed in terms of those in the upper, we have

$$H_I = \int_0^{\bar{x}_2} [(\sigma_{i1}(\bar{x}_1, x_2)u_i^{*}(\bar{x}_1, x_2) + \sigma_{i1}(\bar{x}_1, -x_2)u_i^{*}(\bar{x}_1, -x_2)) - (\sigma_{i1}^{*}(\bar{x}_1, x_2)u_i(\bar{x}_1, x_2) + \sigma_{i1}^{*}(\bar{x}_1, -x_2)u_i(\bar{x}_1, -x_2))]dx_2 \quad (8)$$

*Although the lower case subscripts only range over the integers (1, 2) the usual summation convention for repeated subscripts still applies over this reduced range.

$$+ \int_{\bar{x}_1}^{-\bar{x}_1} [(\sigma_{i2}(x_1, \bar{x}_2)u_i^*(x_1, \bar{x}_2) - \sigma_{i2}(x_1, -\bar{x}_2)u_i^*(x_1, -\bar{x}_2))$$

$$- (\sigma_{i2}^*(x_1, \bar{x}_2)u_i(x_1, \bar{x}_2) - \sigma_{i2}^*(x_1, -\bar{x}_2)u_i(x_1 - \bar{x}_2))]dx_1.$$

Now introducing into (8) the antisymmetry relations satisfied by the antisymmetric parts of σ_{ij}, u_i, namely the equivalent of (4), in conjunction with the symmetry relations satisfied by the symmetric complementary singular eigenfunctions σ_{ij}^*, u_i^*, viz., the equivalent of (3), we see that all the combinations in parentheses () cancel. It follows that the only nontrivial contributions to H_I must come from the symmetric parts of σ_{ij}^*, u_i^*. Further, as proven in [2], only the singular part of these symmetric fields actually contributes, recovering the first of (7). Analogously, H_{II} may be shown to pick off only K_{II} in mixed mode problems.

Thus for general problems containing a mixture of symmetric and antisymmetric fields, in addition to the strategy of separating the given problem into its symmetric and antisymmetric constituents if it occupies a region geometrically symmetrical about the x_1-axis*, one can simply apply the H_I and H_{II} integrals directly on the path of choice to discern K_I and K_{II} respectively. Either technique provides reliable estimates of the stress intensity factors when implemented numerically, and either can be made quite computationally efficient when used together with a superposition procedure or regularizing approach such as [4].

REFERENCES

[1] W.C. Carpenter, *International Journal of Fracture* 24 (1984) 45-58.

[2] G.B. Sinclair, M. Okajima, and J.H. Griffin, *International Journal for Numerical Methods in Engineering* 20 (1984) 999-1008.

[3] W.C. Carpenter, *International Journal of Fracture* 26 (1984) 201-214.

[4] G.B. Sinclair and D. Mullan, *International Journal for Numerical Methods in Engineering* 18 (1982) 1587-1600.

21 January 1985

APPENDIX

Here for completeness we furnish details of the complementary singular eigenfunctions required in the definitions of H_I and H_{II} in (5), (6). These fields are most readily expressed in cylindrical polar coordinates r, θ (Fig. 1). For the H_I integral we then have

$$\sigma_{rr}^* = -K^* r^{-\lambda-1}[(\lambda + 3)\cos(\lambda + 1)\theta - \beta \cos(\lambda - 1)\theta]$$

$$\sigma_{\theta\theta}^* = K^* r^{-\lambda-1}[(\lambda - 1)\cos(\lambda + 1)\theta - \beta \cos(\lambda - 1)\theta]$$

$$\sigma_{r\theta}^* = -K^* r^{-\lambda-1}[(\lambda + 1)\sin(\lambda + 1)\theta - \beta \sin(\lambda - 1)\theta]$$

*Such a strategy offers computational savings with finite element analysis of about a factor of four in terms of operational counts and around a factor of two in storage requirements. See [2], Eqn. (10) et seq. for specifics of the decomposition.

$$u_r^* = \frac{K^* r^{-\lambda}}{2\mu\lambda}\,[(\lambda + \kappa)\cos(\lambda + 1)\theta - \beta\cos(\lambda - 1)\theta]$$

$$u_\theta^* = \frac{K^* r^{-\lambda}}{2\mu\lambda}\,[(\lambda - \kappa)\sin(\lambda + 1)\theta - \beta\sin(\lambda - 1)\theta]$$

$$K^* = \frac{\sqrt{(8\pi)\mu\lambda(\lambda\sin^2\alpha + \sin^2\lambda\alpha)}}{(1 + \kappa)(\sin 2\alpha + 2\alpha\cos 2\lambda\alpha)}$$

in which

$$\lambda = \lambda^+,\ \beta = \frac{\lambda^2 - 1}{\lambda\cos 2\alpha + \cos 2\lambda\alpha}$$

and wherein μ is the shear modulus, and $\kappa = 3 - 4\nu$ for plane strain and $(3 - \nu)/(1 + \nu)$ for plane stress, ν being Poisson's ratio. For the H_{II} integral we have

$$\sigma_{rr}^{**} = -K^{**} r^{-\lambda-1}[\beta\sin(\lambda - 1)\theta - (\lambda + 3)\sin(\lambda + 1)\theta]$$

$$\sigma_{\theta\theta}^{**} = K^{**} r^{-\lambda-1}[\beta\sin(\lambda - 1)\theta - (\lambda - 1)\sin(\lambda + 1)\theta]$$

$$\sigma_{r\theta}^{**} = K^{**} r^{-\lambda-1}[\beta\cos(\lambda - 1)\theta - (\lambda + 1)\cos(\lambda + 1)\theta]$$

$$u_r^{**} = \frac{K^{**} r^{-\lambda}}{2\mu\lambda}\,[\beta\sin(\lambda - 1)\theta - (\lambda + \kappa)\sin(\lambda + 1)\theta]$$

$$u_\theta^* = -\frac{K^{**} r^{-\lambda}}{2\mu\lambda}\,[\beta\cos(\lambda - 1)\theta - (\lambda - \kappa)\cos(\lambda + 1)\theta]$$

$$K^{**} = \frac{\sqrt{(8\pi)\mu\lambda(\lambda\sin^2\alpha - \sin^2\lambda\alpha)}}{(1 + \kappa)(\sin 2\alpha - 2\alpha\cos 2\lambda\alpha)}$$

in which now

$$\lambda = \lambda^-,\ \beta = \frac{\lambda^2 - 1}{\lambda\cos 2\alpha - \cos 2\lambda\alpha}$$

Like fields for the mode III integral H_{III} ($=K_{III}$) can be found in [2].

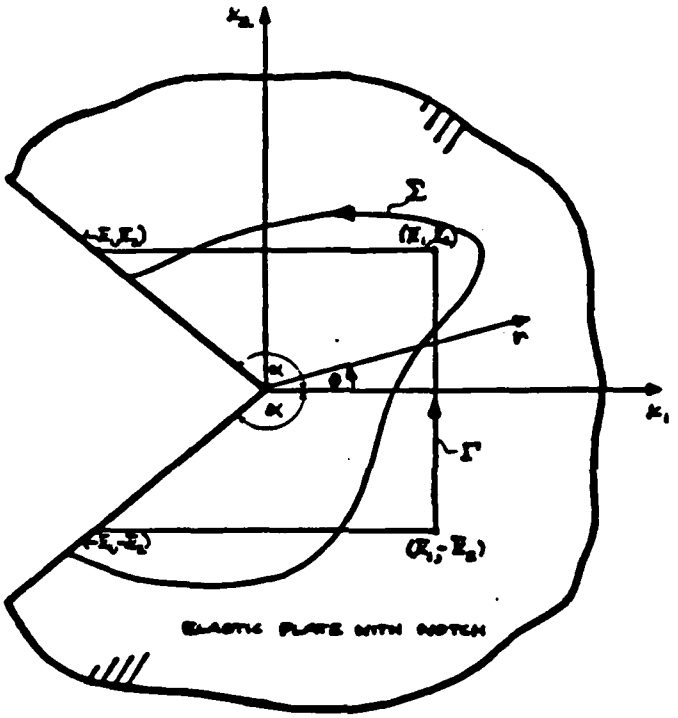

Figure 1. Geometry, coordinates, and integration paths

International Journal of Fracture 29 (1985) R17

CORRIGENDUM

Correction: "A Remark on the Determination of Mode I and Mode II Stress Intensity Factors for Sharp Re-Entrant Corners," G.B. Sinclair, *International Journal of Fracture* 27 (1985) R81-R85.

Equations (5) and (6) on pg R82 should read:

$$H_I = \int_\Sigma (\sigma_{ij}\, u_i^* - \sigma_{ij}^*\, u_i) n_j ds \tag{5}$$

$$H_{II} = \int_\Sigma (\sigma_{ij}\, u_i^{**} - \sigma_{ij}^{**}\, u_i) n_j ds \tag{6}$$

The paragraph following Eqn. (7) on pg R82 should read:
Turning to their application in mixed mode problems which have both symmetric and antisymmetric singular fields present, we first focus on the use of H_I to determine K_I in such cases. In view of the path independence of H_I established for any problem's elastic fields in [2], the general contour Σ can be exchanged for the here more convenient path Γ (Fig. 1)....

Equation (8) is split and occurs on the bottom of pg R82 and the top of pg R83. The arguments for the last displacement field occurring on pg R83 should read:

$$u_i(x_1, -\bar{x}_2)$$

We regret any inconvenience created for our readers by these typographical errors - Ed.

12 July 1985

APPENDIX 3: SOME INHERENTLY UNRELIABLE PRACTICES IN PRESENT DAY FRACTURE MECHANICS / FURTHER EXAMPLES OF THE UNRELIABILITY OF STRESS INTENSITY ESTIMATES FOUND VIA LOCAL FITTING

International Journal of Fracture 28 (1985) 3–16.

Some inherently unreliable practices in present day fracture mechanics

G.B. SINCLAIR

Department of Mechanical Engineering, Carnegie-Mellon University, Pittsburgh, PA 15213, USA

(Received July 30, 1984; in revised form December 7, 1984)

Abstract

A number of current practices in fracture mechanics which use quantities near a crack tip to make conclusions about response at the crack tip itself are examined. Specifically these include: stress and displacement matching to estimate stress intensity factors, monitoring local stress and strain values to predict fracture, and both crack opening angle and crack opening displacement as fracture criteria. By means of a pair of counter applications, all of these procedures are demonstrated to have the potential of leading to completely incorrect conclusions. An understanding of what causes this inadequate performance then indicates that such procedures may be unreliable in general and prompts suggestions as to alternatives.

1. Introduction

In fracture mechanics today there are a number of procedures which in essence draw on field quantities in the vicinity of a crack tip to infer what is happening right at the crack tip. This paper considers two classes of such procedures: local fitting methods for determining stress intensity factors, and local fracture criteria for predicting fracture. The intent is to examine the reliability of these approaches.

Local fitting methods for calculating stress intensity factors at cracks arose out of a need to extract this parameter from numerical analyses, particularly finite element analyses. One of the first discussions as to how best to undertake such exercises is that of Chan et al. [1], though certainly the approach was in use prior to [1] even if somewhat informally. Moreover the approach, together with spin offs such as the nodal force technique of Raju and Newman [2], continues to be used today in conjunction with both finite element and numerical integral equations analyses, as is evident in several papers in recent conferences [3,4]. All of these methods entail matching near but not at the crack tip to estimate the stress intensity factor there; the question considered here is how reliably can the attendant extrapolations be carried out.

Local fracture criteria attempt to predict fracture by checking some quantity in the vicinity of the crack tip. Among the more natural choices of quantity to this end are measures reflecting stresses and strains at the crack tip. Stresses are usually used in elastic analyses and typically in complex configurations (e.g. for failure in composites as in Chamis [5], and for biomedical applications as in Valliappan et al. [6]). * Strains are

* There do exist, though, examples of the direct use of local stresses in elastoplastic treatments, see for instance Miller et al. [7].

normally preferred when significant plastic flow accompanies fracture (e.g. Newman [8], Belie and Reddy [9], Kim and Hsu [10]). Other quantities employed in this role are the crack opening displacement of Wells [11] and the crack opening angle of Andersson [12], the former having gained sufficient acceptance to merit a British Standard [13] to govern its measurement. * All of these criteria involve comparisons made away from the crack tip with a view to gauging what is happening there; the issue of concern here is the certainty with which such comparisons are connected to fracture at the crack tip.

We begin our assessment in Section 2 by specifying the local fitting methods and local fracture criteria for testing/calibrating and thereafter using on simple elastic problems in Section 3. The conceptual applications in Section 3 in fact have known solutions, thereby furnishing demonstrations of local procedure performance. These sample evaluations in turn motivate a discussion of the more general use of local procedures and some suggestions as to alternatives in Section 4. The paper then ends with some concluding remarks.

2. Procedures examined

Here we first define a stress intensity factor and describe two local fitting procedures aimed at estimating it – one using stress, the other displacement. We then specify some local fracture criteria which are based on stress, strain, crack opening angle, and crack opening displacement.

To fix ideas consider a cracked elastic plate which is thick in the out-of-plane direction so that a state of plane strain obtains (Fig. 1). For the in-plane directions, we let (x, y) be rectangular cartesian coordinates having origin O at the crack tip and x-axis aligned with the crack. To further assist the development, we also let (r, θ) be cylindrical polar coordinates, sharing the same origin, and related to the rectangular coordinates by

$$x = r\cos\theta, \quad y = r\sin\theta, \tag{1}$$

for $0 \leqslant r < \infty$, $-\pi < \theta \leqslant \pi$. Next we assume the plate to be under symmetric loading having resultant force per unit thickness, P, acting transverse to the crack. Then the only stress intensity factor present is the mode I factor K_1, defined by

$$K_1 = \lim_{r\to 0} \sqrt{2\pi r}\,\sigma_\theta U(\sigma_\theta) \qquad \text{on} \quad \theta = 0, \tag{2}$$

where σ_θ is the elastic normal stress in the θ-direction and U is the unit step function, here taken as being one for positive arguments and zero otherwise.

We now wish to draw on local quantities to form estimates of the stress intensity factor, $\bar{K}_I$. One straightforward stress estimate is suggested by definition (2) itself and merely sets

$$\bar{K}_I = \sqrt{2\pi r_0}\,\bar{\sigma}_\theta|_{r=r_0} U\big(\bar{\sigma}_\theta|_{r=r_0}\big) \qquad \text{on} \quad \theta = 0, \tag{3}$$

wherein r_0 is some "small" distance from the crack tip and the bar atop σ_θ distinguishes it as being whatever value is found by the numerical solution technique adopted. An analogous displacement estimate is

$$\bar{K}_I = \frac{\mu}{1-\nu}\sqrt{\frac{\pi}{2r_0}}\,\big(-\bar{u}_\theta|_{r=r_0}\big)U\big(-\bar{u}_\theta|_{r=r_0}\big) \qquad \text{on} \quad \theta = \pi. \tag{4}$$

Here, μ is the shear modulus, ν Poisson's ratio, and $-\bar{u}_\theta$ on $\theta = \pi$ the numerically-de-

* Crack opening displacement was also independently introduced by Cottrell [14] to the effect a somewhat different objective, that of classifying brittle versus ductile fracture – see Burdekin [15] for a recent review of its role in fracture mechanics.

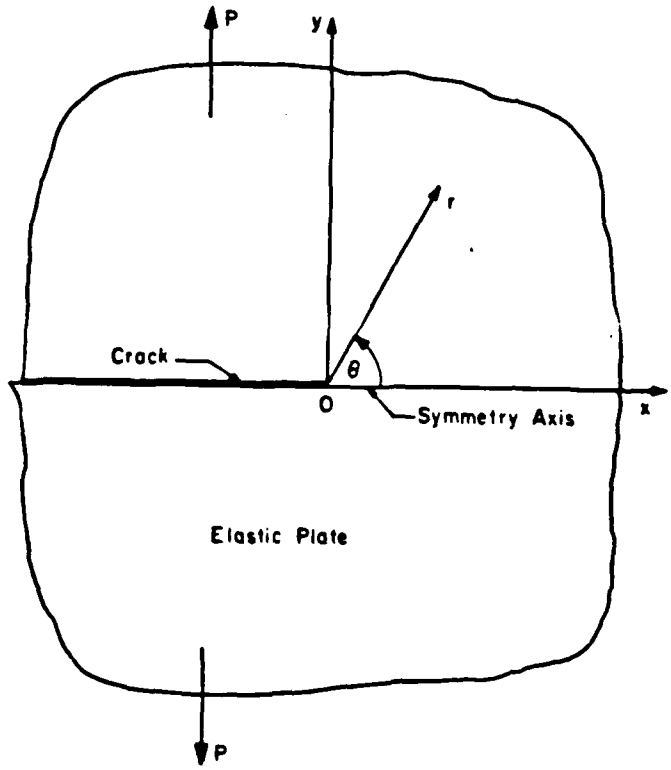

Figure 1. Mode I crack configuration and coordinates.

termined opening displacement of the upper crack flank. Again in (4), for simplicity, we select $r = r_0$ as our "small" distance, a policy we continue throughout the remainder of this discussion without loss of generality. The estimates in (3), (4) both fit the first singular eigenfunction for a symmetrically excited crack to the entire crack fields at a station supposedly close enough to ensure that these singular fields dominate. Thus while (3), (4) do not represent the most sophisticated of local fitting procedures for finding K_I, they do contain the essence of the rationalization for all such approaches. Consequently they are adequate for demonstration purposes here; subsequently we review other, more complex, local fitting methods.

We now turn to fracture criteria based on local quantities. For a stress criterion we choose perhaps the most obvious, namely that the tensile stress ahead of the crack, near but not at the crack tip, attain a critical value for fracture. That is,

$$\tilde{\sigma}_\theta|_{r=r_0} = \sigma_c \qquad \text{on} \quad \theta = 0, \tag{5}$$

for fracture, wherein $\sigma_c (> 0)$ is the critical stress determined on a suitable calibration problem. An analogous strain criterion exists. Instead, with a view to examining a greater variety of local fracture criteria, we consider the more involved condition of Newman [8]. In Newman [8], the crack-tip strain measure is assembled from a finite-element analysis. The result, denoted $\bar{\epsilon}_y$ here, is the average of the element strains in the y-direction, ϵ_{yy}, taken over all the elements connected to the node at the crack tip. Accordingly for fracture

we have (Fig. 2)

$$\bar{\epsilon}_c = \epsilon_c, \ \bar{\epsilon}_c = \sum_{i=1}^{3} \tfrac{1}{3}\epsilon_c\Big|_{\substack{r=r_i \\ \theta=\theta_i}} \tag{6}$$

where $\epsilon_c(>0)$ is a calibrated critical strain and $r_1 = r_2 = \sqrt{5}\, r_0/3$, $r_3 = \sqrt{2}\, r_0/3$, $\theta_1 = \cot^{-1}2$, $\theta_2 = \tan^{-1}2$, $\theta_3 = 3\pi/4$. The sample finite element grid of Fig. 2 also suffices for computing the crack opening angle, α, of Andersson [12], this being the angle subtended by the closest node to the crack tip. The associated fracture criterion has that, at fracture,

$$\alpha = \alpha_c, \quad \alpha = 2\tan^{-1}\left(-u_\theta|_{r=r_0}/r_0\right) \quad \text{on} \quad \theta = \pi, \tag{7}$$

with $\alpha_c(>0)$ being a calibrated critical angle. A similar evaluation of the crack opening displacement, δ, of Wells [11], leads to the fracture criterion that has, at fracture,

$$\delta = \delta_c, \quad \delta = -2u_\theta|_{r=r_0} \quad \text{on} \quad \theta = \pi, \tag{8}$$

$\delta_c(>0)$ being a calibrated critical displacement. Actually δ is usually evaluated as the crack opening displacement at $r = r_y = K_1^2/2\pi\sigma_y^2$, where σ_y is the uniaxial yield stress: here we take σ_y to be such that this station too coincides with $r = r_0$. Equation (8) completes our specification of the set of fracture procedures based on local quantities to be appraised next.

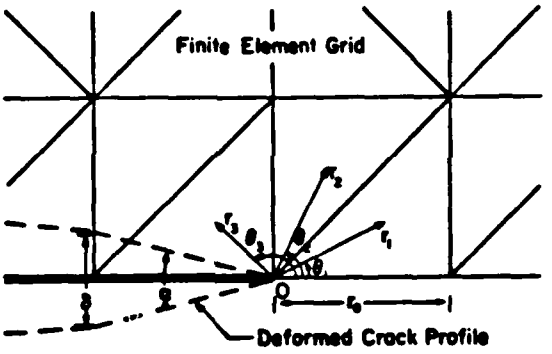

Figure 2. Finite element grid and other features near the crack tip.

3. Test/calibration problem: applications

In this section we start by formulating a test/calibration problem and a pair of problems to serve as "applications". Then we exhibit the closed form solutions to all three problems, employ the first of these to test the local fitting methods and calibrate the local fracture criteria, and thereafter use the last of the solutions to assess performance.

The problems to be treated are drawn from the class of symmetric, plane strain, crack problems outlined in the previous section. We do this conveniently by confining attention to the cracked circular plate of radius R (Fig. 3) and hence, by virtue of symmetry, need only to consider the semicircular region $\mathcal{R}$, defined by

$$\mathcal{R} = \{(r, \theta) | 0 < r < R, 0 < \theta < \pi\}. \tag{9}$$

Throughout this region we seek, in general, the stresses σ_r, σ_θ, $\tau_{r\theta}$ and displacements u_r, u_θ as suitably smooth functions of r, θ meeting the following requirements. All three problems are to satisfy: the plane-strain stress equations of equilibrium in the absence of

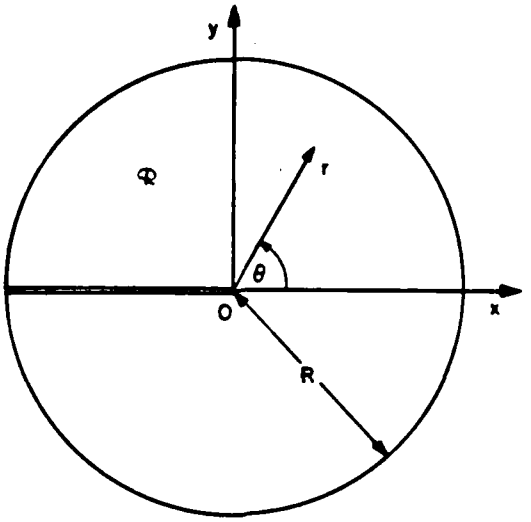

Figure 3. Cracked plate geometry for test problem and applications.

body forces, namely

$$r\sigma_{r,r} + \tau_{r\theta,\theta} + \sigma_r - \sigma_\theta = 0,$$
$$\sigma_{\theta,\theta} + r\tau_{r\theta,r} + 2\tau_{r\theta} = 0, \tag{10}$$

on $\mathscr{R}$, where subscripts preceeded by a comma denote differentiation with respect to that variable; the plane-strain stress-displacement relations for a linear elastic, homogeneous and isotropic, plate with shear modulus μ and Poisson's ratio $\nu = 1/4$, viz.,

$$\sigma_r = \mu\left[3u_{r,r} + r^{-1}(u_r + u_{\theta,\theta})\right],$$
$$\sigma_\theta = \mu\left[3r^{-1}(u_r + u_{\theta,\theta}) + u_{r,r}\right], \tag{11}$$
$$\tau_{r\theta} = \mu\left[u_{\theta,r} + r^{-1}(u_{r,\theta} - u_\theta)\right],$$

on $\mathscr{R}$; the stress-free crack flank conditions which set

$$\sigma_\theta = \tau_{r\theta} = 0 \quad \text{on} \quad \theta = \pi, \tag{12}$$

for $0 < r < R$; and the symmetry conditions ahead of the crack which have

$$u_\theta = 0, \quad \tau_{r\theta} = 0 \quad \text{on} \quad \theta = 0, \tag{13}$$

for $0 < r < R$. In addition each problem individually must comply with its applied stress conditions on the circular boundary. These set

$$\sigma_r = \frac{P}{kR} \sum_{n=0,1,\ldots} a_n \cos\frac{n\theta}{2} \quad \text{on} \quad r = R,$$
$$\tau_{r\theta} = \frac{P}{kR} \sum_{n=1,2,\ldots} b_n \sin\frac{n\theta}{2} \quad \text{on} \quad r = R, \tag{14}$$

for $0 < \theta < \pi (P > 0)$, where, for the test problem,

$$k = 8, \quad a_1 = 5, \quad a_3 = -1, \quad b_1 = b_3 = 1, \tag{15}$$

are the only $a_n \neq 0$, $b_n \neq 0$, and, for the two applications, all nontrivial constants are given in Table 1, wherein $\rho = R/r_0 (> 1)$.

While not strictly needed in the mathematical formulation of the foregoing type of elasticity problem, we adjoin the following regularity requirements on the displacements in

Table 1. Boundary condition constants for the applications

Constant	Application 1	Application 2
k	$8a_{11}(\rho-2+\sqrt{2})^2/63\rho^2$	$8(\rho^2-1)^2$
a_0, a_4	$-7.374.036\rho^{1/2}$	$-5.969.792\rho^{1/2}$
a_1	0	5
a_2, b_2	0	$15.690.918\rho^{3/2}$
a_3	$10(9-4\sqrt{2})\rho^2/49$	$-1-10\rho^2$
a_5	$2(10+\sqrt{2})\rho^3/7$	0
a_6, $-b_6$	0	$47.072.754\rho^{5/2}$
a_7	$3(a_3-a_{11}/7)$	$-3\rho^2(10+9\rho^2)$
a_8, $-b_8$	0	$10.008.616\rho^{5/2}$
a_9, b_9, $-b_9$	$-5a_5$	0
a_{11}, $-b_{11}$	$9(11+6\sqrt{2})\rho^4/7$	$63\rho^4$
b_1	0	1
b_3	$3a_3$	$1-30\rho^2$
b_4	$-a_0$	$-a_0+a_6/2$
b_7	$-3a_3+a_{11}$	$30\rho^2+a_{11}$

all three problems to emphasize their physical admissibility: that the displacements at the crack tip be bounded, that is

$$u_r = O(1), \quad u_\theta = O(1) \qquad \text{as} \quad r \to 0, \tag{16}$$

on $\mathscr{R}$, where O is the large order symbol; and that the crack opening displacement be nowhere negative, i.e.,

$$-u_\theta \geq 0 \qquad \text{on} \quad \theta = \pi, \tag{17}$$

for $0 < r < R$.

We postpone for the moment a discussion of how the test problem and two applications were arrived at together with their solutions and merely exhibit the latter at this point. For all three problems the complete solutions admit to representation by finite sums of eigenfunctions for the crack, viz.,

$$\begin{aligned}
\sigma_r &= \frac{P}{k\sqrt{rR}} \sum_{n=1,2,\ldots} c_n r^{(n-1)/2}\left[(6-n)\cos(n-2)\frac{\theta}{2} + (n+(-)^n 2)\cos(n+2)\frac{\theta}{2}\right],\\
\sigma_\theta &= \frac{P}{k\sqrt{rR}} \sum_{n=1,2,\ldots} c_n r^{(n-1)/2}\left[(n+2)\cos(n-2)\frac{\theta}{2} - (n+(-)^n 2)\cos(n+2)\frac{\theta}{2}\right],\\
\tau_{r\theta} &= \frac{P}{k\sqrt{rR}} \sum_{n=1,2,\ldots} c_n r^{(n-1)/2}\left[(n-2)\sin(n-2)\frac{\theta}{2} - (n+(-)^n 2)\sin(n+2)\frac{\theta}{2}\right],
\end{aligned} \tag{18}$$

$$\begin{aligned}
u_r &= \frac{P}{\mu k}\sqrt{\frac{r}{R}}\\
&\quad \times \sum_{n=1,2,\ldots} \frac{c_n}{n} r^{(n-1)/2}\left[(4-n)\cos(n-2)\frac{\theta}{2} + (n+(-)^n 2)\cos(n+2)\frac{\theta}{2}\right],\\
u_\theta &= \frac{P}{\mu k}\sqrt{\frac{r}{R}}\\
&\quad \times \sum_{n=1,2,\ldots} \frac{c_n}{n} r^{(n-1)/2}\left[(n+4)\sin(n-2)\frac{\theta}{2} - (n+(-)^n 2)\sin(n+2)\frac{\theta}{2}\right],
\end{aligned}$$

on $\mathscr{R}$. For each problem respectively, the solutions have k as previously ((15), Table 1)

Table 2. Coefficients in the solutions for the applications

Coefficient	Application 1	Application 2
c_1	0	1
$r_0^2 c_2$	$-1.843.509$	$-1.492.448$
$r_0^3 c_4$	0	7.845.459
$r_0^3 c_5$	$10(9-4\sqrt{2})/49$	-10
$r_0^4 c_6$	0	1.251.077
$r_0^4 c_7$	$-2(10+\sqrt{2})/7$	0
$r_0^4 c_9$	$9(11+6\sqrt{2})/49$	9

while the only nontrivial coefficients in the above are: for the test problem,

$$c_1 = 1; \tag{19}$$

and for the two applications, those $c_n \neq 0$ in Table 2.

The solutions in (18), (19), Table 2 may be verified directly. Substituting the forms in (18) into (10), (11) establishes that the field equations are complied with, and inspection of (18) shows that the crack flank and symmetry conditions (12), (13) are met. Evaluating σ_r, $\tau_{r\theta}$ of (18) on $r = R$, using (19), Table 2, further shows that the boundary conditions (14), (15), Table 1 are fulfilled. Finally, checking the displacements in (18) under (19) or Table 2 reveals that the regularity requirements (16), (17) are satisfied.

In applying the local fracture procedures to the three problems we begin by assuming that their numerical treatments have been refined to the extent that the exact answers are recovered to all intensive purposes, i.e. $\bar{\sigma}_\theta = \sigma_\theta$, etc. This is the ultimate of situations from an analysis point of view and allows us to focus on whatever errors are introduced by the procedures alone.

Invoking this assumption we next test our local fitting methods before applying them, a precaution commonly undertaken in practice. Using the local fits for the stress intensity factor in (3), (4) with $\nu = 1/4$ on (18) when (19) holds yields, for both methods,

$$\bar{K}_I = \frac{4P}{k}\sqrt{\frac{2\pi}{R}}\,. \tag{20}$$

For comparison, taking the defining limit of (2) in (18), (19) gives

$$K_I = \frac{4P}{k}\sqrt{\frac{2\pi}{R}}\,. \tag{21}$$

Hence the local fitting values of K_I are exact and the performance of the two methods (3), (4) on the test problem is perfect.

In order to calibrate our local fracture criteria we need to determine the load to fracture in our standardizing problem. We do this by regarding fracture as occurring when the stress intensity factor takes on a limiting value of K_c, the fracture toughness for the plate. It follows from (21) that the critical load in the calibration problem, P_c, is

$$P_c = \frac{kK_c}{4}\sqrt{\frac{R}{2\pi}}\,. \tag{22}$$

Thus increasing P to P_c and evaluting the stress in (5), the strain measure of (6) *, the

* For this derivation we note that straightforward manipulation leads to

$$\epsilon_y = \frac{P}{2\mu k\sqrt{rR}} \sum_{n=1,2,\ldots} c_n r^{(n-1)/2}\left[(2-n-(-)^n 2)\cos(n-2)\frac{\theta}{2} + (n-2)\cos(n-6)\frac{\theta}{2}\right]$$

as the normal strain in the y-direction to be calculated at the set of points in (6) et seq., and thereafter averaged to produce ϵ_y.

crack opening angle (COA) of (7), and the crack opening displacement (COD) of (8), using (18), (19) gives, respectively,

$$\begin{aligned}
&\bar{\sigma}_\theta|_{r=r_0} = \frac{4P_c}{k_1\sqrt{r_0 R}} = \frac{K_c}{\sqrt{2\pi r_0}} = \sigma_c \quad \text{on} \quad \theta = 0,\\
&\bar{\epsilon}_1 = \frac{4P_c k'}{k\mu_1\sqrt{r_0 R}} = \frac{K_c k'}{\mu_1\sqrt{2\pi r_0}} = \epsilon_c,\\
&\alpha = 2\tan^{-1}\frac{6P_c}{\mu k_1\sqrt{r_0 R}} = 2\tan^{-1}\frac{3K_c}{2\mu_1\sqrt{2\pi r_0}} = \alpha_c,\\
&\delta = \frac{12P_c}{\mu k}\sqrt{\frac{r_0}{R}} = \frac{3K_c}{\mu}\sqrt{\frac{r_0}{2\pi}} = \delta_c,
\end{aligned} \tag{23}$$

wherein ν has been set to $1/4$ and $k' = 0.303{,}299$.

With our local fitting methods tested and local fracture criterion calibrated we can apply them to the two applications. Introducing (18), together with the coefficients of Table 2, into (3), (4), (5), (6), (7) and (8) with $\nu = 1/4$ and when $P = P_c$ of (22), with k therein now taking on the respective values in Table 1, furnishes the results displayed in Table 3. As opposed to normal engineering practice, we can also determine the corresponding exact answers for the stress intensity factors in our "applications" from (2), (18) and Table 2, and thereby check the values of K_1 when $P = P_c$. These last results are also included in Table 3.

Table 3. Comparison of procedure outcomes with actual results

Activity	Application 1	Application 2
K_1 determination		
Stress fit	$K_1 = \frac{4P}{k}\sqrt{\frac{2\pi}{R}}$	$K_1 = 0$
Displacement fit	$K_1 = \frac{4P}{k}\sqrt{\frac{2\pi}{R}}$	$K_1 = 0$
Exact answer	$K_1 = 0$	$K_1 = \frac{4P}{k}\sqrt{\frac{2\pi}{R}}$
Fracture prediction		
Local stress	$\sigma_\theta\|_{r=r_0} = \sigma_c$	$\sigma_\theta\|_{r=r_0} = 0$
Local strain	$\epsilon_y = \epsilon_c$	$\epsilon_y = 0$
COA	$\alpha = \alpha_c$	$\alpha = 0$
COD	$\delta = \delta_c$	$\delta = 0$
Exact answer	$P = P_c \rightarrow K_1 = 0$	$P = P_c \rightarrow K_1 = K_c$

Several comments on the results in Table 3 are in order. For the first application, the stress intensity factor in reality is zero irrespective of load level P so that the stress right at the crack tip is also always zero and fracture there is not a possibility (at least not prior to fracture elsewhere): the local fitting procedures on the other hand estimate K_1 as being dependent on P and consequently, when this load is sufficiently large ($P = P_c$ in fact), all the local fracture criteria predict fracture at the crack tip. Hence the procedures considered give rise to conservative but gross errors in Application 1. For the second application, the stress intensity factor is not zero and increases linearly with load so that there is indeed a load level at which fracture occurs: the local fitting procedures in contrast give no K_1 whatsoever, independent of the value of P, and companion predictions of no fracture for any load. Hence the procedures give rise to nonconservative gross errors in Application 2. In all the results in Table 3 represent a clear demonstration of the potential

unrealiability of the fracture procedures of Section 2 - we look for means of controlling such unreliability next.

4. Some alternatives

Here we start by examining the nature of the breakdown of the two local fitting methods used to estimate K_1. In the light of this appraisal we review other local fitting methods and advance suggestions for improved methods of extracting stress intensity factors. Finally we discuss what remedial action can be taken for the local fracture criteria.

The reasons underlying the failure of the K_1 estimation via local fitting in the preceding section are as follows. First, the fit must be made away from the crack tip with $r_0 \neq 0$, since the stresses can be singular and thus not fittable at $r_0 = 0$ while the displacements are zero there leaving nothing to fit. Second and as a consequence, other eigenfunctions for the crack that are not being fitted can participate causing incorrect answers. Indeed this is the effect that the applications in Section 3 were constructed to produce. That is, symmetric eigenfunctions for the crack other than the singular one being fitted were added so as to generate the erroneous K_1 estimates of Table 3, then whatever stresses the combination so devised realized on the circular boundary were taken as the prescribed stresses there. *

At first glance it might appear a simple matter to design a local fitting method which does not succomb to such contrivances. Perhaps the simplest candidate stategy to this end is to move the point fitted closer to the crack tip; such an approach however fails if r_0 in the counter applications is then adjusted to coincide with the new point (which it can be). A more sophisticated possibility is the procedure in which $\sqrt{2\pi r}\,\sigma_\theta$ on $\theta = 0$ is plotted as a function of r, a straight line fitted to the data, then the line extrapolated to $r = 0$ to estimate K_1. This type of extrapolation technique in effect matches the first and third eigenfunctions for the crack and would appear to enjoy some popularity in present day practice. There are a number of ways in which the details of this and like extrapolation methods may be implemented with varying results, but typically such an approach does meet with more success on the given applications than that reported in Table 3. In fact, on knowing the answers, it is possible to adjust the technique to recover the correct results exactly. For such a fine tuned method though, it is then possible to devise a further new application on which it does not work by superimposing even more eigenfunctions. By way of illustration of this sort of more extensive counter application, consider Fig. 4. ** In Fig. 4, $\sqrt{2\pi r}\,\sigma_\theta/K$ on $\theta = 0$ is given as a function of r/R on a set of 17 points; here K is a nondimensionalizing, but otherwise arbitrary, constant. A least squares, straight line through these data points passes through the origin, yielding $\bar{K}_1 = 0$. In actuality, $K_1 = K$, illustrating the unrealiability of this approach. Further, gathering more data on $1/9 \leqslant r/R \leqslant 1$ and matching does not improve the incorrect estimate of K_1. Furthermore, similarly erroneous results can occur when using the displacement counterpart – indeed, there is a counter application which has exactly the same data as that depicted in Fig. 4 but with "$\sqrt{2\pi r}\,\sigma_\theta/K$ on $\theta = 0$" there exchanged for "$-\sqrt{\pi/2r}\;\mu u_\theta/K(1-\nu)$ on $\theta = \pi$", thus producing $\bar{K}_1 = 0$ despite the fact that $K_1 = K$. † And this is the situation that prevails in general. That is, irrespective of how apparently refined a local fitting method is and what it fits, once its specifics have been decided on it is then always possible to generate an example on which it proves to be comprehensively inadequate. The reason for this is that

* In this process the choice of $\nu = 1/4$ is simply made to facilitate the construction and not of any significance in itself.

** See Sinclair [16] for details of this example.

† See [16] for details of this second example and others.

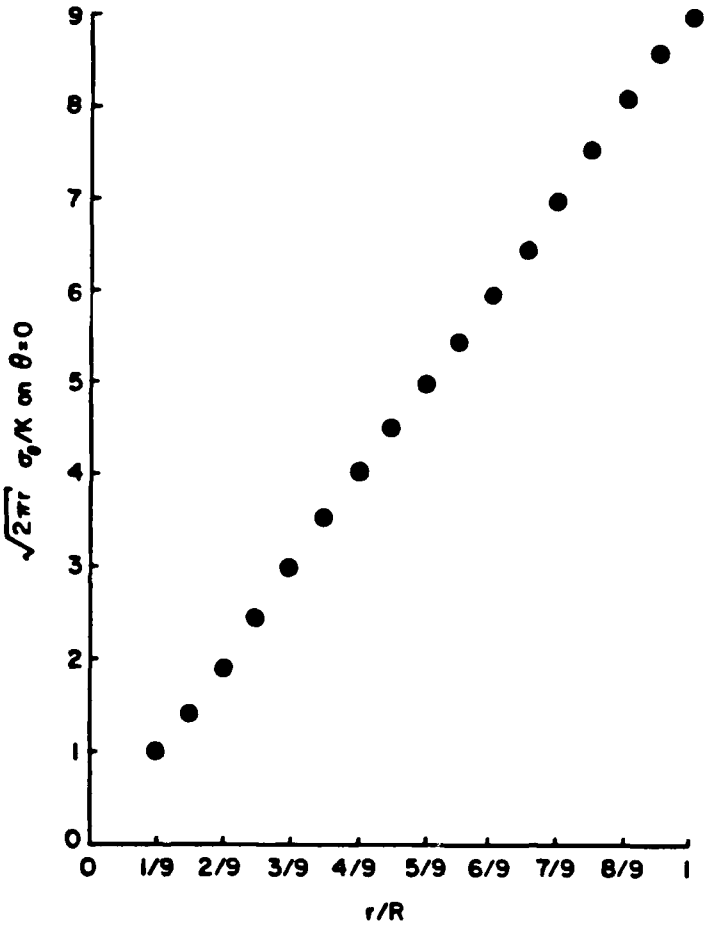

Figure 4. Product of stress ahead of the crack times the square-root of distance from the crack in a more extensive counter application.

any local fitting procedure must match a finite number of quantities on a finite set of points and thereby can only fit a finite number of eigenfunctions; thus any local fitting procedure leaves an infinity of eigenfunctions unfitted whose participation factors can be adjusted to ensure its downfall.

A key question that arises at this point therefore is who has the final say, the analyst making adjustments to his local fitting method so that it does produce good results or the rascal generating the problems on which the given method does not work. Unfortunately in practice the latter always has the option of going last. This is because in practice we must ultimately stop checking our procedure on test problems and apply it. Then, since applications are problems for which we do not know the answers, we cannot tell with certainty how well our procedure really works, and as a result we have to tolerate the possibility of it giving erroneous estimates, maybe even grossly erroneous estimates.

Logically one only needs the possibility of such results in an application to establish that a method is unreliable. In practice, however, one can perhaps rationalize still using the method if one can assign a sufficiently low probability to the occurrence of the disastrous example - the counter application being pathological to a degree. Certainly the

counter applications provided in Section 3 do not appeal as physical problems, being constructed more towards dramatically underscoring how much in error the selected local fitting methods and fracture criteria could be. Even so, the two particular counter applications are one of an infinity of pairs that could be devised to ensure that the methods in (3), (4) give the same completely incorrect estimates as in Table 3. Moreover there are other such sets of pairs that give rise to estimates that are more subtly in error than those of Table 3 but are nonetheless significantly inaccurate. And such is the case for any local fitting method, no matter how apparently refined - one can always construct an indefinitely large number of applications on which it fails. It therefore appears unlikely that the probability of encountering a problem application in engineering can safely be taken as being negligible.

More specifically in this regard, consider the following limited simulation of performance for the simple stress-fitting method of (3) on two problems that could reasonably be viewed as being of practical consequence. In accordance with normal practice, we begin our simulation by testing our method. As a test problem we take the classical Griffith geometry of a center-cracked infinite plate and consider the case when the crack is opened by a uniform far-field tension. Then we adjust r_0 so as to ensure acceptable results which here we take as being up to 5% in error. Picking $r_0 = a/14$, a being the semi-crack length, as a moderately close point at which to obtain accurate stress values by either numerical or experimental methods, we find on assuming negligible errors in the stress determination that

$$\bar{K}_1 = 1.05\, K_1, \tag{24}$$

wherein K_1 is the exact value. Equation (24) represents a satisfactory and encouraging result. Now as an "application" we take the Griffith crack opened by a uniform pressure. Applying (3) with $r_0 = a/14$ as before then yields

$$\bar{K}_1 = 0.67\, K_1. \tag{25}$$

Equation (25) represents an unsatisfactory nonconservative result, showing that the probability of meeting a problem application in practice for this simple method is not zero. *

Of course, as remarked earlier, it is possible to adapt ones local fitting method to overcome the difficulty experienced in this last elementary example. However, while increasing ones efforts considerably when applying local fitting procedures by performing the matching in a variety of ways at a number of locations does tend to increase the chances of detecting spurious results, it does not appear reasonable at this time to assume that any such combination of techniques reduces the probability of unacceptably incorrect results to a negligible level in all situations of practical interest. Continuing to use local fitting methods to determine stress intensity factors in engineering would thus seem to be unjustified and unwise. This is especially so since there are available quite different approaches which are free from the potential of furnishing useless results that local fitting methods have, and which can be implemented with no more effort.

One of the best of such alternative approaches employs path independent integrals, since the integral operators involved are essentially orthogonal to all of the eigenfunctions for the crack except the singular one. That is, contributions to these integrals from the nonsingular eigenfunctions can be shown to be zero analytically **, so that these terms are

* See Efus et al. [17] for further discussion of the effects of the presence of stresses which are independent of r, like the additional hydrostatic pressure here. See also Sinclair and Mullan [18] for a further example, concerning the standard configuration of a single edge notch under tension, wherein local fitting methods have been responsible for less than satisfactory results.

** See e.g., [19] pp. 1002, 1003 for a proof.

in essence eliminated rather than merely hoped-to-be-small as they are to varying degrees in local fitting methods. Two such integrals are the J integral of Eshelby [20], Rice [21] and Sanders' integral [22]; both of these enjoy physical interpretation as the energy release rate at the crack tip in the elastic instance. Other such integrals are those of Carpenter [23] and of Sinclair et al. [19]; these last lack the appeal of a direct physical interpretation but can be expected to perform somewhat better numerically since they involve the calculation of single terms rather than products. * In addition there are also methods, like that developed by Parks [24], which effectively employ a path independent integral and consequently realize similar performance.

Turning to fracture criteria based on local stresses and strains, we find the situation is not improved in terms of their likelihood of furnishing correct information. Again one can conceive of more complex criteria than the simple stress criterion and the average strain criterion specifically examined here; for example, the condition of Belie and Reddy [9] which checks the maximum strain in all the elements near the crack tip to decide if fracture occurs there. Again too one can construct counter applications on which such approaches fail; for example, Application 2 actually has $\epsilon_y = 0$ at each centroid of the elements sharing the crack-tip node (Fig. 2), so that Belie and Reddy's criterion applied to these elements would predict no fracture despite the fact that crack-tip fracture occurs in this application when the load is sufficiently large. Simply put, these methods cannot reliably infer what the physical stresses and strains are near the crack tip given an underlying theory which can lead to infinite stresses and strains at the crack tip in response to infinitesimal loads. Good alternatives here await the development of stress and strain fields for cracks whose physical relevance is unquestionable. In the meantime, the mathematically singular stress and strain fields, while not a physical reality, are a reality of analysis which must be faced, even in the elasto-plastic instance. ** At this point the accepted way of doing this, at least in the elastic situation, is by means of the associated energy release rate, whence the stress intensity factor. Accordingly local stress/strain fracture criteria must be interpreted as trying to estimate stress intensity factors, whether wittingly or otherwise. It follows that such practices are every bit as subject to the uncertainties of explicit estimation via local fitting methods discussed previously, and we recommend that alternatives, such as those suggested earlier, be used in their stead.

The last two local fracture criteria could both be regarded as using measures of the loaded crack profile and thereby avoiding the singular stresses and strains to some extent. Nonetheless their performance in the elastic regime is impaired by the same shortcoming that all of the preceding local procedures have, that of not being able to reliably assign what proportion of their totals are due to benign nonsingular eigenfunctions and accordingly what part is not. As a result they cannot reliably estimate the accepted governing parameter, the stress intensity factor. † Furthermore, being fits of a single parameter at a single point in effect, they cannot even be readily supplemented to reduce the chances of extraneous results. In the light of this inadequacy of both measures in treating elastic response it would not appear reasonable to entertain with any great confidence their use to treat fracture when significant plastic flow is present, the end to which they were originally proposed. Especially since, physically, elastic response must precede plastic irrespective of how much plastic flow ultimately accumulates. In the absence of a sure

* This has in reality been found to be the case in limited numerical experiments undertaken to date, refer [18,19].

** See, for example, Hutchinson [25] for an analysis demonstrating the persistence of singular behavior within the deformation theory of plasticity.

† In passing we observe that, in view of the uncertainty in the elastic situation of COD's relationship to K_I, hence to J, attempts to find a truly general simple relation between δ and J in elasto-plastic instances would seem to be futile.

connection to a physically reasoned explanation of fracture then, these measures remain inherently unreliable and others are to be preferred. The best of these at this time would seem to be the stress intensity factor itself and the J integral, both of which at least have the attribute of being clearly related to the energy release rate in the special case of pure elastic response.

5. Concluding remarks

Fracture mechanics today continues to be faced with the task of making physically sensible interpretations of the nonphysical singular fields which exist at crack tips, be the situation purely elastic or elasto-plastic. A prerequisite to success therefore is an accurate assessment of the degree to which these singular fields are present. The procedures considered here – local fitting methods to estimate stress intensity factors and local fracture criteria to predict fracture – fail to do this in a way which can be shown to be reliable.

The basic reasons for the potential unreliability of the local procedures are as follows. First, all the local procedures must consider quantities near but not at the crack tip. Second, at such stations fields other than the key singular ones can contribute. Third, the extent of such participation cannot be either completely controlled or fully accounted for. As a consequence, for any given local procedure there exist problems on which it produces unacceptably erroneous results.

The question then arises as to how likely is one to come upon such problem problems in practice: the answer unfortunately is not obvious. For local procedures based on a single parameter such as one point stress or displacement matching for K_1, a critical stress at a single station, COA, and COD, the likelihood would appear to be quite high. For local procedures employing a multiplicity of quantities such as some of the more extensive matching techniques to estimate stress intensity factors, the chances would seem to be reduced. However, for the best of these approaches in this regard, the probability of invalid results cannot be shown to be zero. Consequently in real applications wherein the answers are not known, one cannot be sure that such procedures do in fact find them. That is not to say that local procedures may not work on occasions, and even quite well; it is just to say we cannot be certain they do. Accordingly local procedures must be viewed as being unreliable at this time.

Acknowledgements

It is a pleasure to acknowledge the benefit of discussions of this work with J.H. Griffin and P.S. Steif of the Mechanical Engineering Department at Carnegie-Mellon University. The financial support of the Air Force Office of Scientific Research is also appreciated.

References

[1] S.K. Chan, I.S. Tuba and W.K. Wilson, *Engineering Fracture Mechanics* 2 (1970) 1–17.
[2] I.S. Raju and J.C. Newman Jr., *Engineering Fracture Mechanics* 11 (1979) 817–829.
[3] *Numerical Methods in Fracture Mechanics*, Proceedings of the Second International Conference (Swansea, Wales) Pineridge Press, U.K. (1980).
[4] *Fracture Mechanics: Fourteenth Symposium – Volume I: Theory and Analysis* (Los Angeles, California) ASTM Special Technical Publication 791, Philadelphia (1983).
[5] C.C. Chamis, *Failure Criteria for Filamentary Composites*, NASA Technical Note D-5367, National Aeronautics and Space Administration, Washington, D.C. (1969).
[6] S. Vallıappan, S. Kjellberg and N.L. Svensson, *Proceedings of the International Conference on Finite Elements in Biomechanics* (Tucson, Arizona) 2 (1980) 527–548.

[7] R.E. Miller Jr., B.F. Backman, H.B. Hansteen, C.M. Lewis, R.A. Samuel and S.R. Varanasi, *Computers and Structures* 7 (1977) 315–326.
[8] J.C. Newman Jr., in *Cyclic Stress-Strain and Plastic Deformation Aspects of Fatigue Crack Growth*, ASTM Special Technical Publication 637, Philadelphia (1977) 56–78.
[9] R.G. Belie and J.N. Reddy, *Computers and Structures* 11 (1980) 49–53.
[10] Y.J. Kim and T.R. Hsu, *International Journal of Fracture* 20 (1982) 17–32.
[11] A.A. Wells, in *Proceedings of the Crack Propagation Symposium* (Cranfield, England) 1 (1961) 210–230.
[12] H. Andersson, *Journal of the Mechanics and Physics of Solids* 21 (1973) 337–356.
[13] British Standards Institution, *Methods for Crack Opening Displacement (COD) Testing*, BS 5762 (1979).
[14] A.H. Cottrell, The Iron and Steel Institute, Special Report Number 69 (1961) 281–296.
[15] F.M. Burdekin, *Philosophical Transactions of the Royal Society* (London) A299 (1981) 155–167.
[16] G.B. Sinclair, "Further Examples of the Unreliability of Stress Intensity Estimates Found via Local Fitting", Report SM 84-13, Department of Mechanical Engineering, Carnegie-Mellon University, Pittsburgh (1984).
[17] J. Eftis, N. Subramonian and H. Liebowitz, *Engineering Fracture Mechanics* 9 (1977) 189–210.
[18] G.B. Sinclair and D. Mullan, *International Journal for Numerical Methods in Engineering* 18 (1982) 1587–1600.
[19] G.B. Sinclair, M. Okajima and J.H. Griffin, *International Journal for Numerical Methods in Engineering* 20 (1984) 999–1008.
[20] J.D. Eshelby, *Philosophical Transactions of the Royal Society* (London) A244 (1951) 87–112.
[21] J.R. Rice, *Journal of Applied Mechanics* 35 (1968) 379–386.
[22] J.L. Sanders Jr., *Journal of Applied Mechanics* 27 (1960) 352–353.
[23] W.C. Carpenter, *International Journal of Fracture* 24 (1984) 45–58.
[24] D.M. Parks, *International Journal of Fracture* 10 (1974) 487–502.
[25] J.W. Hutchinson, *Journal of the Mechanics and Physics of Solids* 16 (1968) 13–31.

Résumé

On examine diverses pratiques courantes en Mécanique de Rupture qui font usage de grandeurs paramétriques au voisinage de l'extrémité d'une fissure pour tirer des conclusions sur ce qui se passe à cette extrémité même. Ces grandeurs sont notamment: les valeurs de la contrainte et du déplacement correspondant à un facteur d'intensité de contrainte estimé, l'enregistrement des contraintes et déplacements locaux en vue de prédire la rupture, et l'angle et le déplacement d'ouverture d'une fissure en tant que critères de rupture.

En considérant une paire d'applications divergentes, on démontre que toutes ces procédures risquent d'entraîner des conclusions complètement incorrectes.

Une analyse des causes de ces inadéquations montre que ces procédures peuvent se révéler peu fiables en général, et conduit à des suggestions de procédures alternatives.

FURTHER EXAMPLES OF THE UNRELIABILITY OF STRESS INTENSITY ESTIMATES FOUND VIA LOCAL FITTING

G.B. SINCLAIR

SM 84-13

May 1984

Department of Mechanical Engineering

Carnegie Institute of Technology

Carnegie-Mellon University

Pittsburgh, Pennsylvania

FURTHER EXAMPLES OF THE UNRELIABILITY OF STRESS INTENSITY ESTIMATES FOUND VIA LOCAL FITTING

INTRODUCTION

The inherent unreliability of local fitting methods for determining stress intensity factors is established in [1, 2]. In [1, 2], examples of this shortcoming are limited to very simple fitting procedures, although the general nature of source of the difficulty is discussed: the intent in this brief supplementary report is to furnish the details of some more extensive demonstrations. We begin with a precise statement of four chosen problems, then exhibit their complete closed-form solutions*. Using these forms we next extract the exact values of the corresponding stress intensity factors and compare the results with those obtained by fitting stresses and displacements using several eigenfunctions. The report closes with a brief discussion of some of the implications of the examples regarding even more involved local fitting procedures.

FORMULATION OF PROBLEMS

The plane region of concern in all four problems is the cracked circular disk of radius $R = 9$ (Fig. 1). To describe this geometry, we take rectangular cartesian coordinates (x, y) with origin at the crack-tip and x-axis aligned with the crack face, together with cylindrical polar coordinates (r, θ) related to (x, y) by

$$x = r\cos\theta,\ y = r\sin\theta\ (0 \le r < \infty,\ -\pi < \theta \le \pi). \tag{1}$$

Since excitation is restricted to that which is symmetric about the x-axis, we can confine attention to the upper half of the disk, R, where

$$R = \{(r, \theta)\,|\ 0 \le r < R,\ 0 \le \theta < \pi\}. \tag{2}$$

We seek then, the stresses σ_r, σ_θ, $\tau_{r\theta}$, and displacements u_r, u_θ, as sufficiently smooth functions of r, θ throughout R, satisfying the following requirements. The *stress equations of equilibrium* in the absence of body forces,

---

*In the interests of brevity, no information as to how these particular problems were constructed is given: in this regard, see [1, 2] for the basic approach.

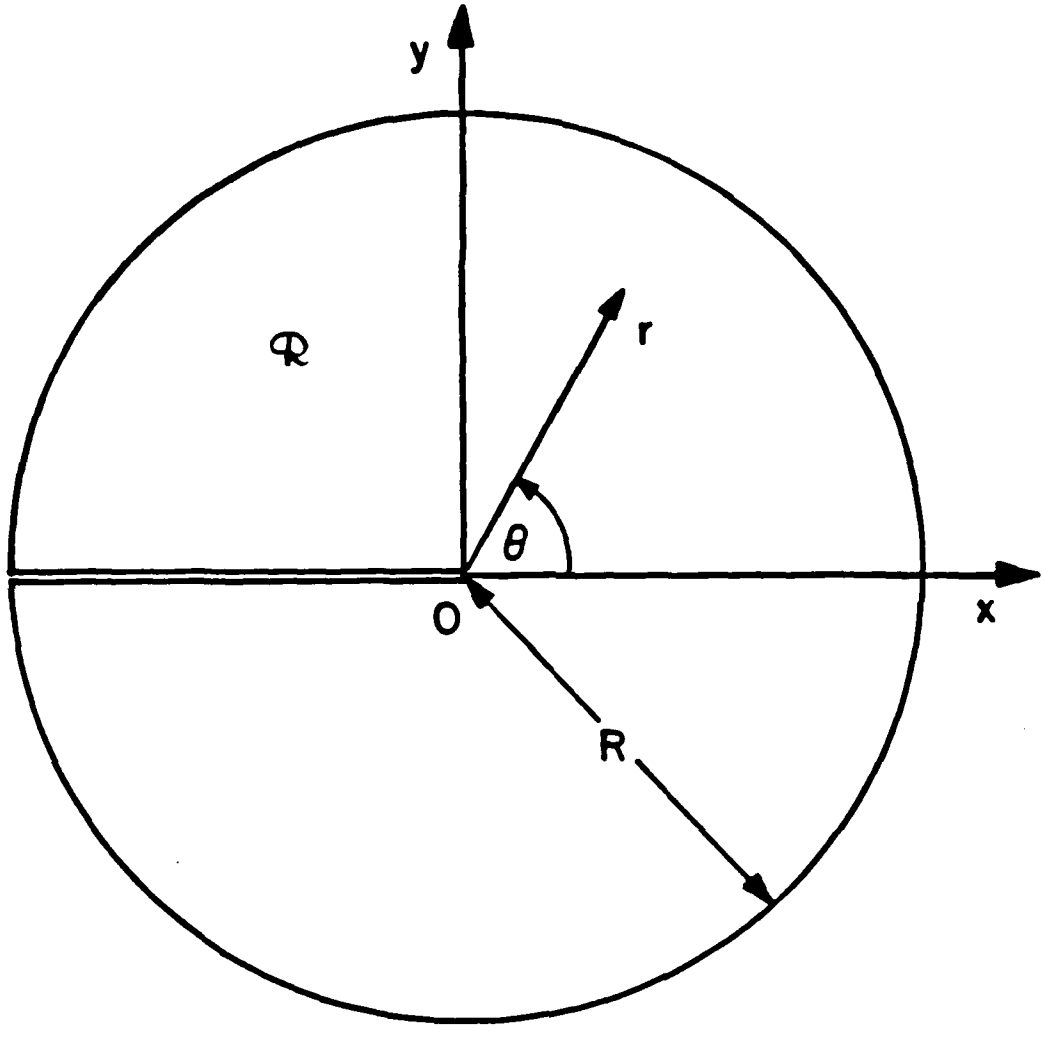

Figure 1. Cracked plate geometry and coordinates

$$\frac{\partial \sigma_r}{\partial r} + \frac{1}{r}\frac{\partial \tau_{r\theta}}{\partial \theta} + \frac{\sigma_r - \sigma_\theta}{r} = 0,$$

$$\frac{1}{r}\frac{\partial \sigma_\theta}{\partial \theta} + \frac{\partial \tau_{r\theta}}{\partial r} + \frac{2\tau_{r\theta}}{r} = 0, \tag{3}$$

on R. The *plain strain stress-displacement relations* for a homogeneous and isotropic, linear, elastic material with shear modulus μ and Poission's ratio ν,

$$\sigma_r = \frac{2\mu}{1-2\nu}\left[(1-\nu)\frac{\partial u_r}{\partial r} + \nu\left(\frac{1}{r}\frac{\partial u_\theta}{\partial \theta} + \frac{u_r}{r}\right)\right],$$

$$\sigma_\theta = \frac{2\mu}{1-2\nu}\left[(1-\nu)\left(\frac{1}{r}\frac{\partial u_\theta}{\partial \theta} + \frac{u_r}{r}\right) + \nu\frac{\partial u_r}{\partial r}\right], \tag{4}$$

$$\tau_{r\theta} = \mu\left(\frac{1}{r}\frac{\partial u_r}{\partial \theta} + \frac{\partial u_\theta}{\partial r} - \frac{u_\theta}{r}\right),$$

on R. The *stress-free crack-face conditions* and the *symmetry conditions* ahead of the crack,

$$\sigma_\theta = \tau_{r\theta} = 0 \text{ when } \theta = \pi,$$

$$u_\theta = 0,\ \tau_{r\theta} = 0 \text{ when } \theta = 0, \tag{5}$$

for $0<r<R$. The *stress boundary conditions* on the outer circular boundary which prescribe

$$\sigma_r = \frac{K}{a_0\sqrt{2\pi}}\sum_{n=1}^{8} a_n \cos\left(\frac{(2n-1)\theta}{2}\right) \text{ when } r = R,$$

$$\tau_{r\theta} = \frac{K}{b_0\sqrt{2\pi}}\sum_{n=1}^{8} b_n \sin\left(\frac{(2n-1)\theta}{2}\right) \text{ when } r = R, \tag{6}$$

for $0<\theta<\pi$, where K is a constant ($K>0$) and a_n, b_n ($n = 0, 1,\ldots 8$) are given in Table 1 for the respective problems (1-4). By way of illustration, Figs.2 display sketches of these stress distributions for Problem 1 (Figs. 2a and 2b share the same scale). And finally the *regularity requirements* which insist that the displacements be integrable at the crack tip and that there is no overlapping of the crack flanks.

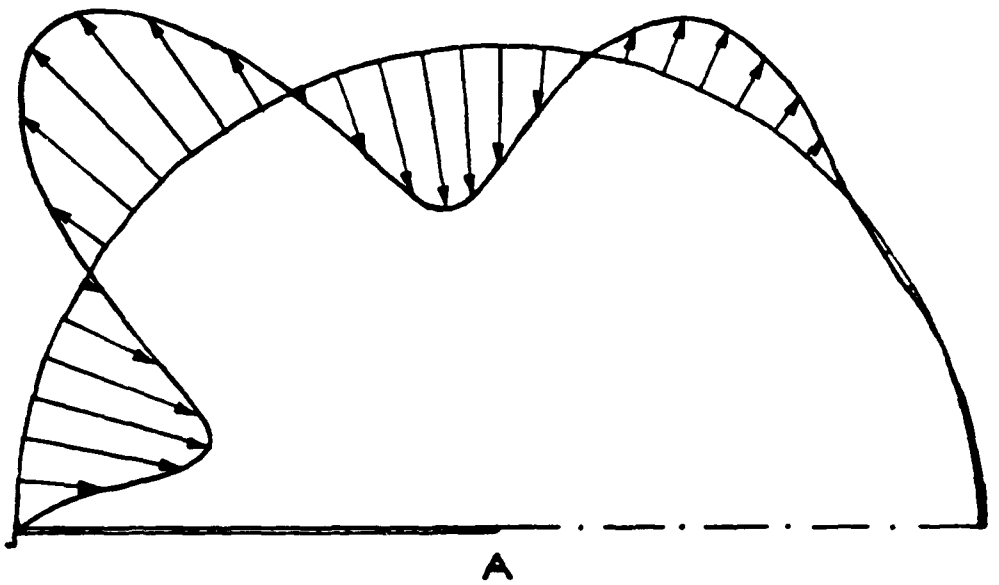

A

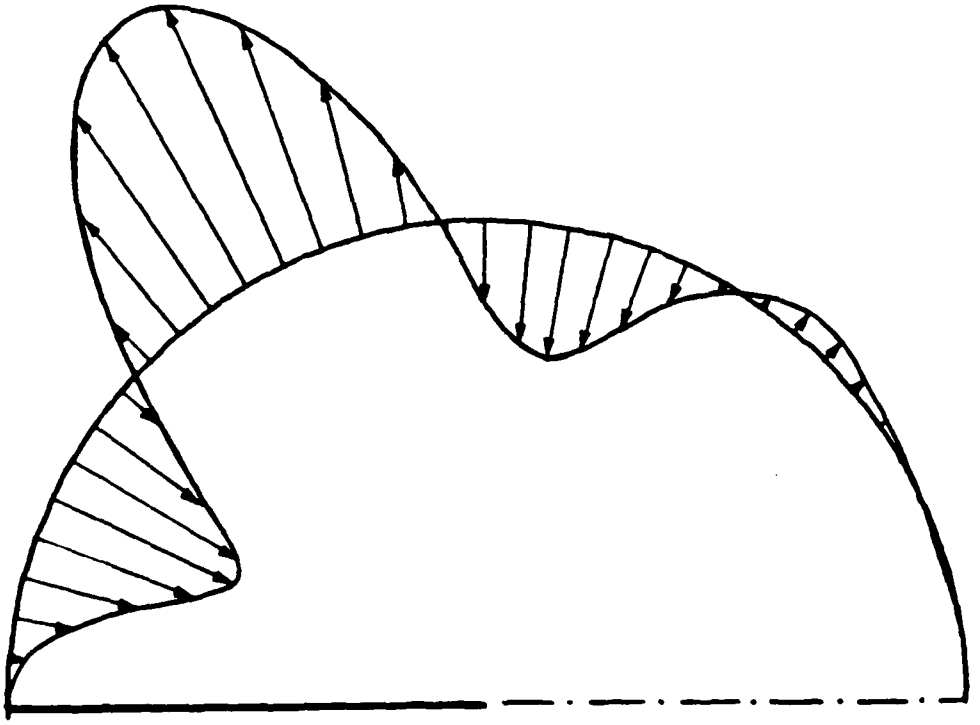

B

Figure 2. Applied stresses for Problem 1:
A - $\sigma_r \mid_{r=9} /K$, B - $\tau_{r\theta} \mid_{r=9} /K$

$$u_r = O(1),\ u_\theta = O(1) \text{ as } r \to 0, \tag{7}$$

for $0 \le \theta \le \pi$, and

$$u_\theta \le 0 \text{ when } \theta = \pi, \tag{8}$$

for $0 < r \le R$.

TABLE 1: BOUNDARY CONDITION CONSTANTS

Constant	Problem 1	Problem 2	Problem 3	Problem 4
$a_0 (= b_0)$	420	420	14,700	-420
a_1	-569	919	0	5067
a_2	2,815	14,215	217,219	14,250
a_3	5,962	-43,222	1,387,200	-41,781
a_4	-9,675	-121,275	-9,199,158	-121,275
a_5	-20,115	97,065	9,782,400	97,065
a_6	45,525	382,725	14,366,268	382,725
$a_7 (= -b_7)$	-19,683	216,513	-30,093,120	216,513
$a_8 (= -b_8)$	0	0	13,544,091	0
b_1	-213	779	0	1,689
b_2	8,585	42,785	651,657	42,750
b_3	-30,802	216,606	-6,936,000	215,661
b_4	33,975	339,975	22,333,578	339,975
b_5	11,367	-837	-23,157,120	-837
b_6	-42,525	-382,725	-9,441,144	-382,725

PROBLEM SOLUTIONS

For all four problems the *complete solutions* can be expressed as *finite sums of eigenfunctions* for the crack. Explicitly we have

$$\sigma_r = \frac{K}{\sqrt{2\pi r}} \sum_{n=0}^{6} \frac{c_n r^n}{c} \left[\left(\frac{5}{2} - n \right) \cos\left(n - \frac{1}{2}\right)\theta + \left(n - \frac{1}{2}\right) \cos\left(n + \frac{3}{2}\right)\theta \right],$$

$$\sigma_\theta = \frac{K}{\sqrt{2\pi r}} \sum_{n=0}^{6} \frac{c_n r^n}{c} \left[\left(n + \frac{3}{2}\right) \cos\left(n - \frac{1}{2}\right)\theta - \left(n - \frac{1}{2}\right) \cos\left(n + \frac{3}{2}\right)\theta \right],$$

$$\tau_{r\theta} = \frac{K}{\sqrt{2\pi r}} \sum_{n=0}^{6} \frac{c_n r^n}{c} \left(n - \frac{1}{2}\right) \left[\sin\left(n - \frac{1}{2}\right)\theta - \sin\left(n + \frac{3}{2}\right)\theta \right], \tag{9}$$

$$u_r = \frac{K}{\mu}\sqrt{\frac{r}{2\pi}}\sum_{n=0}^{6}\frac{c_n r^n}{c(2n+1)}\left[\left(\frac{5}{2} - n - 4\nu\right)\cos\left(n-\frac{1}{2}\right)\theta + \left(n-\frac{1}{2}\right)\cos\left(n+\frac{3}{2}\right)\theta\right],$$

$$u_\theta = \frac{K}{\mu}\sqrt{\frac{r}{2\pi}}\sum_{n=0}^{6}\frac{c_n r^n}{c(2n+1)}\left[\left(n+\frac{7}{2} - 4\nu\right)\sin\left(n-\frac{1}{2}\right)\theta - \left(n-\frac{1}{2}\right)\sin\left(n+\frac{3}{2}\right)\theta\right],$$

where c, c_n (n=0,1,....6) are constants having values for the respective problems as given in Table 2. That (9) and Table 2 constitute the solutions to the four problems posed earlier can be *verified directly*. That is, the forms in (9) for each n individually can be shown to satisfy the governing field equations (3), (4) by substitution and the crack-face and symmetry conditions (5) by inspection, while the combination realized on the boundary r=R=9 using the values in Table 2 can, after come manipualtion, be shown to comply with the prescribed stresses there (6), Table 1. In addition, inspection of (9) shows that the displacements are bounded ar r=0, i.e. (7) is satisfied, and combining the forms in (9) using Table 2 gives positive crack-opening displacements, viz., (8) is met.

TABLE 2: SOLUTION CONSTANTS

Constant	Problem 1	Problem 2	Problem 3	Problem 4
c	1,890	1,890	595,350	-1,890
c_0	945	945	0	0
$c^{-<1>}$	-744	2,232	0	5,067
c_2	950	4,750	651,657	4,750
c_3	-230	1,610	-462,400	1,610
c_4	25	225	121,615	225
c_5	-1	11	-13,760	11
c_6	0	0	563	0

STRESS INTENSITY FACTORS: EXACT AND ESTIMATED VALUES

Defining the Mode I *stress intensity factor*, K_I, by

$$K_I = \lim_{r\to 0}\sqrt{2\pi r}\,\sigma_\theta\big|_{\theta=0}, \tag{10}$$

on R, we have from (9),

$$K_I = K\left(\frac{2c_o}{c}\right). \tag{11}$$

Thus from Table 2 we obtain the exact values of K_I recorded in Table 3 for each of the problems.

As out *local stress-fitting method* we match the transverse stress, σ_θ, on the line of symmetry ahead of the crack ($\theta=0$) at the five radial stations r=1, 3, 4, 7, 9. To do this we take the five eigenfunctions for the crack given by (9) with n=0, 1, 3/2, 2, 5/2 therein[**]. Then, in view of definition (10), we must solve the 5x5 system of equations

$$\bar{K}_I + d_1 r + d_2 r^{3/2} + d_3 r^2 + d_4 r^{5/2} = \sqrt{2\pi r}\,\sigma_\theta\big|_{\theta=0}, \qquad r = 1, 3, 5, 7, 9, \tag{12}$$

where $\bar{K}_I$ is our stress-fitting estimate of the stress intensity factor and d_n (n=1-4) are estimated participation factors for the other eigenfuntions.

As our *local displacement-fitting method* we match the crack opening displacement, $-u_\theta$, on the crack flank ($\theta=\pi$) at the five radial stations r =1, 3, 5, 7, 9. To do this we take the five eigenfunctions for the crack given by (9) with n=0, 1, 2, 3, 4[***]. Then it follows from (10) and the forms in (9) for n=0 that we must treat the 5x5 system

$$\bar{K}_I' + d_1' r + d_2' r^2 + d_3' r^3 + d_4' r^4 = \frac{-\mu}{2(1-\nu)}\sqrt{\frac{2\pi}{r}}\,u_\theta\big|_{\theta=\pi}, \qquad r = 1, 3, 5, 7, 9, \tag{13}$$

where $\bar{K}_I'$ is our displacement-fitting estimate of K_I and d_n' (n = 1-4) are estimated participation factors for the other eigenfunctions.

[**]The eigenfunction associated with n=1/2 is not as given in (9) since $\sigma_\theta \neq 0$ on $\theta=\pi$ when n=1/2 in (9). The eigenfunction for this eigenvalue requires individual analysis and eventually simply reduces to σ_x equal to a constant as the only nonzero stress in the plane. As a result $\sigma_\theta=0$ on $\theta=0$ for this case so that in effect this eigenfuntion is also being matched by our stress-fitting procedure.

[***]Here the actual eigenfunction associated with n = 1/2 has $u_\theta=0$ on $\theta=\pi$ and so contributes nothing to a crack opening displacement fit (just as the corresponding stress does not affect a stress fit). Further, although (9) does give the correct eigenfunctions for n=3/2, 5/2, 7/2, 9/2, none of these terms add to u_θ on $\theta=\pi$. Hence in effect here we are fitting the first ten eigenfunctions.

We now apply our local stress fitting method to Problem 1. From Problem 1, from (9), Table 2, we have

$$\sqrt{2\pi r}\,\sigma_\theta\big|_{\theta=0} = K\sum_{n=0}^{6}\frac{2c_n}{c}r^n$$

$$= K[1 - \frac{248}{315}r + \frac{r^2}{189}(190 - 46r + 5r^2 + \frac{r^3}{5})]. \qquad (14)$$

Hence system (12) becomes

$$\begin{aligned}
\bar{K}_1 + d_1 + d_2 + d_3 + d_4 &= K,\\
\bar{K}_1 + 3d_1 + 3\sqrt{3}d_2 + 9d_3 + 9\sqrt{3}d_4 &= 3K,\\
\bar{K}_1 + 5d_1 + 5\sqrt{5}d_2 + 25d_3 + 25\sqrt{5}d_4 &= 5K, \qquad (15)\\
\bar{K}_1 + 7d_1 + 7\sqrt{7}d_2 + 49d_3 + 49\sqrt{7}d_4 &= 7K,\\
\bar{K}_1 + 9d_1 + 27d_2 + 81d_3 + 243d_4 &= 9K.
\end{aligned}$$

Solving (15) yields $\bar{K}_1 = 0$, $d_1 = K$, $d_2 = d_3 = d_4 = 0$; the first of these is the estimate entered in Table 3.

Similarly we apply our local displacement-fitting method to Problem 2, then our stress-fitting and displacement-fitting methods in turn to Problems 3 and 4. The resulting estimates are entered in Table 3.

TABLE 3: STRESS INTENSITY VALUES, K_I

Problem	Basis of local fitting method	Local fitting estimate of K_I	Actual exact value of K_I
1	Stress	0	K
2	Displacement	0	K
3	Stress	K	0
4	Displacement	K	0

Table 3 shows that it is possible to devise problems which ensure the *comprehensive failure* of the two local fitting methods put forward here.

Several comments are in order at this point. Clearly, *given knowledge of the exact solution* as here, it is possible to modify either of the two local fitting methods so that they do work. In practice, however, one does *not know* the answer in an actual application, so that one does not have the option of fixing up a local fitting approach but can only see if things "look right". In this connection, consider the plot $\sqrt{2\pi r}\,\sigma_\theta(\theta=0)$ for Problem 1, which as it happens coincides with $-\mu u_\theta(\theta = \pi)\sqrt{2\pi/r}\,/\,2(1-\nu)$ for Problem 2 (Fig. 3). Certainly here things "look right". Indeed one could even imagine obtaining results from a sequence of finite element grids at the points 3, 5, 7, 9, then at 2, 3, 4, 5, 6, 7, 8, 9, and ultimately at 3/2, 2, 5/2, 7/2, 4, 9/2, 5, 11/2, 6, 13/2, 7, 15/2, 8, 17/2, 9, and still concluding $K_I = 0$ when, in actuality, $K_I = K$. And it is possible to construct a problem which has both its stress fit and its displacement fit do this. In sum, *once* any local fitting procedure has been tested and decided upon, it is *then* possible to set up an "application" on which the procedure gives completely incorrect results. Finally we remark that while these given problems are not the easiest to solve without hindsight using other methods, they are by no means impossible. In fact, using the superposition method of [3] in conjunction with the path independent integrals of [4] we would judge that reasonable results could be obtained in return for some computational effort. More precisely, for Problem 1 for instance, we estimate from the participation of the regular eigenfunctions in Table 2 relative to that in trial problems in [4], that K_I could be found to within 10% using a uniform grid comprised of around 1000 constant-strain triangle elements, to within 1% using grids with up to 5000 such elements and extrapolation. Moreover, these analyses could be performed in a completely systematic way without drawing on a knowledge of the exact answer at all.

REFERENCES

1. G.B. Sinclair, "The inherent unreliability of local fitting methods for calculating stress intensity factors," Report SM 82-19, Department of Mechanical Engineering, Carnegie-Mellon University (1982).

2. G.B. Sinclair, "Some inherently unreliable practices in present day fracture mechanics," *International Journal of Fracture*, to appear.

3. G.B. Sinclair and D. Mullan, "A simple yet accurate finite element procedure for computing stress intensity factors," *International Journal for Numerical Methods in Engineering*, Vol. 18, pp.1587-1600 (1982).

4. G.B. Sinclair, M. Okajima and J.H. Griffin, "Path independent integrals for computing stress intensity factors at sharp notches in elastic plates", *International Journal for Numerical Methods in Engineering*, Vol. 20 (1984).

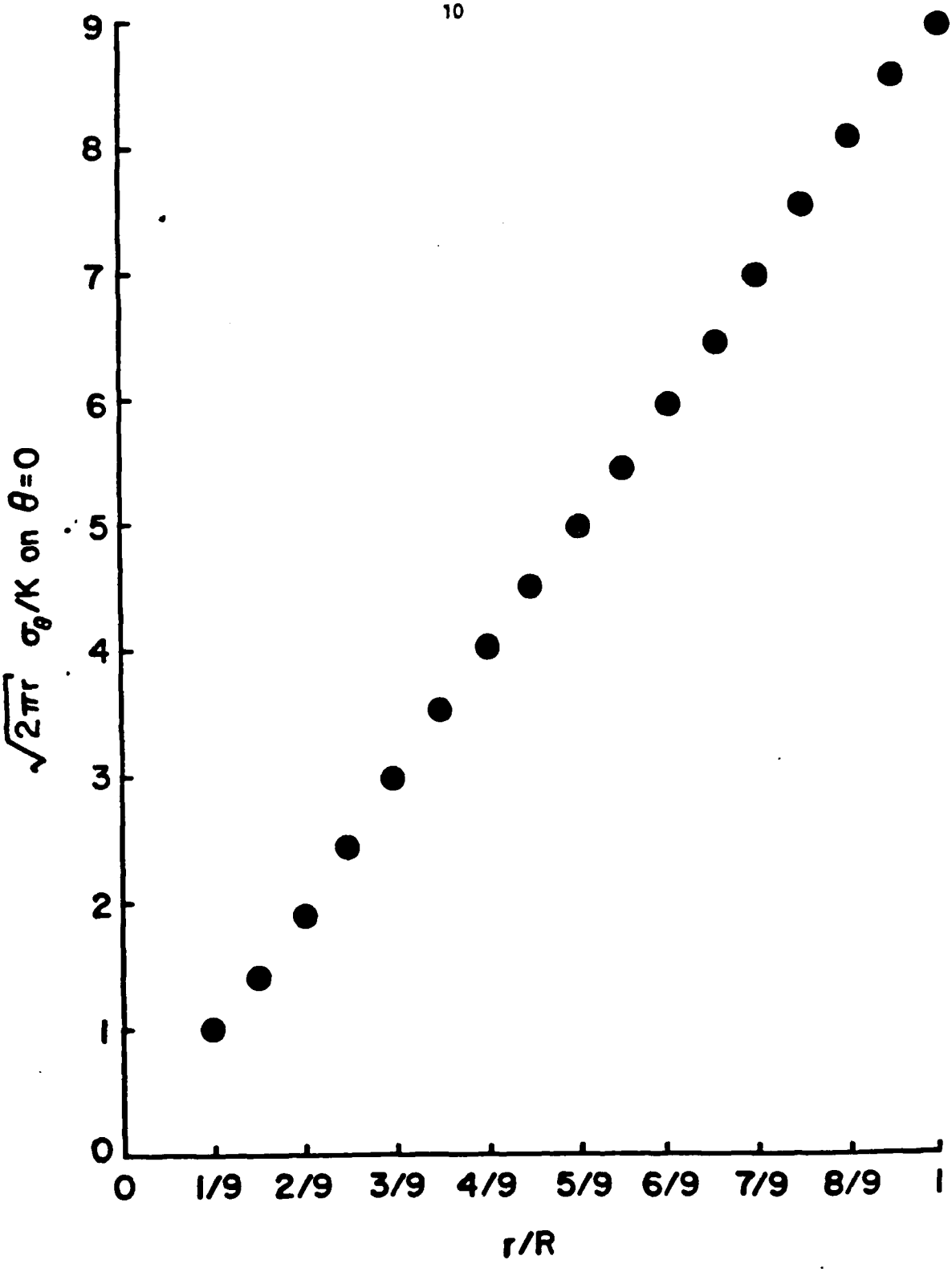

Figure 3. Stress ahead of the crack in Problem 1

APPENDIX 4: ON THE CAPRICIOUS NATURE OF ELASTIC SINGULARITIES / THE ELASTIC ANALYSIS OF THREE RE-ENTRANT CORNERS

ON THE CAPRICIOUS NATURE OF ELASTIC SINGULARITIES

A.E. Chambers and G.B. Sinclair
Department of Mechanical Engineering, Carnegie-Mellon University
Pittsburgh, PA 15213

Classical elastic analysis of re-entrant corners or sharp notches in plates reveals the presence of stress singularities at the notch vertices. As a result, one must make inferences concerning the structural integrity of components containing such features when the stresses become infinite in response to infinitesimal loads, clearly not a simple task. At this time the accepted methodology, for the case of cracks in brittle materials anyway, is to take the coefficient of the singularity – the stress intensity factor – as the parameter governing failure. This choice represents the basic tenet of linear elastic fracture mechanics today.

The usual approach taken in the elastic asymptotic analysis of re-entrant corners is to examine what stress fields, including singular fields, are possible for a given local geometry. Here we adopt an inverse approach of prescribing a field with bounded but nontrivial stresses at the vertex then asking what problem can such fields occur in. In this way we construct a closed form solution with finite stresses for a loaded plate in the shape of a pac-man with a specific angle between its stress-free flanks. This configuration then has a stress concentration factor but no stress intensity factor. By maintaining the same loading on the outer edges of the pac-man yet perturbing the shape of the flanks about their original positions, problems which have participating singularities are generated. These last do not readily admit to the determination of close form solutions but are amenable to numerical analysis of demonstrably high resolution using appropriate path independent integrals and a superposition procedure. Since an identical loading acts in all problems and only very minor changes in geometry occur, it is to be expected that the physical responses would be quite similar. Thus the stress intensity factor's on-off-on-again type behavior makes it difficult to envisage how it could be the controlling damage parameter in this sequence of problems. These results, and other like them (e.g., references), suggest the need for a reconsideration of the role of the stress intensity factor in fracture mechanics.

References

A.E. Chambers and G.B. Sinclair, On obtaining fracture toughness values from the literature *Int. J. Fracture* 30, R11-R15 (1986).

G.B. Sinclair and A.E. Chambers, Strength size effects and fracture mechanics: what does the physical evidence say? *Engng Fracture Mech.* to appear.

THE ELASTIC ANALYSIS OF THREE RE-ENTRANT CORNERS

A. E. Chambers and G. B. Sinclair

SM 86-10

June, 1986

Department of Mechanical Engineering
Carnegie Institute of Technology
Carnegie-Mellon University
Pittsburgh, Pennsylvania 15213

THE ELASTIC ANALYSIS OF THREE RE-ENTRANT CORNERS

INTRODUCTION

Since many engineering structures are designed with what are known as re-entrant corners or notches (Figure 1), it is important to understand the mechanical behavior of these geometries upon loading. Elastic analysis of these notches can result in stress fields near the notch tip that are singular in nature [1]. Physically, these singularities do not make any sense. Unbounded stresses imply failure under even an infinitesimal load, which is inconsistent with everyday experience. For analytical purposes, it is desirable to determine the participation of these singular fields in comparison to the regular fields present.

These singular stress fields are eigenfunctions of the equilibrium problem posed upon loading re-entrant configurations. In general, most regular eigenfunctions stresses acting along the bisector of the re-entrant corner are equal to zero, leaving only the singular fields to dictate the mechanical behavior of the notch (Figure 1). It is these stress fields acting at the notch tip that are analytically unbounded. It is also these stress fields that require making some sense of their significance in the problem under investigation. In order to gain some understanding as to how the singularity plays a role in the overall stress field, one could ask the question, is there a re-entrant geometry which has non-zero and finite stresses acting at the notch tip? Such a configuration would have no singularity participation, i.e. a stress intensity factor of zero. The answer to this question is, in fact, yes. Upon finding a re-entrant corner that has only regular stress fields, the objective of the present work is to track the variations of the stress intensity factor with slight perturbations of geometry. A re-entrant corner under a particular loading that has a stress intensity factor of zero yet nontrivial stresses at the vertex will be determined. The angle near the vertex of the corner will be decreased and then increased slightly. The

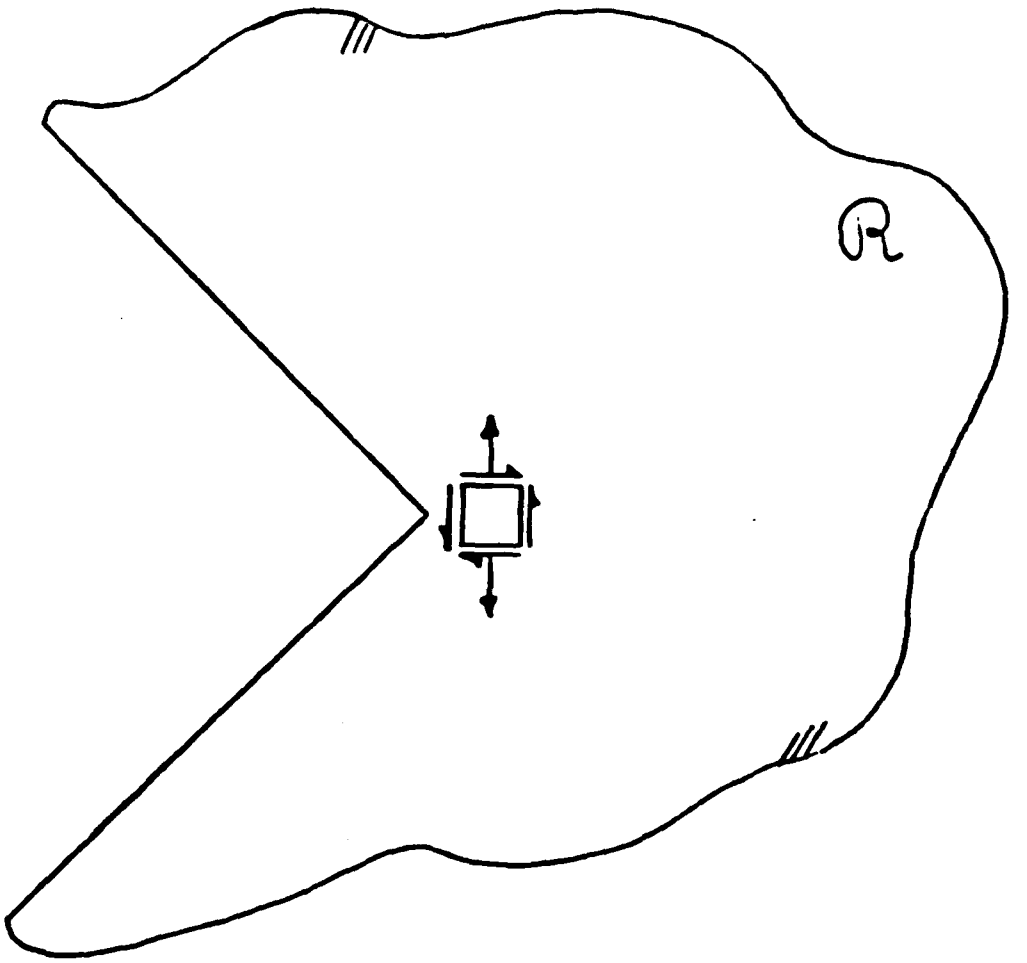

Figure 1

effects of these geometric changes will be studied through the behavior of the stress intensity factor.

The first section presents the formulation of the problem under investigation. The exact geometries to be examined are introduced. The generalized stress intensity factor is defined. The second section presents the numerical analysis. A finite element approach is taken to determine the stress and displacement fields. A path-independent integral is used to calculate the stress intensity factor with the information produced from the finite element analysis. Results will be presented and discussed in the final section.

PROBLEM FORMULATION

In order to study the effects of a stress singularity of a re-entrant corner, three individual regions are analyzed. The basic difference of the three regions is that the material angle local to the notch tip is slightly perturbed from an initially symmetric geometry. The planar region R_i has material angle, $2\alpha_i$ (i=0,1,2). In particular, α_0 = 128.727° , α_1 = 125.863 and α_2 = 131.863° . The choice of these particular values will be explained later. Let (x,y) be cartesian coordinates that have origin at the notch vertex, and the x-axis bisects the material angle there (Figure 2). Let (r,θ) be polar coordinates in the region where $r^2 = x^2 + y^2$ and θ = arctan (y/x). The dimensions of the notch are as follows: a = notch depth and h = half-height of notch.

The region, R_0, is defined as the region enclosed by basically two boundaries. The first boundary, $\partial_1 R_0$, is the boundary to which the prescribed tractions will be applied. It consists of three sides of a rectangle. The line segments that define it are:

$$y = \pm h \quad \text{for} \quad -a \le x \le 2h \quad \text{and} \quad x = 2h \quad \text{for} \quad -h \le y \le h. \tag{1}$$

The second boundary, $\partial_2 R_0$, to enclose the region, R_0, is the two line segments given by

$$\tan\alpha_0 = \pm y/x \quad \text{for} \quad -a \le x \le 0. \tag{2}$$

The region, R_1, is defined in a similar manner. The local (x,y) coordinate system near the vertex of the corner is slightly rotated about the global coordinates by about δ = 3°. The outer rectangular boundary, $\partial_1 R_1$, on which the tractions are applied is left intact, as

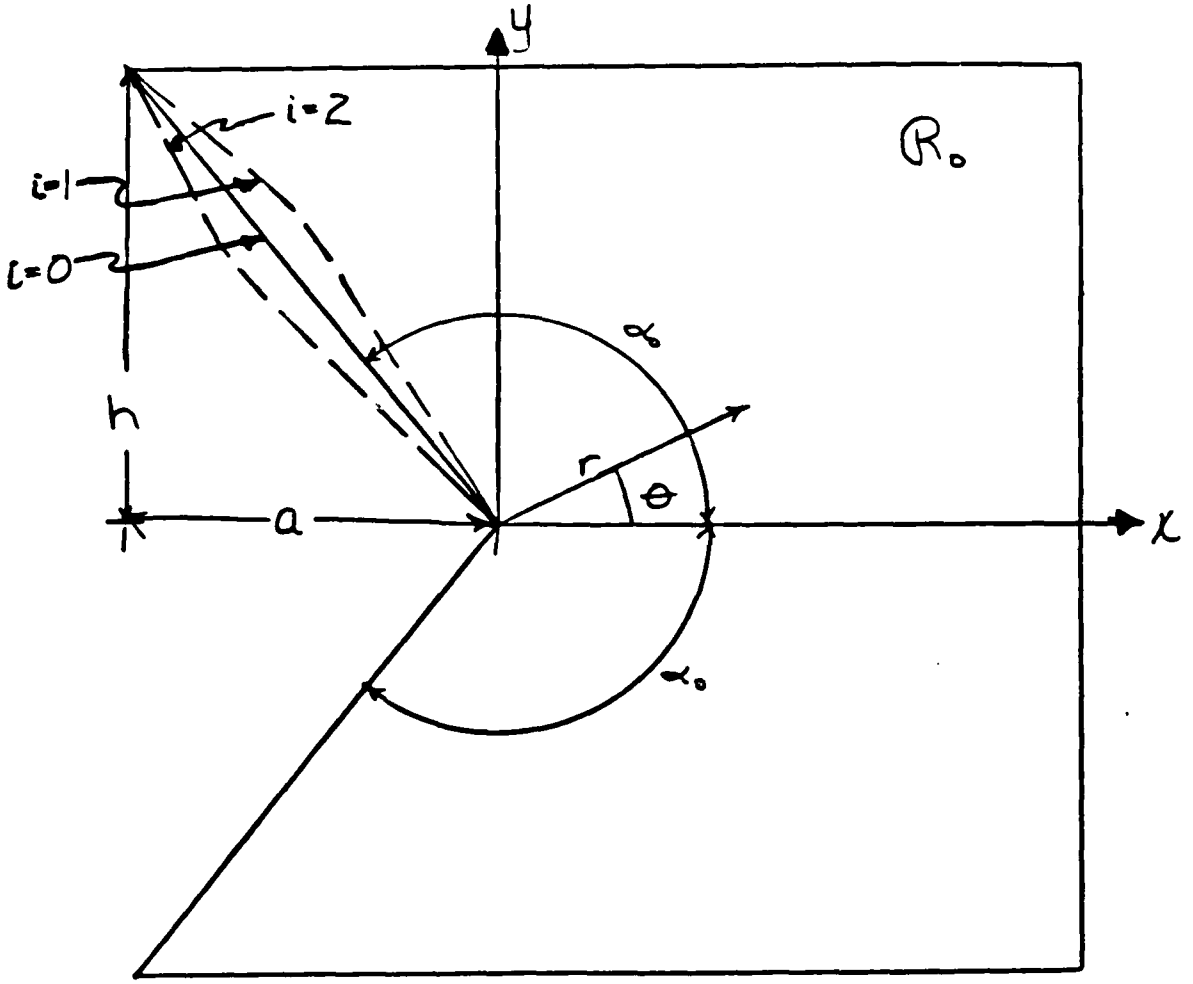

Figure 2.

is the lower flank. The upper flank is rotated by approximately 2δ and extended to y = h/2, thus resulting in less solid material to support the applied loads in the original problem. It is connected by a smooth curve to the point where the positive y-face boundary begins in the second quadrant at y = h. This is boundary $\partial_2 R_1$.

The perturbation of the upper flank for Problem i = 2 is similar to that in the first perturbed problem. However, the rotation of the local axes is in the opposite direction, resulting in more solid material than both Problems i = 0 and 1. This is region R_2. (The dotted lines in Figure 2 represent the upper flanks for Problems i = 1 and 2.)

Formally, we seek the stresses, σ_{rr} , $\sigma_{\theta\theta}$ and $\tau_{r\theta}$, and the displacements, u_θ and u_r, as functions of r and θ in the region R_i, satisfying the following. The stress field must satisfy the two- dimensional stress equations of equilibrium in the region in the absence of body forces,

$$\frac{\partial \sigma_{rr}}{\partial r} + \frac{1}{r}\frac{\partial \tau_{r\theta}}{\partial \theta} + \frac{\sigma_{rr}-\sigma_{\theta\theta}}{r} = 0,$$

$$\frac{1}{r}\frac{\partial \sigma_{\theta\theta}}{\partial \theta} + \frac{\partial \tau_{r\theta}}{\partial r} + \frac{2\tau_{r\theta}}{r} = 0, \tag{3}$$

on R_i. The stress-displacement relations for a homogeneous, isotropic, linear elastic plane hold for the regions,

$$\sigma_{rr} = \frac{2\mu}{C_1}\left[C_2 \frac{\partial u_r}{\partial r} + \nu\left(\frac{1}{r}\frac{\partial u_\theta}{\partial \theta} + \frac{u_r}{r} \right)\right],$$

$$\sigma_{\theta\theta} = \frac{2\mu}{C_1}\left[C_2\left(\frac{1}{r}\frac{\partial u_\theta}{\partial \theta} + \frac{u_r}{r} \right) + \nu \frac{\partial u_r}{\partial r} \right], \tag{4}$$

$$\tau_{r\theta} = \mu\left[\frac{1}{r}\frac{\partial u_r}{\partial \theta} + \frac{\partial u_\theta}{\partial \theta} - \frac{u_\theta}{r} \right],$$

on R_i, where μ is the shear modulus, C_1 equals $1-2\nu$ for plane strain and $1-\nu$ for plane stress, C_2 equals $1-\nu$ for plane strain and 1 for plane stress, and ν is Poisson's ratio. The notch flanks are stress-free which requires that

$$\sigma_{\theta\theta} = \tau_{r\theta} = 0 \quad \text{on} \quad \partial_2 R_i \quad \text{when} \quad \theta = \pm \alpha_i \tag{5}$$

The remaining boundary conditions on $\partial_1 R_i$ are prescribed tractions derived from the following stresses:

$$\begin{aligned}
\sigma_{rr} &= -\sigma_0\left[\sin 2\theta + \frac{\theta}{\alpha_0} \sin 2\theta_0 \right], \\
\sigma_{\theta\theta} &= \sigma_0\left[\sin 2\theta - \frac{\theta}{\alpha_0} \sin 2\theta_0 \right], \\
\tau_{r\theta} &= -\sigma_0\left[\cos 2\theta - \cos 2\theta_0 \right],
\end{aligned} \tag{6}$$

where σ_0 is arbitrary. Finally, the regularity requirements involve the fact that the *displacements at the vertex of the notch must be finite,*

$$u_r \text{ and } u_\theta = O(1) \quad \text{on} \quad R_i \quad \text{as} \quad r \to 0. \tag{7}$$

More specifically, we want to use the stress and displacement fields found in the problems (i = 0, 1 and 2) formulated above to find the generalized stress intensity factors present. There are two possible factors, one arising from any symmetric loading and one arising from any antisymmetric loading in the problem. For the symmetric case, the stress intensity factor is defined as:

$$K_I = \lim_{r \to 0^+} \sqrt{2\pi}\ \sigma_{\theta\theta}\, r^{1-\lambda_i} \quad \text{on} \quad \theta = 0. \tag{8}$$

The subscript I represents mode I loading (symmetric opening mode). The value of λ_i is the eigenvalue identified after Williams [1] that represents the only singular stress field possible at the re-entrant corner under this symmetric mode. That is, λ_i is the root of the eigen-condition

$$\sin 2\lambda_i \alpha_i = -\lambda_i \sin 2\alpha_i \qquad (0 < \lambda_i < 1). \tag{9}$$

For the anti-symmetric case, the stress intensity factor is defined as:

$$K_{II} = \lim_{r\to 0^+} \sqrt{2\pi}\, \tau_{r\theta}\, r^{1-\lambda_i} \quad \text{on} \quad \theta = 0, \tag{10}$$

where the subscript II represents the mode II loading (antisymmetric). The eigenvalue λ_i is evaluated from the antisymmetric eigen-condition,

$$\sin 2\lambda_i \alpha_i = \lambda_i \sin 2\alpha_i \qquad (0<\lambda_i<1). \tag{11}$$

These eigenvalues produce eigenfunctions which are the only singular stress fields possible for the particular notch geometry. As a result of the problem formulation, the displacement fields derived are regular. That is, the fields near the notch tip behave as

$$\sigma_{\theta\theta} \text{ and } \tau_{r\theta} = O(r^{\lambda_i - 1}) \text{ and } u_r \text{ and } u_\theta = O(r^{\lambda_i}) \text{ on } R_i \text{ as } R\to 0. \tag{12}$$

Some explanation of the traction boundary conditions found from (6) is now in order. Recall, that the purpose of this study is to look at slight geometric perturbations of a regular configuration. Therefore, R_0 is taken to be the region in the nonsingular problem under investigation. The approach taken is such that a particular material angle, α_0, is sought that will produce a regular and non-zero stress field for an antisymmetric problem. The following transcendental equation results:

$$\tan 2\alpha_0 = 2\alpha_0 \tag{13}$$

It is in solving this equation that α_0 is found to be approximately 128.7° . The remaining two problems are then posed by simply changing the material angle by plus or minus about three degrees. Note, also, there is now an exact solution for the nonsingular problem that is independent of the radial coordinate, r. It is these regular stress fields that are used as the traction conditions on the boundary $\partial_1 R_i$ (i=0,1,2).

In conclusion, what we have are three problems where the applied tractions and the boundary on which they are applied remain the same. The flanks change in geometry, but remain stress free. An easy way to imagine it all, is that the region R_0 is an ideal geometry of a re-entrant corner that is to be fabricated (i=0). The first singular case examined (i=1) is a result of machining just a little too much material away from the upper flank. The second (i=2) follows from not machining quite enough material away from the

flank. When the three configurations are loaded under the same conditions, what is the result of these slight geometric changes?

ANALYSIS

The analysis of the problems requires two major steps. First, the stress fields in R_i (i = 0,1,2) need to be determined. Secondly, as stated in the problem formulation section, a method is then needed to determine the stress intensity factor of each problem for both mode I and mode II loadings.

A finite element method is used to numerically determine the resultant stress and displacement fields of the three problems.* For each problem, three grids of different sizes are used in the hopes of attaining better accuracy and gauging convergence. The grid refinement is fairly systematic. The coarse grid for the nonsingular problem (i=0) is shown in Figure 3. The nonsingular stress fields defined in (6) are applied on the rectangular boundary, leaving the notch flanks stress-free. Upon finite element analysis, nodes along common θ are of constant stress. (One drawback of the grid pattern chosen is that near the notch vertex there is no refinement in the angular direction. Therefore, convergence as r goes to zero is difficult to judge, though, divergence can be obvious.) The coarse grid for the first singular problem (i=1) is shown in Figure 4, while that for the second singular problem is displayed in Figure 5. The dotted lines in Figures 4 and 5 are the smooth curves that represent the flanks. Since the finite element code uses linear elements, these curves are better approximated upon grid refinement. For all three problems, three grids were used in the stress analysis. The coarse grids have 68 elements and 48 nodes. The medium grids have 264 elements and 159 nodes. The fine grids have 1040 elements and 573 nodes.

The second step of the analysis requires a method of determining the generalized stress intensity factor from the stress and displacement fields generated from the finite element analysis. The method employed, the H-integral [2], is from the family of path-independent integrals. The major advantage of path-independent integrals is that the only

---

*The program used is PLANDJ, originally developed by J.L. Swedlow. It is used on the VMS/VAX at the Mechanical Engineering Department, Carnegie-Mellon University.

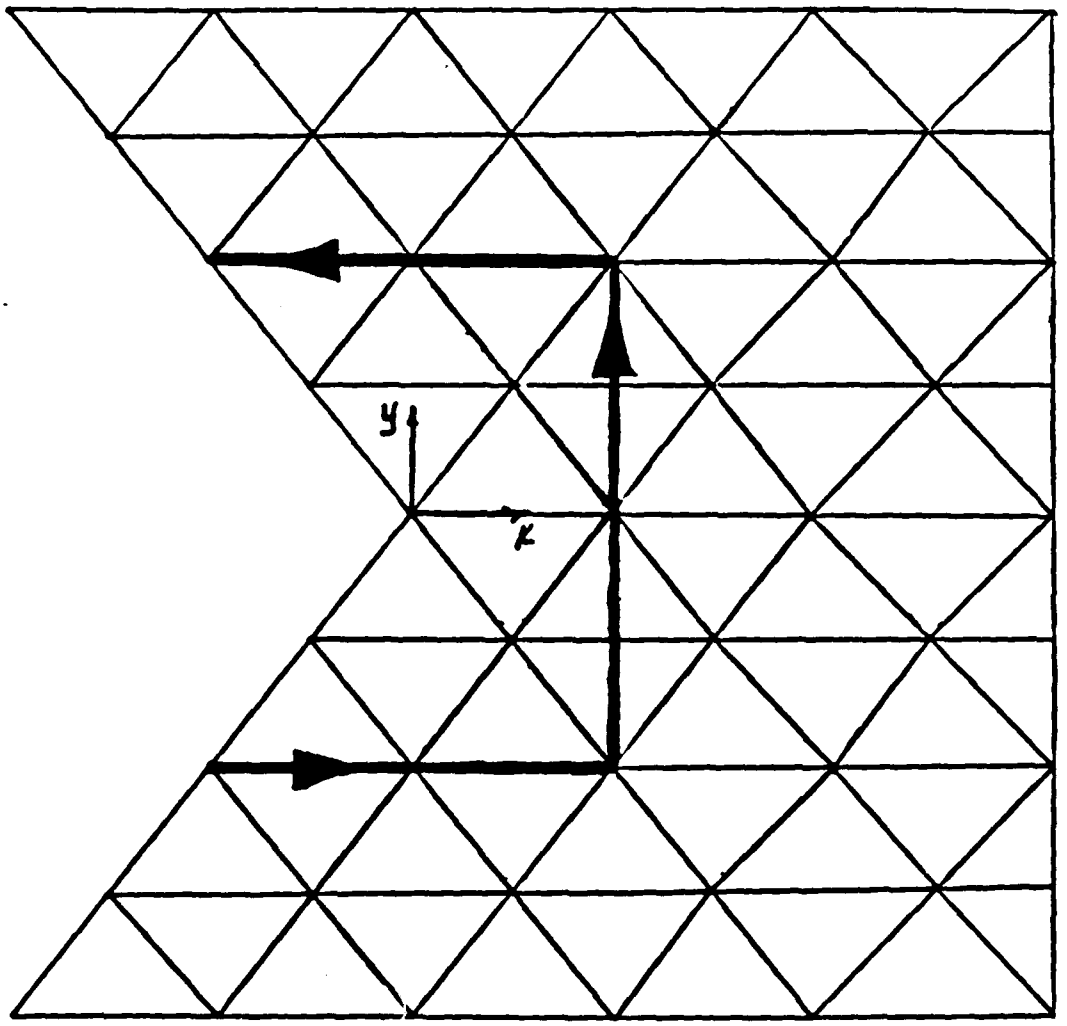

Figure 3

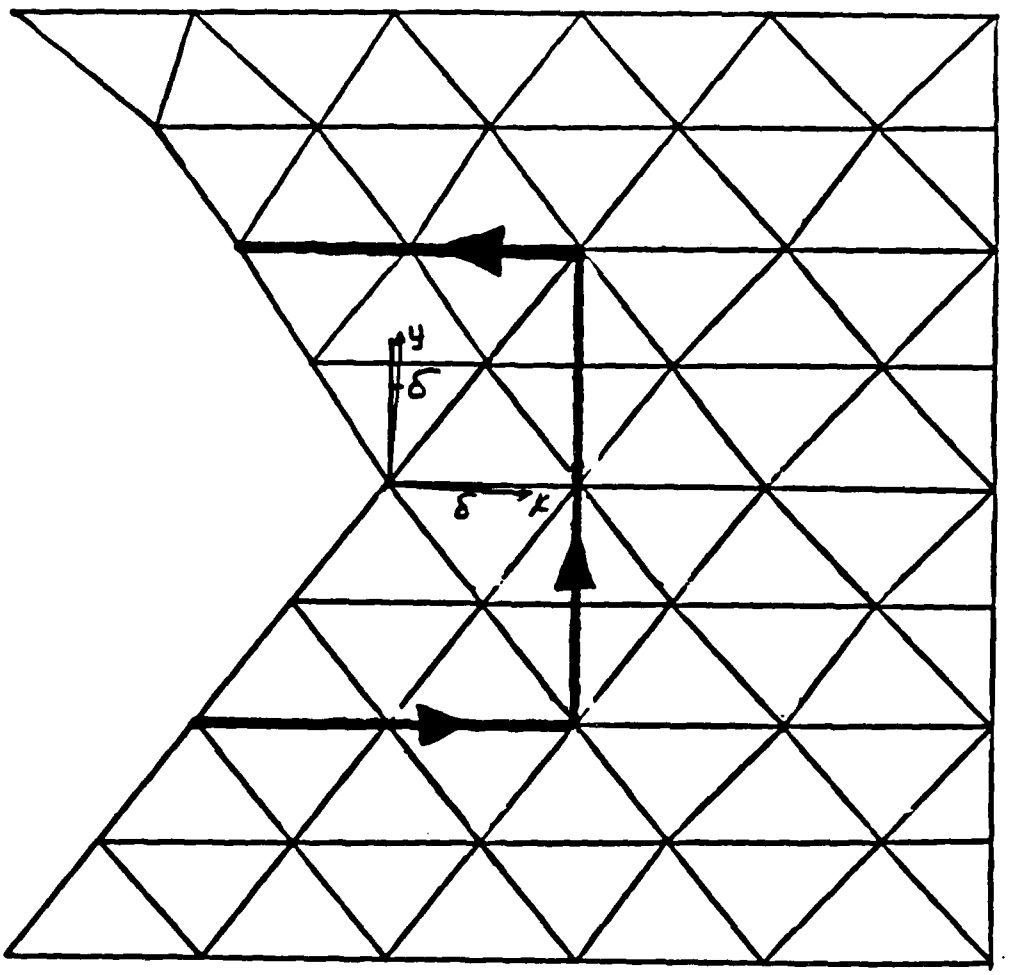

Figure 4.

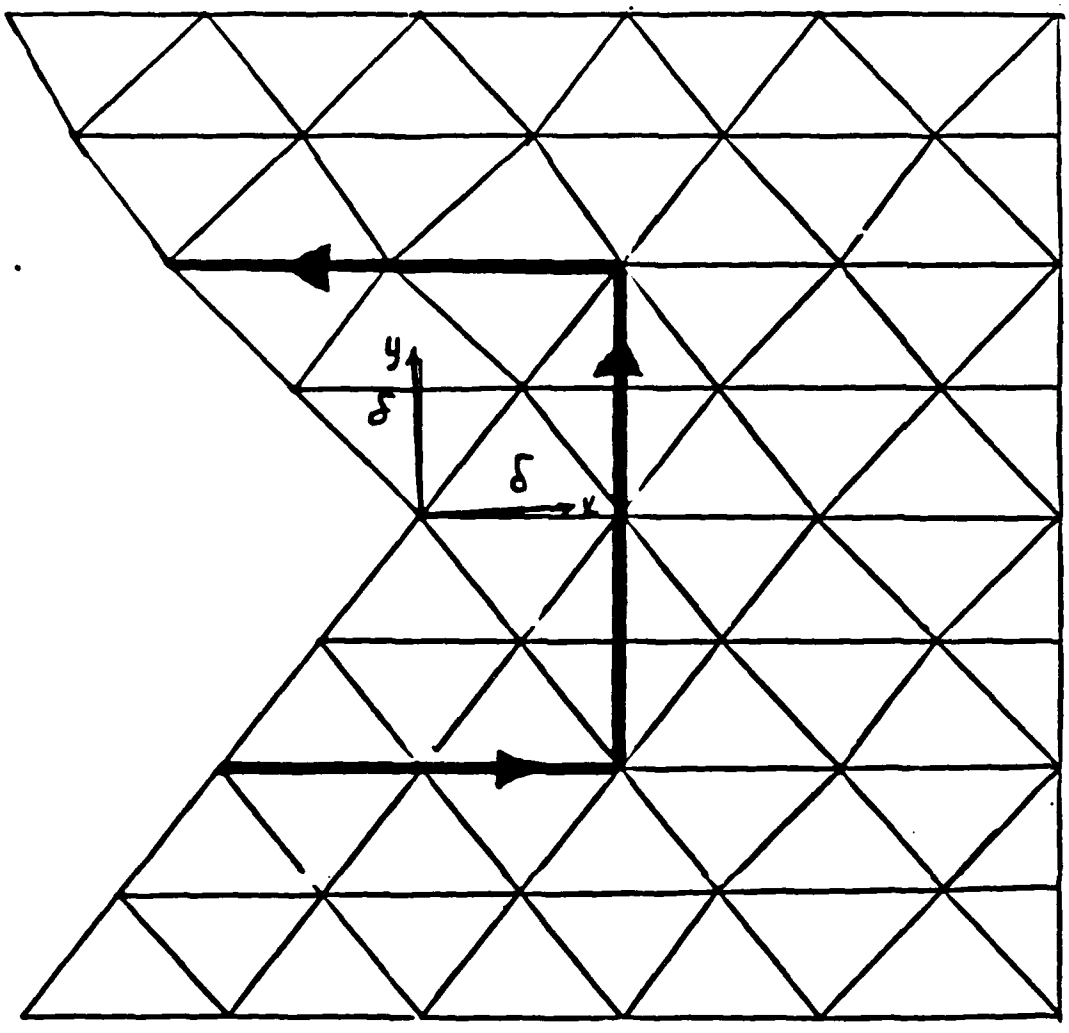

Figure 5.

errors accumulated are those from the numerical approximations present. Another advantage of these integrals is the fact that the symmetric and antisymmetric parts need not be separated in the analysis. (For the argument supporting this statement, see reference [3].) The path of integration is shown in Figures 3, 4 and 5. Notice that the inside path is chosen so that the curvature of the notch flanks in the two singular problems (i = 1 and 2) does not interfere with the independence of the integration path. The H-integral program uses the second-order trapezoidal rule for the integration. The nodal values along the path of integration are used as points of numerical integration. The complementary stress fields and displacement fields used in the H-integral (see reference [2]) are determined from the (r,θ) coordinates of the nodes along the path. The actual nodal displacements are read from the finite element output. The stresses at the nodes are determined from nodal averages of the surrounding elements of each node along the integration path.

RESULTS

In presenting the results of this analysis, some sort of verification is required. One common method of verification of the finite element method is to check convergence at nodes common to all three grids used for each problem. In the nonsingular case, convergence to the exact solution (6) is required. In the other two cases, convergence within the three associated grids is desired. As stated earlier, since there is no grid refinement in the angular direction, convergence near the origin is difficult to assess. Divergence, on the other hand, is clear when present. Therefore, the nodal stresses acting along the x-axis (θ=0) are plotted for all three problems. (Figure 6, 7, and 8.) Convergence to the exact solution in the nonsingular problem (i=0) is seen clearly (Figure 6). The antisymmetry in the problem is observed in that $\sigma_{\theta\theta}$ = 0 and $\tau_{r\theta}$ is finite along the x-axis. Convergence at r=0 for $\tau_{r\theta}$ is not obvious (though, as explained earlier, it is not particularly expected). However, divergence is not noticed.

Comparing the expected singular problems (i = 1 and 2), divergence at the origin is clear. For the singular problem i=1 (Figure 7), $\sigma_{\theta\theta}$ at r = 0 is divergent, where the trend of $\tau_{r\theta}$ is not obvious. This is consistent with what will be seen later, problem i = 1 has a

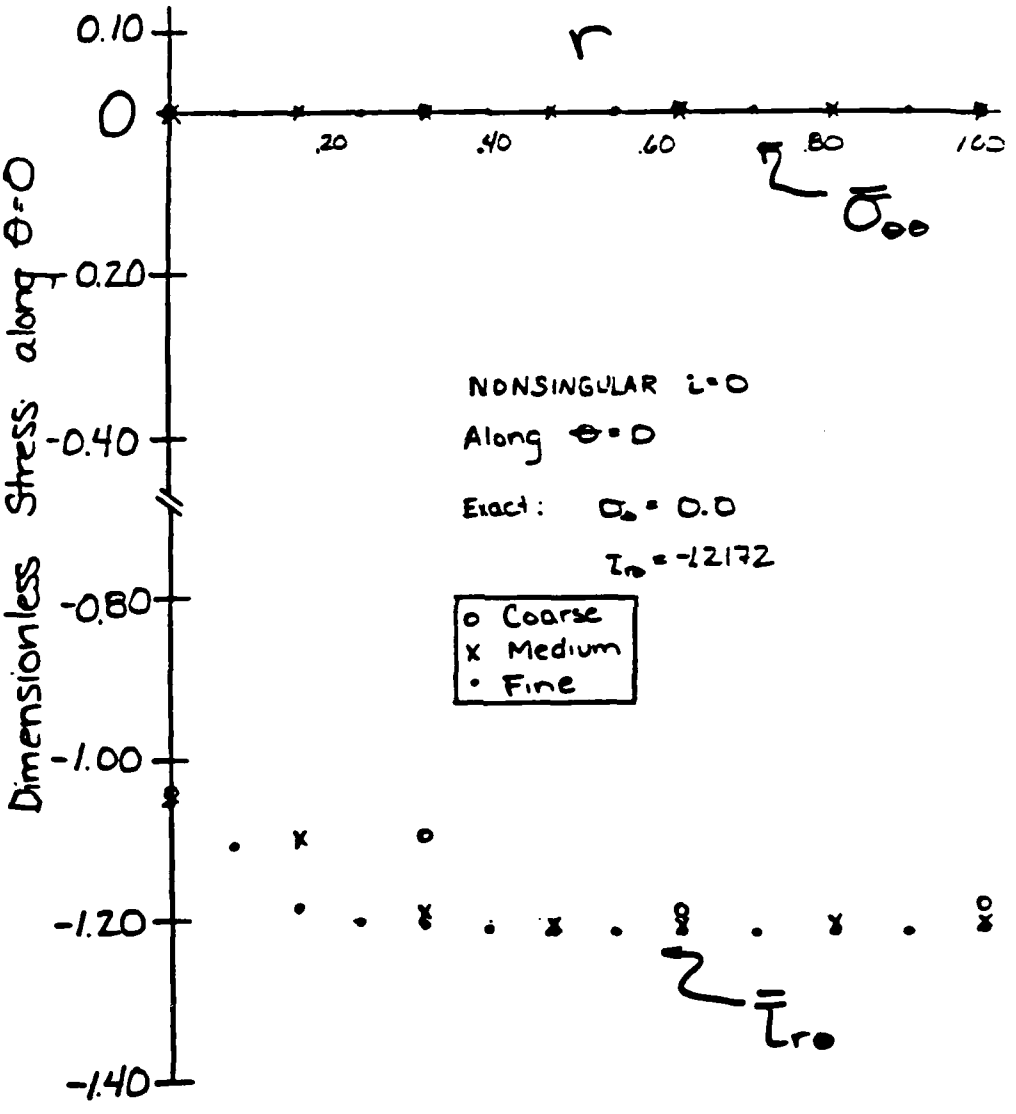
0.10
0
-0.20
-0.40
-0.80
-1.00
-1.20
-1.40
r
.20
.40
.60
.80
1.00
Dimensionless Stress along θ=0
NONSINGULAR i=0
Along θ=0
Exact: σθθ = 0.0
τrθ = -.2172
o Coarse
x Medium
• Fine
σθθ
τrθ

Figure 6.

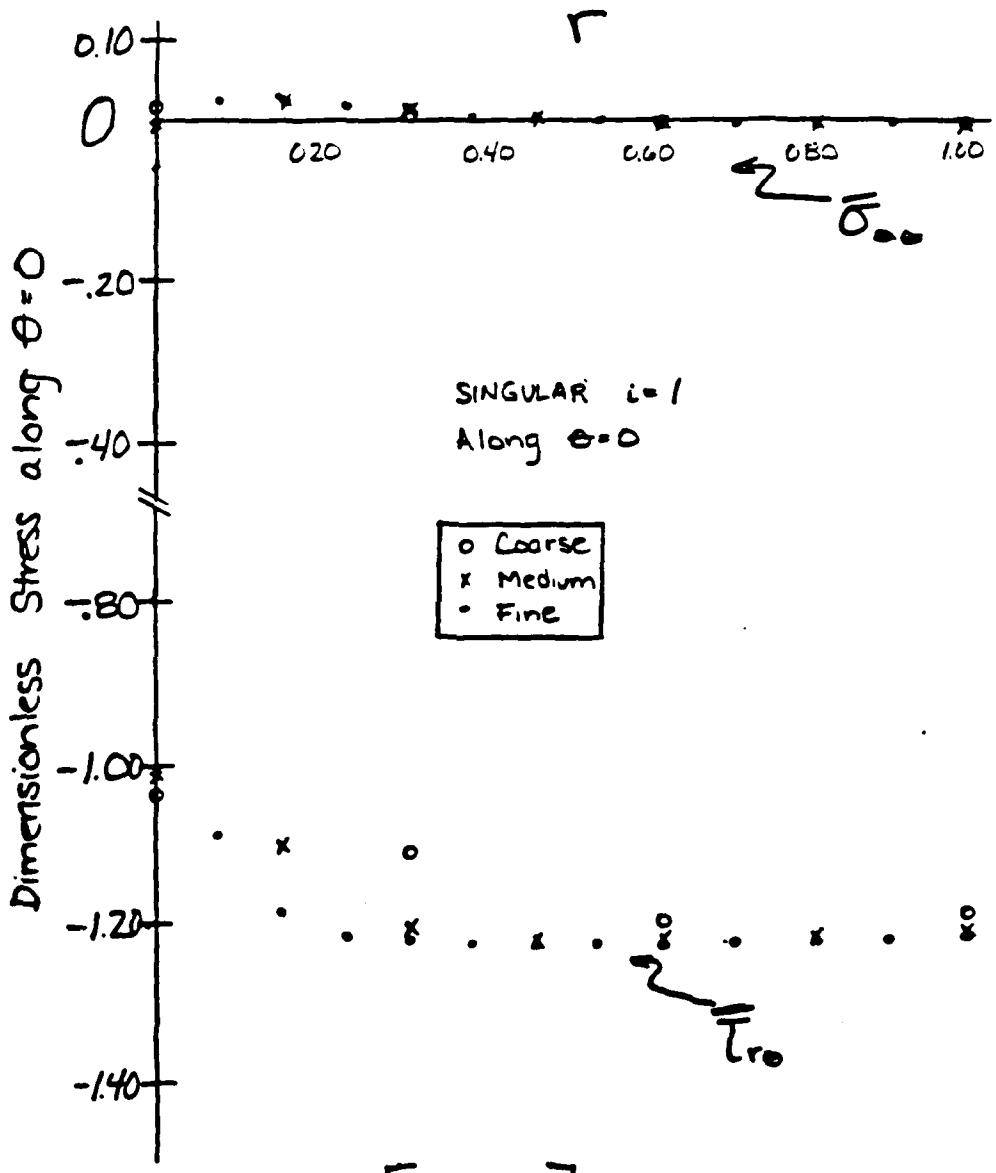
r
0.10
0
0.20
0.40
0.60
0.80
1.00
$\bar{\sigma}_{\theta\theta}$
-.20
-.40
-.80
-1.00
-1.20
-1.40
Dimensionless Stress along θ=0
SINGULAR i=1
Along θ=0
o Coarse
x Medium
• Fine
$\bar{\tau}_{r\theta}$

Figure 7.

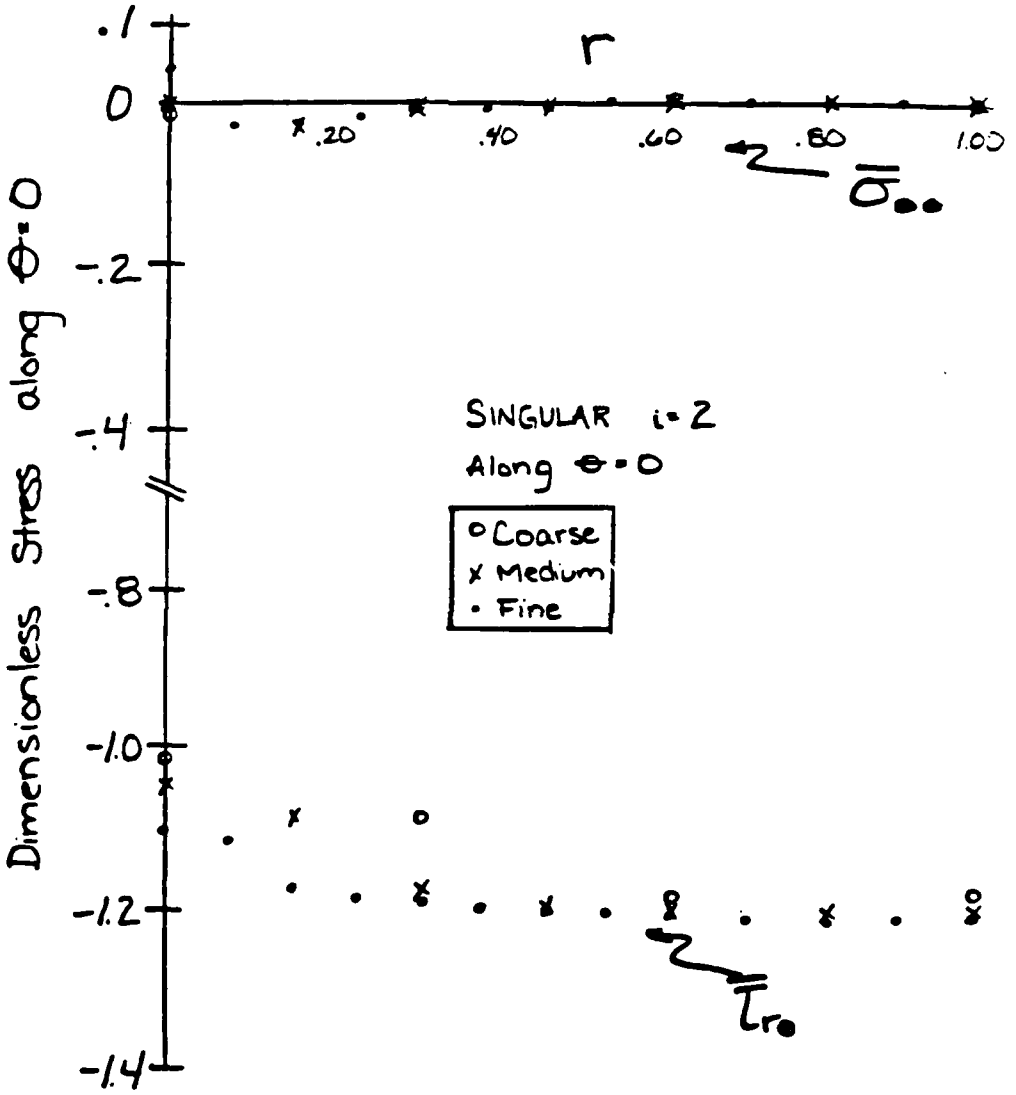
.1
0
-.2
-.4
-.8
-1.0
-1.2
-1.4
r
.20
.40
.60
.80
1.00
$\bar{\sigma}_{\theta\theta}$
Dimensionless Stress along $\theta = 0$
SINGULAR i = 2
Along $\theta = 0$
o Coarse
x Medium
• Fine
$\bar{\tau}_{r\theta}$

Figure 8.

mode I singularity and no mode II. The results for $\sigma_{\theta\theta}$ and $\tau_{r\theta}$ for problem i=2 (Figure 8) are divergent at r=0. This is also consistent since both mode I and II singularities are present in the problem.

Another method of verification is the fact that where there is no singularity present, H = K should be zero. The H_I-integral of the nonsingular problem oscillates about zero. And is, in fact, numerically zero for our purposes. (The H_{II}-integral cannot be determined for the eigenvalue equal to 1.0, see reference [2].)

For the nonsingular problem (i=0), the eigenvalues corresponding to both equations (9) and (11) are simply equal to 1.0. Therefore, the stress and displacement fields are of the order one. The mode I eigenvalue of the first singular problem (i=1) is $\lambda_1^I = 0.5818$: this is the only singular stress field in this problem. For the second singular problem (i=2), however, singularities in both modes exist. That is, $\lambda_2^I = 0.5554$ and $\lambda_2^{II} = 0.9528$. The corresponding results of the H-integration are presented in Table I.

Notice how the value of the dimensionless K_I in problems i=1 and 2 are virtually equal in magnitude but opposite in sign. This could have been expected from the beginning since the original (nonsingular) material angle is perturbed about the same in both directions for each of the singular problems (i.e. $\alpha_1 = \alpha_0 - \delta$ and $\alpha_2 = \alpha_0 + \delta$). Notice, also, that the value of K_{II} for problem i=2 is larger in magnitude than K_I. This is expected since the loading used was derived from an antisymmetric problem. The antisymmetric singularity should then be dominant.

CONCLUDING REMARKS

In general, re-entrant corners produce stress fields which are singular as the notch vertex is approached. However, a configuration can be found at a particular material angle and loading that will produce all regular stress fields. Slight perturbations in geometry produce predictable behavior in the stress intensity factor. Since the applied loading in this particular problem is based on an antisymmetric configuration, the mode II singularity has a larger participation factor than that of the mode I. Perturbing the material angle in equal magnitude but opposite direction, results in equal but opposite stress intensity factors for mode 1.

Table I. Dimensionless Stress Intensity Factors ($\bar{K} = K / (\sigma_0\sqrt{\pi}\ a^{1-\lambda_i})$)

Problem/ Mode	λ_i	α_i	K Coarse	K Medium	K Fine
Problem 0					
Mode I	1.000	128.7°	0.000	0.000	0.000
Problem 1					
Mode I	0.582	125.9°	−0.066	−0.060	−0.058
Problem 2					
Mode I	0.555	131.9°	0.063	0.060	0.059
Mode II	0.953	131.9°	0.648	0.610	0.632

λ_i = eigenvalue after Williams [1]
α_i = half the material angle of re-entrant corner

Even though the behavior of the stress intensity factor may be predictable, the problem still exists in that these singular fields are not able to interact with the other regular stress fields that are present. The divergent stresses acting along y = 0 in the singular problems (i = 1 and 2) highlight this difficulty. Studying the behavior of the stress intensity factor may lead to a better understanding of what is occuring in these re-entrant configurations.

References

1. M.L. Williams, "Stress Singularities Resulting from Various Boundary Conditions in Angular Corners of Plates in Extension," Journal of Applied Mechanics 19 (1952) 526.

2. G.B. Sinclair, M. Okajima and J.H. Griffin, "Path Independent Integrals for Computing Stress Intensity Factors at Sharp Notches in Elastic Plates," International Journal for Numerical Methods in Engineering 20 (1984) 999.

3. G.B. Sinclair, "A Remark on the Determination of Mode I and Mode II Stress Intensity Factors for Sharp Re-entrant Corners," International Journal of Fracture 27 (1985) R81.

APPENDIX 5: ON OBTAINING FRACTURE TOUGHNESS VALUES FROM THE LITERATURE

International Journal of Fracture 30 (1986) R11–R15

ON OBTAINING FRACTURE TOUGHNESS VALUES FROM THE LITERATURE

A.E. Chambers and G.B. Sinclair
Department of Mechanical Engineering, Carnegie-Mellon University
Pittsburgh, Pennsylvania 15213 USA
tel: (412) 578-2504

Recently, extensive compendiums of sources of fracture toughness data have been assembled by Hudson and Seward [1,2]. These lists of references naturally prompt the question as to what an engineer would find upon consulting them in terms of actual values of fracture toughness for a given material. The intent of this note is to indicate an answer.

In choosing specific metals for which to obtain fracture toughness values, we look to ones with large listings of data sources so as to gauge any variability present. To this end we select AISI 4340 steel and 7075-T6 aluminum. We focus on plane strain fracture toughness values (K_{Ic}) as governed by ASTM standards since these are more generally regarded as being material properties. We do not check, however, whether or not a given test furnishing a K_{Ic} value complies with all of the specifications in ASTM E399 [3], simply because none of the references reviewed provided sufficient information to enable a complete check. Hence values are included as valid K_{Ic} if their contributors claim them as such. Since we frequently encountered plane stress fracture toughness values (K_c) in the data for 7075-T6 aluminum, we include these as a separate set for comparison. Further by way of comparison, we note yield strengths (σ_y), since σ_y may reasonably be viewed as the uniaxial tension test quantity analogous to initial unstable crack propagation in a brittle material. In processing the data we distinguish between markedly different specimen types reported in a single source but otherwise use mean values for each source. That is, when what is in essence the same test is repeated a number of times and outcomes recorded, we merely extract the mean*. For these average values, we note the number of essentially independent sources and calculate an overall mean. To estimate the variability we also calculate the ranges and 95 percent confidence intervals (1.96s, s being the standard deviation). In justification of the second, histograms of the data show good agreement with the expected frequencies in a normal distribution (possibly because the individual data typically represent mean values themselves and the central limit theorem applies to some extent). The only exception to this agreement occurs for the K_{Ic} values for 7075-T6. These data, though, conformed well with a normal distribution on taking logs and accordingly a log transformation was used to determine the confidence interval in this instance. The results are summarized in Table 1; details of K_{Ic} values are shown in Tables 2,3 wherein single numbers in brackets denote original sources, hyphenated numbers the corresponding reference in [1] or [2], and a virgule between the two implies as reported in the latter, e.g. [6]/[1-12] is [6]'s data as drawn from [12] in [1]**.

*For the 7075-T6 K_{Ic}, about a quarter of the results were designated as being for a longitudinal orientation and a like fraction as being for a transverse orientation with the remainder being unspecified. Given that the difference between the means for all the longitudinal and transverse cases was found to be less than 2.5 percent, the effects of orientation for this alloy were not regarded as being sufficiently significant to merit distinct classification.

**In the interests of brevity we do not relist references given in [1], [2].

Examining Table 1, we find that the variability in plane strain fracture toughness for AISI 4340 steel is 100 percent of the overall mean when based on the range, 87 percent when based on the confidence interval The corresponding percentages for 7075-T6 aluminum are 162 percent and 108 percent. These wide fluctuations are in marked contrast to the respective percentages for the yield strengths which are 17 percent and 19 percent for the steel, and 22 percent and 21 percent for the aluminum. Indeed they are quite comparable to the variations in plane stress fracture toughness values for 7075-T6, viz, 110 percent and 72 percent*.

Such diverse K_{Ic} data demonstrate that the engineer needs to exercise considerable care in drawing a value of plane strain fracture toughness for a particular material from the literature. Short of undertaking the time consuming task of collecting a sufficient set of references as a way of assessing variations as here, no reasonably certain methodology for ensuring a conservative estimate of fracture toughness appears to exist. Possibly, if a single value is found and then assumed to be at the upper limit of the ranges involved and a safety factor applied to reduce it to the lower, a conservative K_{Ic} could be expected. Such safety factors here would be 2.9, 2.5 for AISI 4340 and 3.7, 2.9 for 7075-T6. These suggest that a safety factor of 3 might be adequate, although there is really no guarantee of this being so for another material. Indeed, the fact that the plane strain fracture toughness data display more than five times greater variability than the yield stress data and vary about as much as the plane stress values which are known to be geometry dependent, raises serious doubts concerning the notion of K_{Ic} being a material property. An engineer continuing to interpret and use it as such may therefore be making significant errors.

Acknowledgement: The financial support of this investigation by the Air Force Office of Scientific Research is gratefully acknowledged.

REFERENCES

[1] C.M. Hudson and S.K. Seward, *International Journal of Fracture* 14 (1978) R151-R184.

[2] C.M. Hudson and S.K. Seward, *International Journal of Fracture* 20 (1982) R59-R117.

[3] E399-83 Standard Test Method for Plane-strain Fracture Toughness of Metallic Materials, *1985 Annual Book of ASTM Standards,* Volume 3.01, American Society for Testing and Materials, Philadelphia (1985) 547-582.

[4] W.F. Brown, Jr., and J.E. Srawley, *Plane Strain Crack Toughness Testing of High Strength Metallic Materials,* STP 410, American Society of Testing and Materials, Philadelphia (1967).

[5] J.E. Srawley, M.H. Jones, and W.F. Brown, Jr., *Materials Research and Standards* 7 (1967) 262-266.

[6] E.A. Steigerwald, Report AFML-TF-67-187, Air Force Materials Laboratory, Wright-Patterson AFB, Ohio (1967).

[7] B. Mravic and J.H. Smith, Report AFML-TR-71-213, Air Force Materials Laboratory, Wright-Paterson AFB, Ohio (1971).

*These plane stress percentages are similar to, though somewhat lower than, the corresponding numbers for 2024-T3 aluminum gathered from nineteen independent sources.

[8] M.F. Amateau and E.A. Steigerwald, Report AD611873 (1965).

[9] M.H. Jones and W.F. Brown, Jr., in *Review of Developments in Plane Strain Fracture Toughness Testing,* STP 463, American Society for Testing and Materials, Philadelphia (1970) 63-91.

[10] R.H. Heyer and D.E. McCabe, in *Review of Developments in Plane Strain Fracture Toughness Testing,* STP 463, American Society for Testing and Materials, Philadelphia (1970) 22-41.

[11] U.H. Lindborg and B.L. Averbach, *Acta Metallurgica* 14 (1966) 1583-1593.

[12] G. Sachs, V. Weiss, and E.P. Klier, *Proceedings of the American Society for Testing and Materials* 56 (1956) 555-565.

[13] G. Succop, M.H. Jones, and W.F. Brown, Jr., "Effect of Some Testing Variables on the Results from Slow Bend Pre-cracked Charpy Tests", NASA Lewis Research Laboratories, Ohio (1975).

[14] T.M.F. Ronald, unpublished data, Air Force Materials Laboratory, Wright-Patterson AFB, Ohio (1974).

[15] W.S. Pellini and J.E. Srawley, NRL Report No. 5609 (1961).

[16] D.Y. Wang and D.E. McCabe, in *Mechanics of Crack Growth,* STP 590, American Society for Testing and Materials, Philadelphia (1976) 169-193.

[17] D.A. Gerdeman, J.C. Wurst, J.A. Cherry, and W.E. Berner, Report AFML-TR-68-53, Air Force Materials Laboratory, Wright-Patterson AFB, Ohio (1968).

[18] A.R. Simpson and J. Fielding, HSA Report ER/MISV/MAN/1050 (1971).

[19] J.G. Kaufman and M. Holt, Technical Paper No. 18, ALCOA Research Laboratories, Pittsburgh, Pennsylvania (1965).

[20] H.P. van Leeuwan et al., NLR Report Nos. TR 72032, TR 72082, TR 72088, Amsterdam, The Netherlands (1972).

[21] G.T. Schaeffer and V. Weiss, Interim Technical Report No. SUI MET-1078-664-12, Syracuse University, New York (1964).

[22] R.J. Goode, unpublished data (1974).

[23] D.W. Hoeppner, in *Case Studies in Fracture Mechanics,* Report No. AMMRC MS 77-5, Army Materials and Mechanics Research Center, Mass. (1977) 3.1.1-3.1.10.

[24] S.O. Davis, N.G. Tupper, and R.M. Niemi, Report AFML-TR-65-150, Air Force Materials Laboratory, Wright-Patterson AFB, Ohio (1965).

[25] W.F. Brown, Jr. and J.E. Srawley, Data presented at Subcommittee III Meeting of ASTM Committee E-24 (1964).

[26] W.F. Brown, Jr., "Progress Report on NASA-NRL Cooperative Plane Strain Testing Program", ASTM Committee E-24 Meeting (1965).

[27] M.V. Hyatt and M.O. Spidel, in *Stress-Corrosion Cracking in High Strength Steels and in Titanium and Aluminum Alloys,* Naval Research Laboratory, Washington, DC (1972) 147-244.

[28] R.E. Jones, Report AFML-TR-69-58, Air Force Materials Laboratory, Wright-Patterson AFB, Ohio (1969).

[29] F.C. Allen, in *Damage Tolerance in Aircraft Structures,* STP 486,

American Society for Testing and Materials, Philadelphia (1971) 16-38.

3 December 1985

Table 1. Mean values and variability of some material data

Material	Quantity	No. of data	Mean value	Range	95% Confidence interval
Steel-	σ_y	36	1500	1370-1630	1360-1650
AISI 4340	K_{Ic}	32	70.5	37.4-108.2	39.8-101.2
Aluminum-	σ_y	42	507	434-545	452-561
7075-T6	K_{Ic}	29	34.5	21.0-76.9	19.4-56.7
	K_c	94	70.7	32.9-111.0	45.1-96.2

Note: σ_y values are in MPa; K_{Ic}, K_c values are in MPa $m^{1/2}$

Table 2. Plane strain fracture toughness values for AISI4340 steel

K_{Ic} (MPa $m^{1/2}$)	Source	K_{Ic} (Mpa $m^{1/2}$)	Source	K_{Ic} (MPa $m^{1/2}$)	Source
64.8	[1-2]	70.8	[11]/[1-15]	108.2	[12]/[1-156]
57.7	[4].[5]/	53.8	[1-25]	57.7	[1-160]
76.9	[1-12]	73.6		58.2	[13]/[2-3]
58.2	[6]/[1-12]	87.9		76.9	
89.0		37.4	[1-152]	89.0	
90.1		65.4		58.2	[14]/[2-3]
74.7	[7]/[1-15]	65.9		57.6	[2-27]
85.7	[8]/[1-15]	65.9		37.8	[15]/[2-130]
74.7	[9]/[1-15]	67.0		63.0	
87.9	[10]/[1-15]	67.0		62.6	[2-329]
		84.5			
		87.9			

Table 3. Plane strain fracture toughness values for 7075-T6 aluminum

K_{Ic} (MPa $m^{1/2}$)	Source	K_{Ic} (MPa $m^{1/2}$)	Source	K_{Ic} (MPa $m^{1/2}$)	Source
37.0	[16]/1-2]	31.6	[20]/[1-51]	26.6	[2-66]
21.0	[1-5]	30.8	[1-52]	28.2	[24]/[2-130]
27.7		24.2	[2-2]	31.9	[25]/[2-130]
38.5	[1-6]	39.1	[21]/[2-3]	29.9	[26]/[2-130]
48.9		25.3	[22]/[2-3]	26.4	[27]/[2-137]
35.9	[1-11]	34.5	[23]/2-27]	35.2	[2-153]
48.1		76.9		21.6	[2-157]
53,7		34.8	[2-39]	32.6	[28]/[2-159]
29.1	[17]/[1-12]	35.7	[2-59]	34.8	[29]/[2-159]
28.6	[18]/]1-15]				
30.8	[19]/[1-24]				

END

12-86

DTIC